DEVELOPMENT OF ASPHALT PAVEMENT TEMPERATURE PREDICTION MODELS FOR THE CLIMATIC CONDITIONS OF GHANA

By

Simon Ntramah

(BSc. Civil Engineering; MSc. Sustainable Engineering Management for International Development)

A thesis submitted to the Department of Civil Engineering, College of Engineering, Kwame Nkrumah University of Science and Technology, Kumasi, in partial fulfillment of the requirements for the award of the degree of

DOCTOR OF PHILOSOPHY IN HIGHWAY AND TRANSPORTATION ENGINEERING

JULY 2023

DECLARATION

I hereby declare that this submission is my own work and that, to the best of my knowledge and belief, it contains no material previously published or written by another person nor material which to a substantial extent has been accepted for the award of any other degree or diploma at Kwame Nkrumah University of Science and Technology, Kumasi or any other educational institution, except where due acknowledgment is made in the thesis.

……………………………..	…………………………	…………………
Simon Ntramah	Signature	Date
PG9984119		
(Student)		

……………………………..	…………………………	…………………
Prof. Yaw A. Tuffour	Signature	Date
(Supervisor)		

……………………………..	…………………………	…………………
Dr. Kenneth A. Tutu	Signature	Date
(Supervisor)		

……………………………..	…………………………	…………………
Prof. S. Oduro Kwarteng	Signature	Date
(Head of Department)		

LIST OF ABBREVIATIONS AND ACRONYMS

AC	Asphalt Concrete
AASHTO	American Association of State Highway and Transportation Officials
ANOVA	Analysis of Variance
BELLS	Baltzer Ertman-Larsen Lukanen Stubstad
DUR	Department of Urban Roads
EICM	Enhanced Integrated Climatic Model
FAO	Food and Agriculture Organisation
FDM	Finite Difference Method
FEM	Finite Element Method
FCVM	Finite Control Volume Method
FWD	Falling Weight Deflectometer
GAS	Global Aging Model
GHA	Ghana Highway Authority
GMet	Ghana Meteorological Agency
GSR	Global Solar Radiation
HMA	Hot Mix Asphalt
IRRF	Integrated Road Research Facility
LOE	Line of Equality
LTPP	Long-Term Pavement Performance

MBE	Mean Bias Error
M-E	Mechanistic-Empirical
MOFA	Ministry of Food and Agriculture
MPE	Mean Percentage Error
PDE	Partial Differential Equations
PG	Performance Grade
RMSE	Root Mean Square Error
S.E.	Standard Error
SHRP	Strategic Highway Research Program
SMP	Seasonal Monitoring Program
Superpave	Superior Performing Asphalt Pavements

ACKNOWLEDGMENTS

I would like to express my deepest appreciation to Prof. Yaw A. Tuffour and Dr. Kenneth A. Tutu, for supervising this work. I am also thankful to Prof. Charles Adams, the then TRECK Director, for supporting me with all the initial documentation and introductory letters to various agencies where I needed support or data. I am indebted to Ing. Dr. Daniel Asenso-Gyambibi, the Director of the CSIR - Building and Road Research Institute (BRRI), where I work, for granting me the opportunity to undertake this study. I am also thankful to my workplace staff and all who assisted me in diverse ways to get this work completed. Finally, may my family and loved ones be blessed for their understanding, prayers, sacrifice, and encouragement during this academic pursuit.

ABSTRACT

Asphalt pavement temperature finds application in several areas of pavement engineering including pavement structural evaluation and design, asphalt mixture design, asphalt material aging characterisation, and asphalt binder grade selection. Predictive models may be used in the estimation of asphalt pavement temperature when necessary, however, such models tend to have limited transferability and applicability to other regions where the environmental conditions are significantly different from those under which the models were developed. To avoid the risk of using foreign-developed models in estimating the temperature of asphalt pavements in Ghana using local data, this research set out to develop asphalt pavement temperature prediction models applicable to the climatic conditions of the country. Two locations in the country, one within the Savannah climatic zone and the other within the Forest climatic zone, were used for the study. Mid-depth and surface asphalt pavement temperatures, along with climatic data, were collected over a 12-month period (May 2022 to April 2023) at the two study locations. The dataset was then used to develop separate asphalt pavement temperature prediction models applicable to each climatic zones. Additional pavement temperature and climatic data were also collected on separate roads within the corresponding climatic zones for model validation. When tested against some high-rated foreign-developed models, using local environmental data inputs, the locally-developed models predicted asphalt pavement temperatures that were much superior in accuracy ($R^2 \geq 0.919$, RMSE < 2.8 ºC) to those predicted using the best-performing foreign-based model ($R^2 \leq 0.905$, RMSE ≥ 3.2 ºC). The local models are, therefore, recommended for predicting mid-depth asphalt pavement temperatures in the Forest and Savannah zones of Ghana for pavement engineering purposes.

Table of Contents

LIST OF TABLES

LIST OF FIGURES

CHAPTER 1: INTRODUCTION

1.1 Problem Statement

Asphalt concrete (AC) behaves essentially as an elastic material at low temperatures; so, its deformation at such temperatures under low strain levels is recoverable (Diefenderfer *et al.*, 2006). However, in hot environment, the material behaves as a thick fluid and suffers irrecoverable strain under load. Between the low and high temperature extremes, AC exhibits viscoelastic behaviour. Due to the viscoelastic behaviour, the material's modulus is temperature dependent. For a variety of applications in pavement engineering, such as pavement structural evaluation and design, asphalt binder grade selection, asphalt mixture design and aging characterisation, knowledge of in-situ asphalt pavement temperature is important.

Currently, Ghana implements the empirical pavement design method of the American Association of State Highway and Transportation Officials (AASHTO), which does not directly consider temperature effects on AC modulus. The concern with this is that the geographical characteristics and seasonal variation of air temperature can have significant influence on AC modulus and, hence, on pavement performance. For this reason, pavement structural design in several countries across the world is shifting from a purely empirical approach to a mechanistic-empirical (M-E) approach (AASHTO, 2015; Koranteng-Yorke *et al*., 2015). Unlike empirical pavement design methods, M-E design considers seasonal changes in the AC modulus and is seen as a robust approach to the consideration of the impacts of environmental factors on pavement performance (Koranteng-Yorke *et al*., 2015; Saliko *et al*., 2023).

A crucial component of any M-E design system is pavement temperature estimation (Saliko *et al*., 2023). For instance, the AASHTOWare Pavement M-E Design (developed to replace the

AASHTO empirical design method) has an in-built climate model for estimating temperature variation in the AC layer (Papagiannakis, 2013; AASHTO, 2015). This helps to account for local environmental conditions and their impact on pavement response to loading and, hence, performance.

The selection of an appropriate laboratory asphalt mixture aging and testing temperature is crucial in designing and constructing durable pavements. For instance, the Marshall mix design method assumes 60ºC to be the hottest pavement surface temperature. This temperature has been adopted in Ghana, although maximum pavement surface temperatures in some parts of the country could be higher. This suggests that the laboratory mixture aging and testing protocols associated with the Marshall mix design may not accurately characterise some local conditions in the country, and may result in problematic pavement performance.

In the superior performing asphalt pavements (Superpave) binder grading system, an asphalt binder grade is selected for a project location based on the traffic and weather conditions (Kennedy *et al.*, 1994). The Superpave binder grade is described by the lowest and highest pavement temperature under which the asphalt mixture is expected to serve (Kennedy *et al.*, 1994). Asphalt pavement temperatures may be obtained through in-situ measurements or predicted using mathematical models. In-situ measurements may provide a more accurate data, but the process is time-consuming, labour-intensive and could interrupt traffic flow. In addition, in-situ measurement provides temperature data only for the period of measurement (Minhoto *et al.*, 2005; Gedafa *et al*., 2014). These challenges associated with in-situ pavement temperature measurement have led to the development of pavement temperature prediction models. Asphalt pavement temperature prediction models provide a quicker means for obtaining data, are resource-efficient, and provide temperature data over a broad range of site conditions.

In recent times, several projects in Ghana have utilized Superpave performance-grade (PG) binders but the country lacks a locally-developed model for predicting asphalt pavement temperatures for effective Superpave binder grade selection. As part of a broader scope of developing a framework for pavement design in Ghana, Koranteng-Yorke (2012) formulated mathematical relationships between ambient air temperature and AC layer temperature. However, these relationships were not validated nor were goodness-of-fit parameters reported to judge their applicability. Lekea and Steyn (2023) evaluated models developed by SHRP (Huber, 1994), Viljoen (2001), and Diefenderfer *et al.* (2006) using Koranteng-Yorke's (2012) asphalt pavement temperature data collected in two Ghanaian towns (Sogakope and Akumadan), and found them to perform poorly. It should be noted that data provided by Koranteng-Yorke (2012) excluded the Savannah climatic zone of Ghana. The study by Lekea and Steyn (2023) demonstrated the risk of using foreign-developed models in estimating the temperature of an asphalt pavement using local data.

Despite the availability of several models for predicting asphalt pavement temperature, the accuracy of such models is often applicable to the locations for which they were developed (Alavi *et al.*, 2014). Therefore, before applying foreign models in a significantly different environment, it is necessary to evaluate the accuracy of their predictions to guide their applicability. The consequence of ignoring the climatic conditions of Ghana in asphalt pavement temperature prediction models for Ghana is uncertainty in the model estimates. A validated asphalt pavement temperature prediction model, based on the climatic data of Ghana, will be useful for various pavement engineering applications, such as pavement structural design and evaluation, asphalt binder grade selection, and asphalt material aging evaluation.

1.2 Aim and Objectives

The aim of this study was to develop asphalt pavement temperature prediction models for the Forest and Savannah climatic zones of Ghana. The objectives were to:

i. Establish the state of practice of asphalt pavement temperature determination in Ghana.
ii. Evaluate the prediction accuracy of some foreign asphalt pavement temperature models using data from Ghana.
iii. Develop asphalt pavement temperature prediction models for the Savannah and Forest climatic zones of Ghana.

1.3 Scope of Work

The scope of work comprised interviews, in-situ pavement temperature and climate data collection. The state of practice of asphalt pavement temperature determination in Ghana was established through interview of practicing engineers from road agencies, consulting firms and contractors. The climate and asphalt pavement temperature data were gathered in the Forest and Savannah zones represented by Kumasi and Tamale, respectively. The measured pavement temperature, along with other relevant climatic data, were used to evaluate six foreign asphalt pavement temperature prediction models to ascertain if they could be adopted for Ghana. The study then proceeded to develop a model each for the Forest and Savannah climatic zones, employing regression modelling with SPSS Statistics (Version 23) and R studio packages.

Unlike Koranteng-Yorke (2012), the current study formulated, calibrated and validated non-linear regression models for predicting mid-depth asphalt pavement temperatures for the Forest and Savannah climatic zones of Ghana. Again, the current study utilised the input parameters of pavement surface temperature, mean air temperature of previous day and time of pavement temperature measurement to predict asphalt layer temperature compared with the sole use of ambient temperature by Koranteng-Yorke (2012).

1.4 Justification of the Study

Koranteng-Yorke (2016) recommended that developing countries should develop local M-E pavement design systems that incorporate pavement temperature prediction models. Tutu *et al*.

(2022) reiterated the need for locally-developed models for Superpave PG binder selection for Ghana. Additionally, knowledge of asphalt pavement temperature is required for characterising AC material aging. The aging process renders AC material brittle, making it susceptible to cracking (Sirin *et al*., 2018). Hence, some M-E pavement design systems consider the effect of AC modulus aging (Tsai and Wu, 2009; Ullidtz *et al.*, 2010). A proper understanding of the AC material aging process will help to select appropriate laboratory testing protocols for asphalt mixture.

Currently, pavement structural design in Ghana does not consider AC material aging. Hence, a major step toward incorporating aging effects in pavement design is to develop models for estimating in-situ temperature of asphalt pavement layer.

Further, in-situ pavement temperature is a key input in using the Falling Weight Deflectometer (FWD) device for the structural evaluation of asphalt pavements. FWD deflection measurements are dependent on the pavement temperature at the time of testing. Considering the sensitivity of the AC modulus to temperature variation, the back-calculated AC modulus should be adjusted to a preferred temperature (Chowdhury and Hossain, 1999; Gedafa *et al.*, 2014). Temperature-corrected AC modulus is then used in pavement structural evaluation. There is, therefore, a need for a validated asphalt pavement temperature model for pavement structural analysis and evaluation. With the increasing popularity of Superpave PG binder grade application in Ghana, a validated asphalt pavement temperature prediction model will help to leverage advanced asphalt pavement technology for local adaptation.

CHAPTER 2: LITERATURE REVIEW

2.1 Introduction

Whether it is the application of the M-E design systems, the investigation of asphalt material aging, Superpave binder grade selection, or pavement structural evaluation through falling weight deflectometer testing, asphalt pavement temperature is an indispensable input. The approaches to determining asphalt pavement temperature are gradually shifting to the use of mathematical models due to challenges associated with direct measurement methods, especially on large scale projects (Minhoto *et al.*, 2005; Gedafa *et al.*, 2014). While such temperature prediction models exist mainly in the temperature regions, simply applying them in different environments without recalibration may result in significant prediction inaccuracies. This chapter discusses the climatology of Ghana and the applications of temperature of asphalt pavement layer in pavement engineering, and models for predicting asphalt pavement temperature by highlighting the theoretical underpinnings, assumptions, strengths, and weaknesses of each model type. Also, interview methodology, empirical model evaluation, regression analysis, and solar radiation computations are discussed.

2.2 Climatology of Ghana

2.2.1 Climatic Zoning

A climatic zone is a geographical region that exhibits steady climatic conditions (Bessah *et al.*, 2022). Distinctive climatic zones have been proposed based on either climate parameters, vegetation type, or agro-ecological factors. As seen in Table 2.1, Arulansandan *et al*. (1963), Dickson and Benneh (1988), and Klutse *et al*. (2013) categorised Ghana into four climatic zones. Gidigasu (1972) and the Ministry of Food and Agriculture (MOFA, 2016) suggested six zones while Bessah *et al.* (2022) identified three zones. Lastly, the Food and Agriculture Organisation's (FAO, 2006) seven agro-ecological zones remain the highest number of climatic zones proposed for Ghana. Dickson and Benneh's (1988) Tropical Continental or

Savannah zone is comparable with the Semi-Arid used by Arulanandan *et al*. (1963), the Northern Savannah by Klutse *et al*. (2013), and Bessah *et al.'s* (2022) Savannah zone. The combined Guinea and Sudan Savannahs, as used by Gidigasu (1972) and the Ministry of Food and Agriculture (MOFA, 2016), plus the Transitional zone of FAO (FAO, 2006) together describe the same zone as the Tropical Continental or Savannah zone by Dickson and Benneh (1988).

Similarly, the Wet Semi-Equatorial is synonymous with the Dry Moist Sub-Humid and the Moist Semi-Deciduous Forest. Again, the Wet Semi-Equatorial zones are subdivided into the Deciduous Forest and Moist Evergreen (FAO, 2006) or the Transitional and Deciduous Forest by the Ministry of Food and Agriculture (MOFA, 2016), while Klutse *et al*. (2013) adopted the Forest and Transition zones for the same Wet Semi-Equatorial, with the Forest zone covering the South-western Equatorial. A critical look at Table 2.1 reveals that the South-Western Equatorial falls under the Humid, Rain Forest zone, and the Wet Evergreen zones, with some portions being covered by the Coastal zone (as per Bessah *et al*., 2022). The Dry Equatorial feeds into the Coastal Thicket and Coastal Savannah or simply Coastal and the Semi-Arid or Dry Sub-Humid climatic zones, as depicted by Table 2.1.

Clearly, there has not been a single climatic zone demarcation for Ghana. For example the use of the four climatic zones— Coastal Savannah, Forest, Transition and Northern Savannah by the Ghana Meteorological Agency (GMet)—were intended for weather condition forecasting and agricultural purposes (Yamba *et al.*, 2023). This climatic zone was used by Klutse *et al*. (2013) to examine climate change impact on maize production in the Forest and Transitional zones of Ghana. Aryee *et al.* (2018) used rainfall data and the k-means clustering technique for a climatic zone delineation of Ghana and came out with four zones that were consistent with the zoning proposed by Dickson and Benneh (1988) and Arulanandan *et al*. (1963). However, the use of Aryee *et al.'s* (2018) zoning is limited to rainfall applications, such as hydrological modelling. Recently, Yamba *et al.* (2023) has used rainfall and temperature data from 1981 – 2010 to demarcate the country into five zones: the Coastal, Forest, Transition, Sudan Savannah and Guinea Savannah zones.

Bessah *et al.'s* (2022) re-demarcation of the country into three climatic zones appears to bring the curtain down on the long-standing debate surrounding this subject. Their approach utilized wider climate variables comprising maximum and minimum temperatures, rainfall, and air humidity data from all 22 GMet synoptic weather stations over four decades (1976 – 2018). The zones proposed by Bessah *et al*. (2022) are shown in Figure 2.1.

Table 2.1. Proposed Climatic Zones of Ghana

<table>
<tr><th>Dickson and Benneh (1988)</th><th>Arulanandan et al. (1963)</th><th>Gidigasu (1972)</th><th>FAO (2006)</th><th>MOFA (2016)</th><th>Klutse et al. (2013)</th><th>Bessah et al. (2022)</th></tr>
<tr><td rowspan="3">Tropical Continental or Savannah</td><td rowspan="3">Semi-Arid</td><td rowspan="2">Guinea Savannah</td><td>Guinea Savannah</td><td rowspan="2">Guinea Savannah</td><td rowspan="3">Northern Savannah</td><td rowspan="3">Savannah</td></tr>
<tr><td>Sudan Savannah</td></tr>
<tr><td>Sudan Savannah</td><td>Transitional</td><td>Sudan Savannah</td></tr>
<tr><td rowspan="2">Wet Semi-Equatorial</td><td rowspan="2">Dry Moist Sub-Humid</td><td rowspan="2">Moist Semi-Deciduous Forest</td><td>Deciduous Forest</td><td>Transitional</td><td>Transition</td><td rowspan="3">Forest</td></tr>
<tr><td>Moist Evergreen</td><td>Deciduous Forest</td><td rowspan="3">Forest</td></tr>
<tr><td rowspan="2">South-Western Equatorial</td><td rowspan="2">Humid</td><td rowspan="2">Rain Forest</td><td rowspan="2">Wet Evergreen</td><td rowspan="2">Rain Forest</td></tr>
<tr><td rowspan="3">Coastal</td></tr>
<tr><td rowspan="2">Dry Equatorial</td><td rowspan="2">Semi-Arid/Dry Sub-Humid</td><td>Coastal Thicket</td><td rowspan="2">Coastal Savannah</td><td rowspan="2">Coastal Savannah</td><td rowspan="2">Coastal Savannah</td></tr>
<tr><td>Coastal Savannah</td></tr>
</table>

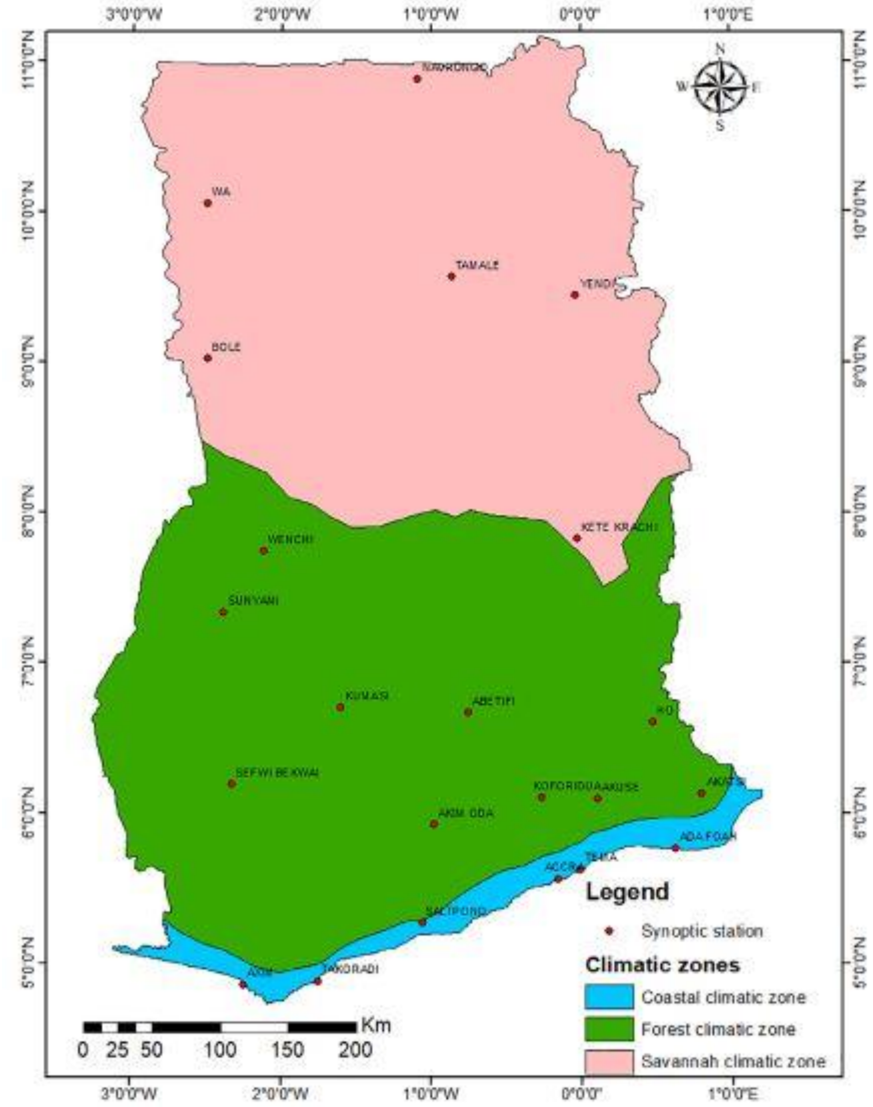

Figure 2.1. Climatic Zoning of Ghana (Bessah *et al.*, 2022)

2.2.2 Climatic Patterns

Based on the climatic zoning by Bessah *et al.* (2022), the Savannah zone spans between latitudes 11°0´0´´ to 7°0´0´´N. The Coastal zone stretches from the coastline to 30 km inland while the Forest zone covers the area between the Coastal and Savannah zones. There is a bimodal rainfall pattern in the Coastal and Forest areas, while uni-modal rainfall exists in the Savannah zone (Klutse *et al*., 2013; MOFA, 2016; Tutu *et al*., 2022). The average annual rainfall for the Savannah ranges between 900mm and 1,200mm, that of the Forest zone between 1,300mm and 1,800mm, while the Coastal zone ranges between 1,100mm and

1,200mm (Yamba *et al.*, 2023). According to Yamba *et al.*, (2023), the length of the single wet season of the Savannah zone varies from four to seven months. The major rainy season spans from March to July, and the minor is from September to October (Klutse *et al*., 2013, Bessah *et al*., 2022) with about 60% of rains occurring in the major season (Bessah *et al.*, 2022). Despite Axim's location in the Coastal zone, it exhibits similar rainfall characteristics as the Forest zone with its peak monthly rainfall being higher than all other Coastal synoptic stations (Bessah *et al*., 2022).

It has been reported by Bessah *et al.* (2022) that the Savannah zone is the driest part of the country, with relative humidity increasing towards the coast. Monthly relative humidity ranges from 20% in January to 70% in August in the zone. The Forest zone records 30% to 80% mean monthly relative humidity, with January experiencing the lowest and June – September experiencing the highest. The Coastal zone records mean monthly relative humidity of 68–80% (Koranteng-Yorke, 2012; Bessah *et al.*, 2022).

In terms of global solar radiation (GSR), Asilevi *et al.* (2019) indicated that the Savannah zone experiences its maximum mean daily insolation (i.e. the incoming solar radiation) during February–May, with Navrongo recording the highest value of 22.57 $MJm^{-2}day^{-1}$, while its lowest daily insolation of 15.80 $MJm^{-2}day^{-1}$ is experienced during June –September at Yendi. The average monthly GSR for the Savannah zone is 20.22 $MJm^{-2}day^{-1}$. The Forest zone is characterised by two maximum insolation patterns, first between February and May with mean daily GSR of 19.5–21.0 $MJm^{-2}day^{-1}$, and then a shorter period between October and November, with average value of 17.7–20.5 $MJm^{-2}day^{-1}$ (Asilevi *et al.*, 2019). The Coastal zone exhibits the same pattern of mean daily GSR as the Forest zone but with the maximum and minimum values being relatively higher. Asilevi *et al.* (2019) estimated maximum insolation values of 20.3–21.8 $MJm^{-2}day^{-1}$ and 18.5–21.3 $MJm^{-2}day^{-1}$ for the period February–May and October–November, respectively, for the Coastal zone, while a lowest insolation of 12.4– 5.4 $MJm^{-2}day^{-}$

^{1} was estimated for the period June–August. Also, Tutu *et al.* (2022) reported maximum duration of sunshine of 7 hours, 8 hours, and 9 hours in the Forest, Coastal, and Savannah zones respectively.

The Savannah zone records its highest mean monthly maximum air temperature between 34 °C in November and 40°C in April, and its lowest of 29°C in August. Mean monthly minimum air temperature is experienced between November and January at 21°C but a highest of 25°C is recorded in April (Bessah *et al.*, 2022). For the Forest zone, the mean monthly maximum air temperature varies from 28°C in August to 34°C in February. Also, mean monthly minimum air temperature varies from 21°C in January to 23°C in April but could be in the broad range of 20°C – 25°C year round (Bessah *et al.*, 2022). The mean monthly maximum air temperature in the Coastal zone reaches extreme values between August (27°C) and March (32°C) and generally less than 30 °C from July – September. Monthly mean minimum air temperature for the Coastal zone is typically 25°C in March (Bessah *et al.*, 2022). Clearly, the varying climatic patterns may be expected to influence asphalt pavement temperature and, hence, pavement performance.

2.3 Applications of Asphalt Pavement Temperature

2.3.1 Pavement Structural Design

The temperature of the asphalt pavement layers influence its performance (Hasan and Tarefder, 2017). Changes in pavement temperature influence pavement distress development. For instance, permanent deformation (rutting) in asphalt pavements, although a load-associated distress, is exacerbated by extremely high temperatures, whereas thermal cracking is induced by low temperatures (Breakah *et al.*, 2011; Hasan and Tarefder, 2017). For this reason, asphalt pavement temperature variation is considered in the M-E pavement design process (Wistuba and Walther, 2013; Koranteng-Yorke *et al.*, 2015). In contrast, empirical pavement design methods hardly require direct consideration of asphalt pavement temperature variation.

The AASHTOWare Pavement M-E design software has an in-built Enhanced Integrated Climatic Model (EICM) for predicting temperature profile in an asphalt pavement (Breakah *et al.*, 2011; Hasan and Tarefder, 2017). The EICM implements the finite difference method, a numerical model, which depends on heat transfer theory. The model provides pavement temperature distribution over time and depth (Houston *et al*., 2006). The input data requirements of the EICM includes wind velocity, percentage of sunshine and ambient temperature (Hasan and Tarefder, 2017). Bryce and Ihnat (2020) have suggested in the current EICM model to curtail an overestimation of pavement temperature, and this requires local climate data.

2.3.2 Pavement Structural Evaluation

Falling weight deflectometer (FWD)-measured deflections are affected by temperature (Chang *et al.*, 2002). Hence, during FWD testing, either a temperature probe is used to measure the temperature of the pavement or mathematical models are used to estimate it. Fernando *et al*. (2001) refer to this temperature as the base temperature, while others (e.g., Chowdhury and Hossain, 1999) refer to it as the effective temperature.

For large projects, challenges in conducting direct pavement temperature measurements at every FWD test location may motivate enumerators to resort to measuring temperatures only at the beginning and end of the FWD testing and, thereafter, interpolate pavement temperatures based on time of deflection measurement (Lukanen *et al*., 2000; Fernando *et al*., 2001). Some researchers (e.g., Chowdhury and Hossain, 1999; Fernando *et al*., 2001) measured AC pavement temperature at three depths (25mm from the surface, mid-depth, and 25mm from the bottom) and suggested the average of these measurements as the effective temperature for the FWD data analysis. The average temperature, thus determined, was similar to the mid-depth temperature (Fernando *et al*., 2001). As a result, some studies have focused on the mid-depth temperature measurement during FWD deflection testing (e.g., Park *et al*., 2001; Gedafa *et al*., 2014).

Back-calculation of AC modulus is performed using software such as WESDEF, ELMOD, MODULUS (Lukanen *et al*., 2000), MICHBACK (Park *et al*., 2001) and CalBack (Tsai and Wu, 2009). Back-calculated AC modulus is corrected to a user-defined reference temperature to account for the effect of temperature (Lukanen *et al*., 2000; Fernando *et al*., 2001; Park *et al*., 2001; Chang *et al*., 2002). The reason for the temperature correction is the sensitivity of the AC modulus to temperature. Studies show that the logarithm of AC modulus has a negative correlation with mid-depth asphalt pavement temperature (Lukanen *et al*., 2000; Park *et al*., 2001). Different procedures are available for temperature correction of deflection data and the back-calculated modulus. Park *et al*. (2001) and Fernando *et al*. (2001) expressed corrected AC modulus as a function of back-calculated AC modulus and a correction factor (Eq. (2.1)):

$$\mathrm{E_{T_r}} = \mathrm{E_T} \times \mathrm{CF} \tag{2.1}$$

where;

$\mathrm{E_{T_r}}$ = AC modulus corrected to a reference temperature, T_r (ºC)

$\mathrm{E_T}$ = Measured AC modulus at temperature, T (ºC)

CF = correction factor

To determine the value of the correction factor, a graph of back-calculated AC modulus against AC layer mid-depth temperature is plotted on a semi-logarithmic scale and a regression model Eq. (2.2) fitted, as proposed by Lukanen *et al*. (2000) and Park *et al*. (2001).

$$\log_{10} \mathrm{E_T} = \mathrm{b} + \mathrm{aT} \tag{2.2}$$

where;

a, b = regression coefficients

T = Mid-depth AC temperature (ºC)

E_T = Measured AC modulus

The correction factor shown in Eq. (2.3) has been suggested by Lukanen *et al*. (2000) and Park *et al*. (2001).

$$CF = 10^{a\,(T_r - T)} \qquad (2.3)$$

where;

a = coefficient determined from Eq. (2.2). Lukanen *et al*. (2000) recommended values of "a" as -0.0195 for the wheel paths and -0.021 for mid-lane.

T_r= reference mid-depth AC temperature (ºC)

T= measured mid-depth AC temperature (ºC)

The foregoing discussion shows the key importance of pavement temperature in the FWD data analysis.

2.3.3 Superpave Binder Grade Selection

Traffic, environmental conditions, and anticipated average vehicle speed are used in the selection of asphalt binder grade under the Superpave system. Environmental conditions are described by the 7-day mean high pavement design and the low pavement design temperatures (Kennedy *et al*., 1994). To obtain these temperatures, historical air temperature data for various weather stations in a given geographical area spanning not less than 20 years are required (Kennedy *et al*., 1994). The actual calculation of the pavement design high and low temperatures from the historic air temperature data requires the use of a mathematical model. Superpave base binder grade is designated as PG XX – YY, where PG refers to performance grade, XX and YY, respectively, represent high pavement design temperature and low pavement design temperature.

The ability of the Superpave performance grades to cater for traffic and environmental conditions at a project site makes them preferable compared to penetration- and viscosity-based grading. The restriction of the penetration and the viscosity grades to temperatures of 25 ºC and 60 ºC, respectively, is addressed by the Superpave PG system, which accounts for a broader temperature range. The PG system links binder properties with field performance (Denneman *et al.*, 2022), an important aspect missing in penetration- and viscosity-based binder grading systems. Superpave binder grade selection has been based on the SHRP models (Huber, 1994; Kennedy *et al*., 1994) and LTPP models (Mohseni, 1998). For instance, Tutu *et al*. (2022) recommended the LTPP models for Superpave binder grade selection in Ghana; Mirza *et al*. (2011) used the SHRP models suitable for Pakistani conditions to determine a PG 70-10 binder grade for Pakistan (Mirza *et al*., 2011). Lee *et al.* (2018) concluded that the SHRP models better specified binder grades for North Korea compared to local models developed from nearby countries of South Korea and Japan. Other researchers, such as Abbas (2017) and Asi (2007), have utilised both the SHRP and LTPP models for base binder grade determination in Iraq and the Kingdom of Jordan, respectively.

The SHRP model for predicting the high pavement design temperature is given by Eq. (2.4) Huber (1994).

$$\mathrm{T_{20mm}} = 0.9545\mathrm{T_{air}} - 0.00590\mathrm{Lat}^2 + 0.21849\mathrm{Lat} + 22.50 \qquad (2.4)$$

where;

$\mathrm{T_{20mm}}$ = High pavement temperature at 20mm depth below the surface (°C)

$\mathrm{T_{air}}$ = Seven-day mean high air temperature (°C)

Lat = Geographical latitude of the project location (degrees)

Similarly, the SHRP model for predicting the low pavement design temperature is given by Eq. (2.5), according to Kennedy *et al*. (1994).

$$T_{pav} = T_{air} + 0.051d - 0.000063d^2 \quad (2.5)$$

where;

T_{pav} = Low pavement design temperature in (°C) at depth, d

T_{air} = Low Air temperature (°C)

d = Depth from pavement surface (mm)

The LTPP models (Mohseni, 1998) for predicting the high and low pavement design temperatures are given by Eqs. (2.6) and (2.7), respectively.

$$T_{pav,h} = 54.32 + 0.78T_{air} - 0.0025Lat^2 - 15.14\log_{10}(d + 25) + z(9 + 0.61{\sigma^2}_{air})^{0.5} \quad (2.6)$$

where;

$T_{pav,h}$ = High pavement design temperature at depth d, below the surface (°C)

T_{air} = Seven-day mean high air temperature (°C)

Lat = Geographical latitude of project location (degrees)

d = Depth below pavement surface (mm)

z = Standard normal deviate corresponding to a selected reliability level

σ_{air} = Standard deviation of average 7-day high air temperature (°C)

$$T_{pav,l} = -1.56 + 0.72T_{air} - 0.004Lat^2 + 6.26\ \log_{10}(d + 25) - z(4.4 + 0.52\sigma_{air}{}^2)^{\frac{1}{2}} \tag{2.7}$$

where;

$T_{pav,l}$ = low pavement design temperature at depth, d (°C)

T_{air} = low air temperature (°C)

d = depth below pavement surface (mm)

z = standard normal deviate corresponding to a selected reliability level

σ_{air} = standard deviation of low air temperature (°C)

Denneman *et al.* (2022) applied the SHRP (Huber, 1994), Beecroft (2019), and Viljoen (2001) models developed in USA, Australia, and South Africa, respectively, to forecast the high and low pavement design temperatures for Australia. The models accurately predicted high pavement design temperatures but the SHRP model was recommended, since it had easily available inputs. Swarna and Hossain (2022) concluded that, in 2070, PG binder grades determined for Canada based on the SHRP, LTPP, and EICM models will require two grade increments in the high-temperature grades (i.e. 12 ºC). However, the SHRP and LTPP models will need four grade increments (-24 ºC) in the low-temperature grades, while EICM prediction will increase by three low-temperature grades.

2.3.4 Asphalt Material Aging Characterisation

Material aging, which is caused by the diffusion of oxygen into asphalt material and subsequent reaction with the binder over time, to cause changes in the chemical composition of the asphalt binder, leads to changes in the physical and rheological properties of the material (Sirin *et al*., 2018; Liang *et al*., 2019). The aging process is accelerated by temperature and oxygen. Oxidative aging occurs in two stages; short-term which occurs during the hot-mix plant production process (Idham *et al.*, 2013; Sirin *et al*., 2018; Liang *et al*., 2019) and long-term which occurs in-service when the asphalt concrete material is exposed to environmental conditions over a long period (Idham *et al*., 2013). This means that the mix production temperature and, the in-service pavement temperature, are key to the asphalt aging phenomenon. Hence, knowledge of the in-service pavement temperature can help to characterise the aging process. Asphalt aging could be either positive or negative. While a stiffer asphalt (due to aging) will have a high modulus and, hence, improved resistance to permanent deformation (Idham *et al*., 2013; Sirin *et al*., 2018), the AC material could become brittle and, thus, prone to cracking and raveling.

The AASHTOWare Pavement M-E Design software has an asphalt concrete material aging prediction model referred to as Global Aging System (Zhang *et al.*, 2019). A fresh model that predicts long-term aging with field-aging temperature as a predictor variable has been proposed by Zhang *et al*. (2019).

2.4 Asphalt Pavement Temperature Prediction Models

Asphalt pavement temperature prediction models may be broadly categorised as empirical, numerical, or analytical, based on their theoretical underpinnings, and method of analysis (Wang *et al*., 2009; Chen *et al*., 2019; Rigabadi *et al*., 2021). The numerical and analytical models, jointly referred to as theoretical models, are based on heat flow theories and are analysed by solving partial differential equations for defined boundary conditions. On the other hand, empirical models use regression methods to establish a relationship between pavement temperature and prediction factors, such as climate, meteorological, geographic, and surface temperature of pavement (Wang *et al*., 2009).

2.4.1 Empirical Models

Empirical models are very common and are mostly preferred because of certain advantages. These models are mostly simple mathematical equations for determining pavement temperature based on known characteristics like the temperature of the pavement surface or pavement depth (Wang *et al*., 2009; Chao and Jinxi, 2018). They are simply statistics-based and are not underlined by any theory. Empirical models are user-friendly and are easy to develop (Diefenderfer *et al*., 2006; Gedafa *et al*., 2014). Notwithstanding, the disadvantage of such models is the fact that they are developed within specific databases and their accuracies are restricted to the confines of the original model formulation database (Wang *et al*., 2009; Alavi *et al*., 2014). According to Chen *et al*. (2019), pavement temperature variation with layer depth and time is non-linear, making it improper to predict using linear regression models. Rather, non-linear regression models and neural network models may be more appropriate for the time-dependent temperature profile of pavements (Cheng *et al*., 2019).

The key findings of empirical models reviewed for this study have been summarised in Table 2.2.

Table 2.2. Summary of Key Findings from Review of Empirical Models

Reference	Method	Country	Predictors	Model Purpose
Ghalandari *et al.* (2023)	Autoencoder network (machine learning)	Belgium	• Air temperature • Solar radiation • Wind speed • Day of year • Relative humidity	• Predict asphalt pavement temperature at different depths
Walia *et al*. (2022)	Non-linear regression	Iran	• Ambient temperature • Time of day • Asphalt layer depth	• Predict asphalt layer pavement temperature
Rigabadi *et al.* (2021)	Artificial neuron network (ANN)	India	• Remote sensing technology	• Predict temperatures at the pavement surface and depths of 200mm and 250mm from the pavement surface.
Tabrizi *et al.* (2021)	Convolutional neural network with long short-term memory (CNN-LSTM)	Canada	• Hourly solar radiation • Hourly air temperature •	• Predict pavement surface temperature
Milad *et al.* (2021)	Bidirectional long short-term memory (Bi-LSTM)	Gaza, Palestine	• Air temperature • Time of day • Depth below the pavement surface	• Predict pavement temperature at a given time and depth
Milad *et al.* (2021)	Hybrid Random Forest Markov chain Monte Carlo (RF-MCMC)	Gaza, Palestine	• Air temperature • Time of day • Depth below the pavement surface	• Predict pavement temperature at a given time and depth
Khan *et al*. (2019)	Linear regression	USA	• Solar radiation • Wind velocity • Relative humidity • Ambient temperature	• Predict temperature of asphalt pavement surface

Table 2.2. Cont'd

Reference	**Method**	**Country**	**Predictors**	**Model Purpose**
Li *et al*. (2018)	Non-linear regression	China	• Average air temperature over cumulative hours • Total solar radiation over cumulative hour historical mean monthly air temperature • Depth from the pavement surface	• Predict asphalt pavement temperature at a specified depth. • Specifically useful for asphalt pavements with asphalt layer thickness above 200 mm.
Chao and Jinxi (2018)	Linear regression	China	• Air temperature • Wind speed • Cloud cover • Relative humidity • Precipitation.	• Predict asphalt pavement temperatures at depths of 50mm, 190mm, and 240mm from the pavement surface.
Xu *et al*. (2017)	Back propagation neural network	China	• Air temperature • Wind speed • Air humidity • Pavement surface temperature • Wind direction • Rainfall • Road condition	• Predict asphalt pavement temperature at depth from the pavement surface.
Asefzadeh *et al*. (2017)	Linear and non-linear regressions	Canada	• Solar radiation • Daily air temperature (average, minimum, or maximum) • Depth below asphalt layer surface	• Predict daily mean pavement temperature for warm and cold seasons • Predict daily minimum, and maximum pavement temperatures.
Chandrappa and Biligri (2016)	Non-linear regression	India	• Mean monthly air temperature • Total solar radiation • Latitude • Month and year	• Predict asphalt pavement surface temperature

Table 2.2. Cont'd

Reference	**Method**	**Country**	**Predictors**	**Model Purpose**
Taamneh (2016)	Linear regression	USA	• Highest and lowest ambient temperature • Solar radiation • Asphalt layer depth • Wind speed	• Predict daily maximum and daily minimum asphalt pavement temperatures
Islam *et al*. (2015)	Linear regression	USA	• Depth from pavement surface • Pavement surface temperature; and/or • Solar radiation	• Predict daily maximum, average, and minimum pavement temperatures.
Marchetti *et al*. (2015)	Linear regression	France	• Pavement surface temperature • Relative humidity • Nebulosity • 24hr period of precipitation • Wind speed • Solar radiation • Time of day and • Traffic situation.	• Predict asphalt pavement surface temperature.
Gedafa *et al*. (2014)	Non-linear regression	USA	• Mid-depth AC layer thickness • Asphalt layer surface temperature • Time of day • Mean air temperature of the preceding day	• Predict mid-depth temperature of perpetual asphalt pavement temperature at a given time
Krsmanc *et al*. (2012)	Linear regression	Slovenia	• Long- and shortwave radiation • Wind speed • Relative humidity • Air temperature • Cloudiness • Precipitation	• Predict surface temperature of asphalt pavement in winter conditions.

Table 2.2. Cont'd

Reference	Method	Country	Predictors	Model Purpose
Diefenderfer *et al*. (2006)	Linear regression	USA	• Ambient temperature • Solar radiation • Asphalt layer depth	• Predict daily maximum and daily minimum asphalt pavement temperatures
Park *et al.* (2001)	Non-linear regression	USA	• Surface temperature • Pavement depth • Time of field pavement measurement.	• Predict daily asphalt pavement temperature at given depths and times.
Viljoen (2001)	Non-linear regression	South Africa	• Ambient temperature • Depth from the pavement surface • Zenith angle • Cloud cover	• Predict pavement surface temperature and pavement temperature at a given depth
Lukanen *et al*. (2000)	Non-linear regression	USA	• Depth from the pavement surface • Pavement surface temperature • Time of day • Mean air temperature of the previous day	• Predict daily asphalt layer pavement temperature

2.4.2 Numerical Models

The procedures involved in using numerical models have been described by Wang *et al*. (2009), as follows. Firstly, a partial differential equation (PDE) describing heat conduction in the pavement must be solved. Second, after defining the boundary conditions at the pavement surface using the energy balance concept, it is necessary to ascertain the relationship between climate data and pavement material properties. Depending on the number of dimensions of the analysis, it may require discretisation of the thickness and/or radial distance into control cells. Numerical models can be applied universally without restrictions. However, it can be difficult to define the boundary conditions and solve the PDE when the initial pavement temperature profile is unknown (Wang *et al*., 2009). Again, the large datasets used as input parameters make their analyses complicated and non-practicable (Gedafa *et al*., 2014; Asefzadeh *et al*., 2017; Rigabadi *et al*., 2021). The accuracy of such models is often impacted by the difficulty of obtaining the pavement property inputs for numerical models (Krsmanc *et al.*, 2012). These pavement properties are either obtained from existing literature or estimated (Chen *et al*., 2019).

The finite element method (FEM), finite difference method (FDM) and finite control volume method (FCVM) are the main categories of numerical models. Chen *et al*. (2019) posit that both the FDM and FCVM have better computational efficiency than the FEM. However, FEM can handle complex geometries such as three dimensions (e.g., Minhoto *et al*., 2005) as well as simpler dimensions (e.g., Teltayev *et al*., 2016). Comparatively, FDM is widely regarded as simple and efficient, hence its frequent use for numerical models (e.g., Han *et al*., 2011; Qin and Hiller, 2011; Nuijten, 2016).

The main heat transfer processes in a pavement structure are conduction, radiation, and convection. Some researchers neglect the heat transfer caused by precipitation and evaporation (e.g., Han *et al*., 2011; Alavi *et al*., 2014). Heat conduction (diffusion) is the only means of heat transfer within the pavement layers. However, the pavement surface and the surrounding environment interact through radiation and convection. The different types of radiation comprise solar radiation (including its reflected fraction by albedo from the surface of pavement), incoming atmospheric longwave radiation, and outgoing longwave radiation from the pavement surface. Heat convection takes place at the pavement surface due to the presence of fluid, such as wind. Figure 2.2 illustrates the heat transfer schematic of a pavement.

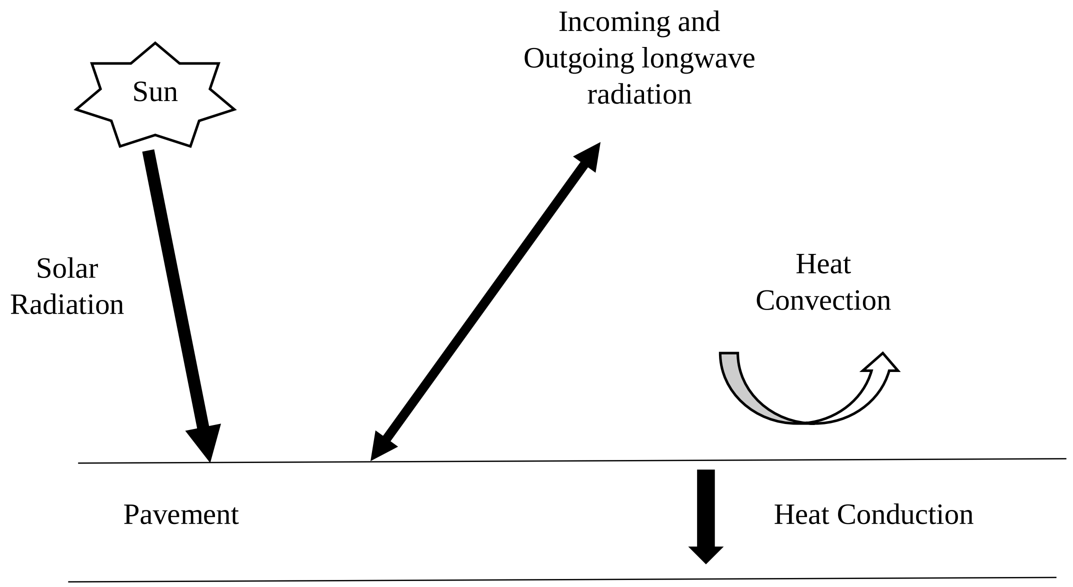

Figure 2.2. Schematic of Heat transfer of pavement and environment (Alavi *et al*., 2014)

Heat transfer equations are in the form of partial differential equations (PDE) and are solved by determining the various boundary conditions (i.e. expressing the various heat fluxes at those boundaries as equations), which are usually complex. From the literature (e.g., Han *et al*., 2011; Alavi *et al*., 2014), the surface boundary condition is usually catered for but the extent of consideration of various heat fluxes may vary. However, the bottom boundary conditions happen to vary based on depth from surface of pavement. Researchers, such as Han *et al.* (2011), set the bottom boundary at a depth of 3m, while others (e.g., Wang and Roesler, 2014) considered temperature as depth approaches infinity.

The expression of the energy balance equation at the various boundary conditions is illustrated below.

A. *Surface Boundary Condition*

The energy balance equation at the pavement surface defines the surface boundary condition heat fluxes, which is given by Eq. (2.8).

$$Q_{solar} + Q_{rad} - Q_{conv} - Q_f = \rho_{suf} \times c_{sur} \times \delta \times \left(\frac{\partial T_{sur}}{\partial t}\right) \tag{2.8}$$

where;

Q_{solar} = heat flux due to solar radiation

Q_{rad} = heat flux from net thermal radiation

Q_{conv} = heat flux from convection

Q_f = conduction from the surface into the pavement

ρ_{suf}, c_{sur} = density and specific heat capacity of the surface material respectively

δ = assumend thickness of the surface material

∂T_{sur} = Differential of pavement surface temperature

∂t = differential of time

Solar Radiation Heat Flux

The Q_{solar} is given by Eq. (2.9).

$$Q_{solar} = (1 - \acute{\alpha})Q_s \tag{2.9}$$

$\acute{\alpha}$ = pavement surface albedo (fraction of the solar radiation that is reflected).

Q_s = incident global solar radiation. This is usually computed from a formula.

Net Radiation Heat Flux

The longwave radiation emitted from the pavement surface, as well as the longwave radiation absorbed by the pavement surface, makes up the net radiation heat flow. This is expressed mathematically in Eq. (2.10).

$$Q_{rad} = Q_{incoming} - Q_{outgoing} = \varepsilon_a \sigma {T_{air}}^4 - \varepsilon_r \sigma {T_{sur}}^4 \tag{2.10}$$

where;

ε_a = Absorption coefficient of the pavement surface

σ = Stefan − Boltzmann constant

ε_r = Emissivity of the pavement surface

T_{air} = Air temperature, K

T_{sur} = Surface temperature, K

$Q_{incoming}$ = Incoming longwave radiation

$Q_{outgoing}$ = Outgoing longwave radiation

Convection Heat Flux

Convection heat flux is computed using Eq. (2.11).

$$Q_{conv} = h_c (T_{sur} - T_{air}) \tag{2.11}$$

where;

h_c = convection coefficient. This is dependent on wind speed

T_{air} = air temperature, K

T_{sur} = surface temperature, K

Conduction Heat Flux

The heat conduction (Q_f) within the top surface and underneath pavement layers is demonstrated by Fourier's law, as shown in Eq. (2.12).

$$Q_f = -k(\partial T/\partial x) \tag{2.12}$$

where;

k = asphaltic material's thermal conductivity

∂T = temperature differential

∂x = differential of the depth of the pavement structure, x

B. *Heat Transfer within the Pavement*

A one-dimensional PDE, also known as the classical thermal diffusion equation (Han *et al.*, 2011), defines the heat conduction within the pavement as shown in Eq. (2.13). The PDE (Eq. 2.13) compares the differential temperature with time to the temperature differential with pavement depth.

$$\partial T/\partial t = \alpha\left(\frac{\partial^2 T}{\partial x^2}\right) \tag{2.13}$$

where;

$$\alpha = \frac{k}{\rho.c} = \text{thermal diffusivity} \tag{2.14}$$

The literature review on numerical models have been summarised in Table 2.3.

Table 2.3. Summary of Key Findings from Review of Numerical Models

Reference	**Method**	**Country**	**Predictors**	**Model Purpose**
Manikkunambi *et al.* (2023)	Finite Element Method	USA	• Air temperature • Layer thickness • Conductivity • Heat capacity • Density • Emissivity • Absorptivity • Solar Radiation • Wind velocity	• Predict the asphalt layer's temperature of flexible pavement
Saliko *et al.* (2023)	Finite Control Volume Method	Sweden	• Air temperature • Solar radiation • Wind speed	• Predict pavement temperature profile at given time and depth
Nuijten (2016)	Finite Difference Method	Norway	• Air temperature • Relative humidity • Wind speed • Precipitation • Shortwave radiation • Cloud cover • Pavement dimension • Density • Specific heat capacity • Thermal conductivity • Air traffic data • Surface condition • Chemicals present on the runway.	• Predict airport runway surface temperature for winter conditions

Table 2.3. Cont'd

Reference	Method	Country	Predictors	Model Purpose
Teltayev *et al.* (2016)	Finite Element Method	Kazakhstan	• Air temperature • Pavement surface temperature • Pavement layers' thermal conductivity • Specific heat capacities • Densities of layer materials • Emissivity • Absorptivity	• Predict temperature profile fluctuations.
Alavi *et al.* (2014)	Finite Control Volume Method	USA	• Air temperature • Wind speed • Solar radiation • Pavement surface albedo; • Surface emissivity • Absorption coefficient • Diffusivity.	• Study the temperature profile of asphalt pavement
Qin and Hiller (2011)	Finite Difference Method	USA	• Air temperature • Wind velocity • Cloud cover • Dew point temperature • Thermal conductivities of pavement layers • Densities of pavement layers • Specific heat capacities of pavement layers • The emissivity of pavement surface • Absorptivity of the pavement surface.	• Predict temperature fluctuation in rigid pavements. • Found it feasible to replace air temperature data with sinusoidal approximation function as model input.

Table 2.3. Cont'd

Reference	Method	Country	Predictors	Model Purpose
Han *et al*. (2011)	Finite Difference Method	USA	• Solar radiation • Wind speed • Air temperature • Pavement surface albedo • Surface emissivity • Absorption coefficient • Diffusivity.	• Predict asphalt pavement temperature and is useful for binder oxidation.
Minhoto *et al.* (2005)	Finite Element Method	Portugal	• Hourly air temperature • Hourly solar radiation • Mean daily wind speed • Pavement surface emissivity • The absorption coefficient of pavement surface • Specific heat capacity of pavement layers • The density of pavement layers	• Predict the temperature at various asphalt pavement depths.
Yavuzturk *et al.* (2005)	Finite Difference Method	USA	• Thermal conductivity • Specific heat capacity • Pavement surface emissivity • Pavement surface absorptivity • Pavement geometry and orientation • Air temperature • Solar radiation • Wind speed • Dew point temperature	• Predict temperature variation in asphalt pavement in vertical and horizontal planes.
Hermansson (2001)	Finite Difference Method	USA	• Solar radiation • Air temperature • Wind speed • Pavement surface temperature • Pavement surface albedo • Emissivity and Absorptivity	• Predict the summertime temperature.

2.4.3 Analytical Models

Analytical models share similar characteristics with numerical models regarding their theoretical underpinnings but are much more complicated to analyse. They offer a better avenue to solving partial differential equations emanating from the definition of boundary conditions in situations where the initial condition (initial pavement temperature) is unknown (Wang *et al.*, 2009). The pioneering work on analytical models is attributed to Barber (1957), who established a model for predicting the maximum asphalt pavement temperature based on climatic and pavement thermal property data. Based on high ambient temperature, high hourly solar radiation, and other pavement parameters, Solaimanian and Kennedy (1993) provided an analytical solution to estimate the high pavement surface temperature, in furtherance of Barber's (1957) work. In recent times, several attempts have been made to improve analytical models. Table 2.4 provides summary findings of some analytical models reviewed in this study.

Table 2.4. Summary of Key Findings from Review of Analytical Models

Reference	Mathematical tools	Country	Predictors	Model Purpose
Ayasrah *et al.* (2023)	Infinite series	Jordan	• Solar radiation & wind speed • Air temperature • Diffusivity	• Predict temperature profile through a pavement structure
Chen *et al*. (2017)	Green's function	China	• Air temperature; solar radiation; • Pavement surface albedo • Emissivity • Thermal conductivity • Specific heat capacity.	• Predict the temperature profile of the asphalt layer of flexible pavement.
Wang (2016)	Eigenfunction expansion	USA	• Pavement surface temperature history thermal diffusivity of surface material • Total time of interest.	• Predict time variation of temperature of asphalt layer of flexible pavement from FWD testing data.
Chen *et al*. (2015)	Green's function	China	• Solar radiation • Air temperature • Cloud cover • Wind speed • Thermal conductivity • Specific heat capacity • Surface temperature • Emissivity • Absorptivity of surface material.	• Predict asphalt pavement's temperature field.
Wang (2015)	Separation of variables/Duhamel's principle	USA	• Pavement surface temperature; • Thermal diffusivity of the asphaltic layer; • Initial pavement temperature at specified depths • Deep soil temperature.	• Predict variation of temperature with time within the asphalt layer of a single-layered flexible pavement.

Table 2.4. Cont'd

Reference	Mathematical tools	Country	Predictors	Model Purpose
Wang and Roesler (2014)	Separation of variables method	USA	• Air temperature • Solar radiation • Layer thicknesses • Material thermal properties	• Predict the time variation of temperature.
Wang (2013)	Odd extension Gaussian quadrature formula	USA	• Pavement surface temperature • Initial pavement temperature profile • Thermal diffusivity of the AC layer.	• Predict the inherent temperature of the asphalt layer of a flexible pavement during FWD testing.
Alawi and Helal (2012)	Finite integral transform	Saudi Arabia	• Air temperature • Solar radiation	• Predict transient pavement temperature for spherical roads with non-linear boundaries.
Wang (2012)	Laplace transformation	USA	• Pavement surface temperature • Layer thicknesses • Thermal conductivities • Diffusivities of layer materials • Average initial pavement temperature along depths.	• Predict the temperature profile of multi-layered asphalt pavement
Wang *et al*. (2009)	Hankel integral transform	USA	• Air temperature • Solar radiation • Wind speed • Emissivity • Absorptivity • Thermal conductivity • Thermal diffusivity of pavement layers.	• Predict the temperature of rigid pavement with unknown initial conditions.

2.4.4 Factors Influencing Asphalt Pavement Temperature

A. Climatic Factors

Attempts to quantify climate variables to determine which of them have the greatest impact on pavement temperature have generated a variety of opinions. Climate parameters, including air temperature, solar radiation, and wind speed, individually exert greater influence on pavement temperature (Minhoto *et al*., 2005; Yavuzturk *et al*., 2005; Alavi *et al*., 2014). However, Chen *et al.* (2019) opined that the debate surrounding the quantification of the impact of climatic factors on pavement temperature has resulted from the non-recognition of the interrelation among the climatic factors. Hence, proper quantification of influential climatic factors of pavement temperature must consider the dependency among them.

The importance of air temperature, solar radiation, and wind speed is seen in the analysis of the heat flux at the pavement surface. Incident solar radiation is required in computing the short-wave radiation on the pavement surface, while computing the net longwave radiation on the pavement surface uses air temperature and pavement surface temperature. Wind speed, on the other hand, is required for computing convection heat flux. In several empirical models, air temperature (e.g., Mohseni, 1998; Taamneh, 2016) and solar radiation (e.g., Taamneh, 2016) have a positive correlation with the daily maximum and daily minimum asphalt pavement temperatures. According to Taamneh (2016), wind speed is negatively correlated with both the daily maximum and daily minimum asphalt pavement temperatures.

Non-climatic influencing factors of pavement temperature, such as latitude (e.g., Mohseni, 1998), depth from pavement surface (e.g., Gedafa *et al*., 2014), month and year of field data collection (e.g., Chandrappa and Biligiri, 2016), are often used in pavement temperature models. In some studies (e.g., Mohseni, 1998; Taamneh, 2016), maximum daily pavement temperature was found to have an inverse relationship with AC layer depth, while minimum daily temperature showed a positive relationship with depth. Mohseni (1998) found the latitude of pavement location to be non-linearly related to both low and high pavement temperatures. However, according to Chandrappa and Biligiri (2016), latitude is positively and inversely related to the maximum and minimum mean monthly pavement surface temperatures, respectively.

B. Internal Factors

I. Pavement surface albedo

Surface albedo, also known as solar reflectivity, is the fraction of the incident solar radiation at the pavement surface that is reflected into the sky. Mathematically, albedo is the ratio of the radiation reflected to the solar radiation incident on the pavement surface. It is a dimensionless value ranging from 0 to 1. An albedo of 0 indicates a perfectly absorbing black surface with non-reflection of the solar radiation, whereas an albedo of 1 indicates a perfectly reflecting white surface, where all radiation is reflected *(*Li *et al*., 2013). Li *et al.* (2013) postulated that the temperature of a pavement surface is affected by the incident solar radiation, depending on its albedo. If the material surface has low albedo such as a black stone, the extent of influence of the solar radiation on the surface temperature is large due to the increased absorbed radiation. In contrast, in a material with high surface albedo (little absorption), there is a low influence of solar radiation on the surface temperature. The effect of albedo on pavement surface temperature is significant in the daytime. Li *et al.* (2013) reported higher surface albedo measured in the morning and late afternoon than during the mid-day. Pomerantz *et al.* (2000) found a correlation between albedo and pavement age. The albedo of asphalt concrete increases with age (Pomerantz *et al*., 2000; Carnielo and Zinzi, 2013; Li *et al*., 2013; Chen *et al*., 2019). In comparison with Portland cement concrete, asphalt concrete has a relatively low albedo (Pomerantz *et al*., 2000; Chen *et al*., 2019). This is because asphalt concrete, being black, absorbs more incident solar radiation. Albedo for cement concrete, in contrast, decreases with age (Chen *et al*., 2019). According to Chen *et al*. (2017), a negative correlation exists between albedo and an asphalt layer's maximum temperature and that pavement surface temperature decreases by 33.3°C for every 0.1 increase in surface albedo. Surface albedo greatly affects daytime maximum pavement temperature more than daytime minimum pavement temperature (Qin *et al.*, 2022).

II. Surface Absorptivity and Emissivity

Surface absorptivity, which is related to incoming longwave radiation at the pavement surface, is the portion of incident radiation that is absorbed into the pavement. Its value ranges from 0 to 1. The sum of the surface absorptivity and albedo equals unity (Chen *et al*., 2019). The solar radiation absorption rate is positively related to pavement temperature (Yinfei *et al*., 2015). In contrast, the difference between the radiation released by a surface at a certain temperature and the same radiation emitted by a black body at the same temperature is known as emissivity. While both absorptivity and emissivity are associated with longwave radiations, their values are different due to differences in wavelengths so their summation may not be equal to unity always (Chen *et al.*, 2019). Chen *et al.* (2019) observed variations in the emissivity of different pavement surfaces. Asphalt concrete surfaces have higher emissivity compared with Portland cement concrete surfaces (Chen *et al*., 2019).

III. Pavement Material's Thermal Properties

The commonly-used thermal parameters of pavement materials in most numerical and analytical models are thermal conductivity, specific heat capacity, and thermal diffusivity (as seen in Tables 2.2 and 2.3). Thermal conductivity is a metric for a material's capacity to conduct heat, according to Cengel (2003). When exposed to solar light, thermal conductivity enables heat to transfer between pavement layers. Thermal conductivity has a similar impact on heat flow at the pavement surface (as shown in Eq. 2.12). Feng *et al*. (2013) concluded that where several asphalt layers exist, it is the top asphalt layer whose thermal conductivity significantly influences the temperature gradient in the pavement. Chen *et al*. (2017) found that, while the maximum surface and minimum bottom temperatures were inversely related to the asphalt mixture's thermal conductivity, the minimum surface and maximum bottom temperatures were actually positively associated.

Specific heat capacity is the energy per unit mass and unit temperature (Chen *et al*., 2019). Specific heat capacity measures the amount of heat stored by a material per unit volume (Cengel, 2003) and has an inverse relationship with the maximum pavement surface temperature, but it is positively related to the minimum surface temperature (Gui *et al*., 2007). A high specific heat capacity indicates high heat storage in a material; this causes massive heat sink into the pavement from the surface during the day and, thus, reduces the maximum pavement surface temperature.

Thermal diffusivity measures the comparison of heat conducted to the heat stored by a material per unit volume (as shown in Eq. 2.14). Gui *et al*. (2007) reported that thermal diffusivity has an inverse and positive relationship, respectively, with the maximum surface and minimum surface temperatures.

2.5 Asphalt Pavement Temperature Prediction Model Evaluation Techniques

Model evaluation compares the level of agreement between model predictions and measured values. Parameters that may be used to judge the level of agreement include; Root Mean Square Error (RMSE), Mean Percentage Error (MPE), Mean Absolute Percentage Error (MAPE) and Mean Bias Error (MBE). In addition, the line of equality (LOE) and the coefficient of determination (R^2) have also been used for judging the prediction accuracies of models (e.g., Park *et al*., 2001; Diefenderfer *et al*., 2006; Khalil and Shaffie, 2013; Gedafa *et al*., 2014; Quansah *et al*., 2014; Taamneh, 2016).

The RMSE, MPE, MBE and R^2 are calculated by Eqs. (2.15), (2.16), (2.17) and (2.18), respectively.

$$RMSE = \sqrt{\frac{1}{n}\sum_{i=1}^{n}(T_{cal} - T_{mea})^2} \quad (2.15)$$

$$MPE = \frac{1}{n}\sum_{i=1}^{n}\left(\frac{T_{mea}-T_{cal}}{T_{mea}} \times 100\right) \quad (2.16)$$

$$MBE = \frac{1}{n}\sum_{i=1}^{n}(T_{cal} - T_{mea}) \quad (2.17)$$

$$R^2 = 1 - \frac{SSR}{TSS} \quad (2.18)$$

where;

T_{mea} = Measured values

T_{cal} = Predicted values

n = Number of observations

SSR = sum of square of residuals

TSS = total sum of squares

The RMSE quantifies the variation of the model-predicted values from observed values, with an RMSE of zero indicating a perfect prediction. MBE determines over-prediction or under-prediction by a model. A positive MBE indicates over-prediction and vice versa. MPE accounts for the level of divergence of predicted values from measured values and is expressed as a percentage. Muzathik *et al*. (2011) suggested an acceptable range of MPE as between -10% and +10%. MAPE is similar to MPE but the deviation of predicted values from measured values is given in absolute terms. The LOE, on the other hand, is a 45-degree line drawn from the origin of a scatter plot of predicted against measured values. A well-fitted model has both predicted and measured values equally displaced on either side of the LOE. The R^2 shows the goodness-of-fit of the model. The value of R^2 indicates the proportion of variance in the outcome variable that can be explained by the predictor variable. Higher values of R^2 indicate a well-fitted model; a perfect fit will have $R^2 = 1$. Hence, low values of MPE, MBE, RMSE, and high value of R^2 indicate a model with high prediction accuracy.

As noted by Khalil and Shaffie (2013) and Muzathik *et al* (2011), although the above error estimates provide a reasonable comparison of models, they do not indicate the level of statistical significance of the model estimates. Hence, a t-test, at a given confidence level, is employed to determine the statistical significance of such estimates. Gedafa *et al*. (2014) employed both the two-sample t-test and paired sample t-test to check for significant differences between predicted mid-depth asphalt pavement temperature at 0% sensitivity level and various independent variables at all other sensitivity levels. They concluded that the time of pavement temperature measurement was the most influential independent variable to predicted mid-depth pavement temperature. The paired sample t-test is used to compare the mean difference between two measures of a variable observed on the same samples (Bluman, 2012). One-way analysis of variance (ANOVA) may also be used (Ibili *et al.*, 2022).

A prerequisite of using the paired sample t-test, the two-sample t-test and ANOVA (all parametric tests) is normality assumption. However, violation of the normality assumption should not pose significant issue for large sample sizes (> 30), indicating that parametric approaches may be utilised although the data are not normally distributed (Ghasemi and Zahediasl, 2012; Bluman, 2012).

2.6 Empirical Models of Routine Industry Application

A thorough search of the literature, revealed six asphalt pavement temperature prediction models which are currently being used by industry, and practitioners. The models are briefly described, below.

a) BELLS 3 (Lukanen *et al*., 2000) Model

The model was developed by Lukanen *et al*. (2000) from the first version of the Baltzer Ertman-Larsen Lukanen Stubstad (BELLS) pavement temperature prediction model, using data collected over two years (1994–1996) from 41 sites, under the Long-Term Pavement Performance (LTPP) study in the U.S. The AC layer thicknesses used for the model ranged from 46 mm to 305 mm. The BELLS 3 model, which is a revised version of the first, corrects for pavement surface shading to enable wider field application (Lukanen *et al*., 2000). The model, which is expressed by Eq. (2.19), predicts asphalt pavement temperature at a given time using the pavement depth, pavement surface temperature, time of day, and mean air temperature of the preceding day.

$$\mathrm{T_d} = 0.95 + 0.892(\mathrm{IR}) + [\log(\mathrm{d}) - 1.25]\left[1.83\sin(\mathrm{hr}_{18} - 15.5) - 0.448(\mathrm{IR}) + 0.621\mathrm{T_{avg}}\right] + 0.042(\mathrm{IR})\sin(\mathrm{hr}_{18} - 13.5) \qquad (2.19)$$

where;

$\mathrm{T_d}$ =pavement temperature at a specified depth, d (ºC)

IR = pavement surface temperature (ºC)

d = Depth from pavement surface (mm)

$\mathrm{T_{avg}}$ = Mean air temperature of the preceding day to the test (ºC)

sin = sine function on an 18-hour clock system (one 18-hour cycle equal to 2π radians)

hr_{18} = time of day in 24-hr (converted to 18-hr asphalt concrete (AC) rise and fall cycle). Calculation of the $\sin(\mathrm{hr}_{18} - 15.5)$ and $\sin(\mathrm{hr}_{18} - 13.5)$ has been detailed in Lukanen *et al.* (2000).

The model's adjusted coefficient of determination (adjusted R^2) was reported to be 0.975, and the standard error (S.E.) was 1.9 ºC (Lukanen *et al.*, 2000). Marshall *et al*. (2001) evaluated the BELLS 3 model for four counties in the state of Tennessee, U.S. and found the predicted mid-depth AC temperature to be reasonably accurate.

b) Diefenderfer *et al*. (2006) Model

Diefenderfer *et al.* (2006) developed models to predict high and low daily temperatures of asphalt pavements using data from the Virginia Smart Road and validated them using data from the LTPP sites (Diefenderfer *et al.,* 2006). The model for daily maximum pavement temperature prediction (see Eq. (2.20)) had an adjusted R^2 of 0.78 and a root mean square error (RMSE) of 5.8 ºC.

$$\mathrm{T_{p,max}} = 2.78752 + 0.686\mathrm{T_{a\ max}} + 5.6736 \times 10^{-4}\mathrm{R_s} - 27.8739\mathrm{P_d} \qquad (2.20)$$

where;

$\mathrm{T_{p,max}}$ = Predicted maximum pavement temperature (ºC)

$\mathrm{T_{a\ max}}$ = Daily maximum air temperature (ºC)

$\mathrm{R_s}$ = Daily solar radiation (kJ/m^{2}day)

$\mathrm{P_d}$ = Asphalt layer depth (m)

c) Taamneh (2016) Model

Using data collected in two years on Interstate 90 in the Ohio state of U.S., Taamneh (2016) built models for predicting daily maximum and daily minimum asphalt pavement temperatures. The daily maximum pavement temperature prediction model is presented in Eq. (2.21) and had an adjusted R^2 of 0.83 and RMSE of 5.1 ºC.

$$\mathrm{T_{P-max}} = 9.720 + 0.947\mathrm{T_{A-max}} - 24.179\mathrm{D} - 1.231\mathrm{WS} + (4.01 \times 10^{-4}\mathrm{RS}) \qquad (2.21)$$

where;

T_{P-max}= Predicted maximum pavement temperature (ºC)

T_{A-max} =Daily maximum air temperature (ºC)

WS = Daily wind speed (m/s)

D = Desired depth below the pavement surface (m)

RS = Daily Solar Radiation (kJ/m^{2}day)

The Taamneh (2016) model is useful for Superpave PG binder selection.

d) Gedafa *et al*. (2014) Model

This model uses inputs of pavement surface temperature, the day-time (in decimal hours), the average air temperature of previous day and mid-depth AC layer thickness to predict mid-depth asphalt pavement temperature. This model was developed and validated using data from six pavement sections in the U.S. state of Kansas. The Gedafa *et al*. (2014) model is presented in Eq. (2.22) and was reported to have an adjusted R^2 of 0.94.

$$T_{pave} = -5.374 - 0.752T_{sur} + 0.022T^2{}_{sur} + 2.016T_{avg} - \left(0.032T_{sur} \times T_{avg}\right) + 1.549t_d - 0.022D \qquad (2.22)$$

where;

T_{pave}= mid-depth AC pavement temperature (ºC)

T_{sur} = Pavement surface temperature (ºC)

T_{avg} = Mean air temperature of the preceding day (ºC)

t_d = Time of day (decimal hours)

D = AC Mid-depth thickness (mm)

e) Park *et al*. (2001) Model

The model developed by Park *et al*. (2001), based on asphalt pavement surface temperature, depth below the pavement surface, and time of surface temperature measurement, predicts AC pavement temperature that is depth- and time-dependent. The model was developed using data from three test roads in the U.S. State of Michigan. The model does not directly depend on climate information. The adjusted R^2 of the validated model exceeds 0.9. The Park *et al*. (2001) model is expressed by Eq. (2.23).

$$T_z = T_{surf} + \{(-0.3451z - 0.0432z^2 + 0.00196z^3) * \sin(-6.3252t + 5.0967)\} \quad (2.23)$$

where;

T_z = AC pavement temperature at depth, z (ºC)

z = Depth where pavement temperature is required (cm)

t = Time when AC surface temperature was measured (days). [0<t<1 (e.g., 2:15pm = 14.25/24 =0.59375 days].

The Park *et al*. (2001) model was calibrated by Asefzadeh *et al*. (2017) for Edmonton, Canada, using data from the Integrated Road Research Facility (IRRF) and found the prediction accuracy to be good.

f) Asefzadeh *et al*. (2017) Models

The daily maximum pavement temperature prediction model developed by Asefzadeh *et al*., (2017), based on two years of data collected from an instrumented road test section in Edmonton, Canada, is given by Eq. (2.24). The model was based on asphalt concrete layer depths ranging from 9 mm to 250 mm.

$$T_{max} = 2.0237 + 0.8709(T_{air-max}) + (7.6 \times 10^{-4} SR) - 16.1886D, \; R^2 = 0.91 \quad (2.24)$$

where;

T_{max} = Daily maximum pavement temperature (ºC)

$T_{air-max}$ = Daily maximum ambient temperature (ºC)

SR = Daily solar radiation (kJ/m^2day)

D = Depth from pavement surface (m)

2.7 Interview Methodology

2.6.1 Interview Data Collection

Interviews are conducted either through telephone, in-person, or by focus groups. These interviews usually involve limited, unstructured, and usually open-ended questions that are meant to elicit the participants' views and opinions (Cresswell and Cresswell, 2018). Roulston and Choi (2018) describe three interview types: structured, semi-structured, and unstructured interviews. In a structured interview, candidates are asked a sequence of predetermined questions with a constrained number of response options. Thus, organizing and measuring the results is usually simple. Because the interviewer reads from a script and tries to stay as close to it as possible, structured interviews are rigorous (Qu and Dumay, 2011).

Gubrium and Holstein (2002) note that unstructured interviews take place in an informal atmosphere that gives both interviewers and interviewees flexibility in how the interview questions responses are framed. The interviewer would, therefore, be eager to track fascinating events and to have the interviewee clarify numerous themes in this instance. Roulston and Choi (2018) note that, in unstructured interviews, topics are determined by the interviewee, and because there may not have been a pre-formatted interview guide, the dialogue is more likely to resemble a casual chat.

In a semi-structured interview, however, questions are guided by defined themes and may be interspersed with probes to elicit in-depth responses. To steer the conversation toward issues the interviewers want to learn more about, the interview guide will incorporate a number of major themes (Qu and Dumay, 2011).

Interview has its disadvantages. Roulston *et al*. (2003) argue that unexpected participant behavior, handling the effects of the interviewer's actions and subjectivities, developing and delivering questions, and handling delicate subjects are some challenges interviewers may encounter. In-depth interviews may also produce unreliable data because of their flexibility. They also need interviewers who are quite skilled. Respondents' subjectivity makes it possible for them to "say" whatever the interviewer wants to hear, which calls into question the reliability and validity of the interview findings.

Alshenqeeti (2014) argues that using several data-collecting instruments would aid in getting detailed information and confirming the research findings. Researchers should consider improving their interviewing skills and choose the approach that best answers their research questions, keeping in mind that the more precise the researchers are with their questioning, the more accurate the data will be (Alshenqeeti, 2014).

2.6.2 Interview Data Analysis

Thematic analysis is a technique for analysing data that aids in finding themes and patterns of meaning concerning a certain research question or questions (SAGE, 2019). It is widely used for analysing interview data. To meaningfully respond to the study's research questions, the researcher can use this data analysis technique to find significant patterns and relationships. This approach entails seven processes, according to Braun and Clarke (2013) and Cresswell and Cresswell (2018): data organisation and preparation, reading and familiarization, data coding, finding themes, examining themes, naming and characterizing themes, and conclusion development.

a) Data organisation and preparation

This involves the transcription of recorded interview data and typing of notes from the interview and arranging them in a meaningful order to make analysis easier. Any extra source of information obtained during the interview data is considered at this stage.

b) Reading and Familiarisation of Data

This automatically begins from the first step which gives a broad understanding of the data and a chance to consider its overall significance. By carefully reading and re-reading the interview data, the researcher can ask himself certain questions. For instance, what are participants saying generally? What kind of tone do the thoughts have? What impression do you have of the information's overall depth, reliability, and application? The researcher must, therefore, carefully examine the material while keeping the theoretical lenses in the back of their mind to see how these are reflected in the data (SAGE, 2019).

c) Coding of Data

Coding is the process of locating all pertinent data within the full dataset to respond to the research questions (SAGE, 2019). It entails gathering text or image data acquired during data collection, dividing it into paragraphs, and then identifying those categories with a phrase, frequently based on the participant's actual language (Cresswell and Cresswell, 2018). Coding can be done either manually or through the use of software such as Nvivo and MAXDA.

d) Identifying Patterns (Codes to Themes)

Once the full dataset has been coded, it is time to search for patterns that may be present in the data. The frequency with which a given code appears is crucial in determining which patterns are most pertinent to addressing a specific research subject. Even so, there will be some codes that are less common but nonetheless important for addressing the study subject. Therefore, when analyzing patterns in the data, it is also necessary to consider the frequency of each code, as well as how crucial it is to answering the study issue (SAGE, 2019).

e) Finding, Examining and Concluding Themes

The next stage is to find the major data patterns that can be used to address the research topic. By looking at the patterns in the data, themes and sub-themes can be found (SAGE, 2019). A theme captures a key aspect of the data with respect to the study question and illustrates the degree to which the data collection contains patterned responses or meaning (SAGE, 2019). These themes are the ones that typically appear as major findings in qualitative research and are used as headings in the findings section of the report. They should provide a variety of perspectives from diverse people and be supported by several quotes and specific examples (Cresswell and Cresswell, 2018). Braun and Clarke (2013) advise updating the identified themes as necessary. Secondly, because qualitative research tells a story about the data in a way that responds to the research questions, themes need not encompass all of the data (SAGE, 2019).

2.8 Regression Model Development

The most common forms of regression employed in building models for asphalt pavement temperature prediction are multiple regression (e.g., Krsmanc *et al*., 2012; Asefzadeh *et al*., 2017; Khan *et al*., 2019), principal component analysis (PCA) (e.g., Marchetti *et al.*, 2014; Marchetti *et al*., 2015) and partial least square (PLS) regression (e.g., Marchetti *et al.*, 2015; Chao and Jinxi, 2018).

PCA makes use of the statistical tool variance-covariance matrix. Also, PCA employs linear transformation of a correlated matrix to produce uncorrelated transformed variables with orthogonal eigenvectors (Marchetti *et al.*, 2014). PCA is used to describe links between variables (columns) in a multivariate table. Chao and Jinxi (2018) noted that PLS regression, as a modelling approach, is very powerful compared with ordinary multivariate regression, as the former allows for multiple response and predictor variables. It also allows for the simplification of models by reducing multi-dimensional data to two-dimensional data (Marchetti *et al.*, 2015; Chao and Jinxi, 2018). PCA is mostly used in conjunction with PLS but they are much more complicated to implement compared with multiple regression.

Multiple regression describes a relationship between a set of independent variables and a dependent variable. Multiple regression could be either linear or non-linear. Bluman (2012), describes the following assumptions of multiple linear regression:

i. A linear relationship must exist between the dependent variable and each of the independent variables (linearity assumption). A scatter plot of the dependent variable versus independent variables is used to check the type of relationship. In case of non-linear relationship, a non-linear transformation of the independent variable is done (e.g., Mohseni, 1998) to achieve linearity. Some non-linear transformations are logarithmic transformation, square root transformation, inverse transformation, or multiplicative function of one variable with another variable (interaction terms).
ii. There should be no strong correlation between the independent variables (non-multicollinearity assumption). A Pearson correlation coefficient matrix or the variance inflation factor is used to check if any of the independent variables strongly correlates with each other.
iii. The regression residuals must follow a normal distribution (normality assumption). This is examined using a histogram with a normal curve. If the curve is bell-shaped, then the normality assumption is satisfied.

iv. Residuals must have equal variances (equal variance assumption). This is examined using a scatter plot of regression standardised residual against standardised predicted values. If the data points are evenly clustered at the centre and do not form a triangle, then there is equal variance.

Multiple linear regression is carried out using any statistical software (e.g., R, Minitab, SPSS, Microsoft Excel) to determine the model's good-of-fit parameters (e.g., R-square, F-statistic) and coefficients of the independent variables and the intercept. This process can be done by the standard regression or stepwise regression approaches.

In standard multiple regression, all the independent variables are entered at once into the regression equation to determine the unique contribution of each independent variable to the dependent variable. For instance, Taamneh (2016) and Diefenderfer *et al*. (2006) used this approach. However, with stepwise regression, the list of independent variables is added or removed one at a time, based on a statistical criterion. The criteria could be the variable's contribution to the coefficient of determination (R^2) and the level of significance. When a stepwise regression adds independent variables one at a time, it is known as a forward stepwise regression. A backward stepwise regression removes predictor variables which make no significant statistical contribution to the model, one at a time. Asefzadeh *et al*. (2017) and Krsmanc *et al*. (2012) utilised backward stepwise regression in their model development.

Having fitted an adequate model fulfilling the multiple linear regression assumptions, the model is validated with different datasets (as done by Taamneh, 2016 and Asefzadeh *et al*., 2017). Some researchers use 80% of the datasets for the calibration (fitting) of the model and the remaining 20% for the validation (e.g., Lukanen *et al*., 2000). The error statistics, LOE, R^2 and statistical significance test, as explained earlier, are employed to finalise the model validation process (e.g., Walia *et al*., 2022).

2.9 Global Solar Radiation Computation

The incident global solar radiation on a horizontal surface has two components: diffuse radiation and direct radiation. It is measured with a pyranometer. The high cost of the device makes it unavailable at various meteorological stations. As such, models are used to compute the global solar radiation. Several factors—ranging from meteorological factors such as sunshine duration and air temperature and geographic factors, including the location latitude and day of the year—have been used to compute the global solar radiation. Some models used to compute global solar radiation are discussed below:

2.9.1 Angstrom-Prescott Equation

The Angstrom-Prescott equation (Quansah *et al.*, 2014) for predicting monthly mean global solar radiation is given by Eq. (2.25).

$$G_m = R_{ext}\left\{A + B\left(\frac{k}{N}\right)\right\} \tag{2.25}$$

where;

$G_m =$ Predicted mean monthly global solar radiation (MJ/m^{2}day)

R_{ext} = Monthly mean of extra-terrestrial solar radiation (MJ/m^{2}day). R_{ext} depends on the location latitude (φ), solar declination angle (δ), eccentricity factor (E_0), solar constant (I_{sc}), and hour angle (ω).

k = Monthly mean daily sunshine hours

N = Maximum monthly mean daily sunshine duration = day length

A, B = location-specific empirical coefficients, from measured solar radiation data. Quansah *et al*. (2014) found A=0.22 and B=0.43 for Kumasi, while Asilevi *et al*. (2019) estimated A=0.25 and B=0.5 for Ghana.

Solar declination angle (δ) indicates how the axis of the sun through the north-south direction is tilted such that different portions of the earth's surface receive varying amounts of the sun's radiation as the earth revolves around the sun (Diefenderfer *et al*., 2006). Eccentricity factor (E_0), however, is the average Earth-Sun distance, while the sun hour angle (ω) indicates the angle between the observer's meridian (the line of longitude passing through the observer's location) and the meridian that contains the Sun (Diefenderfer *et al*., 2006).

The Angstrom-Prescott model estimates the monthly mean solar radiation rather than daily solar radiation.

2.9.2 Weather Condition-Based Models

a) Ho and Romero's (2009) Model

Ho and Romero (2009) provided a model given by Eq. (2.26) for computing the daily incident solar radiation.

$$G_d = I_{ext} \cos\theta_z \left\{\frac{2}{3}\exp\left[\frac{-T_R}{0.9+9.4\theta_z}\right] + \frac{1}{3}\right\} \tag{2.26}$$

where;

G_d = daily incident solar radiation (kWh/m^{2}day)

I_{ext} = intensity of extra-terrestrial radiation, which is a product of the solar constant and the eccentricity factor

T_R = turbidity factor for flat land which is 1.8 for sunny conditions and in January, 5 for partly cloudy and 10 for most cloudy conditions.

θ_z = zenith angle, the angle between the sun's rays and a 90 degree line to the horizontal plane. Zenith angle is a function of $\varphi, \omega\ and\ \delta$.

b) Huang et al.'s (2017) Model

This model gives no information on how the angles, as well as indirect and direct solar radiations are calculated. Huang *et al.* (2017) provided the model given by Eq. (2.27).

$$G_d = [I_d \sin\theta + I_i(1 + \cos\gamma)/2] \tag{2.27}$$

where;

G_d = Total solar radiation (W/m^2)

I_d = Direct solar radiation (W/m^2)

I_i = Indirect solar radiation (W/m^2)

θ = Incident angle (degrees)

γ = Inclination angle (degrees)

On a cloudy day, I_d =0 and I_i = 10%-100% (Huang *et al*., 2017).

2.9.3 Peak Solar Radiation-Based Models

a) *Li et al.'s (2014) Model*

A model for computing the daily solar radiation, as suggested by Li *et al*. (2014), is by Eq. (2.28) as a function of time (*t*).

$$G_d = H_o \cos m\omega(t - t_{so}) \; for \; t_{so} - 0.5c \leq t \leq t_{so} + 0.5c \tag{2.28}$$

where;

G_d = Daily solar radiation (kJ/m^{2}day)

H_o = Noontime peak solar radiation (h) = 0.131mQ

m = Solar radiation's coefficient of distribution = 12/c

c = Effective sunshine hours in a day (h)

Q = Volume of overall solar radiation in a day (J)

t_{so} = Peak position =13

ω = Angular frequency (radians per second)

The calculation of the daily solar radiation is iterative and requires the application of Fourier series. The total daily solar radiation is only provided but how to obtain it is not covered by the model.

b) Qin et al.'s (2016) Model

This approach to computing solar radiation is complicated and may be associated with uncertainty in obtaining the daily sunrise and sunset times from respective meteorological agencies.

Equation (2.29) illustrates Qin *et al*.'s (2016) model for computing incident solar radiation.

$$G_d = H_o \cos(\omega t - \emptyset_s) \;\; for \; t_{sr} < t < t_{ss} \qquad (2.29)$$

where;

G_d = Incident solar irradiation (W/m^2)

H_o = peak solar irradiation at noon (W/m^2)

ω = sunshine hour angle (degrees)

$\emptyset_s$ = phase of the incident solar irradiation = π at noon.

t_{sr}= sunrise time

t_{ss} =sunset time

2.9.4 Other Model Types

a) Diefenderfer et al.'s (2006) Model

Equation (2.30) gives the Diefenderfer *et al*. (2006) solar radiation prediction model. It is mainly from the latitude of the meteorological station where solar radiation is required and the day of the year.

$$G_d = \left(\frac{24}{\pi}\right) \times I_{sc} \times E_0 \times \sin(\varphi) \sin(\delta) \times \left\{\frac{\omega_s \times \pi}{180} - \tan(\omega_s)\right\} \tag{2.30}$$

G_d = solar radiation recorded daily on a horizontal surface (kJ/m^{2}day)

I_{sc} = solar constant =4,871 kJ/m^2 h

φ = location latitude (degrees)

δ = solar declination angle (degrees)

ω_s = sunrise hour angle (degrees)

E_0 = eccentricity factor

The eccentricity factor, E_o, is computed using Eq. (2.31) as follows;

$$E_0 = 1.000110 + 0.034221 \cos T + 0.001280 \sin T + 0.000719 \cos 2T + 0.000077 \sin 2T \tag{2.31}$$

where;

T = day angle (radians). T is computed with Eq. (2.32)

$$T = 2\pi(d_n - 1)/365 \tag{2.32}$$

d_n = day number of the year (e.g., d_n = 33 for February 2, and so on).

Equations (2.33) and (2.34) are used to respectively calculate the values of δ and ω_s;

$$\delta = (0.006918 - 0.399912 \cos T + 0.070257 \sin T - 0.006758 \cos 2T + 0.000907 \sin 2T - 0.002697 \cos 3T + 0.00148 \sin 3T) \times \frac{180}{\pi} \tag{2.33}$$

$\omega_s = cos^{-1}(-\tan\varphi\tan\delta)$ (2.34)

This approach to calculating the daily solar radiation is relatively straightforward with only two inputs – latitude and day of the year, which are easily obtainable from any meteorological station.

b) Nuijten's (2016) Model

Nuijten's (2016) equation for the incoming solar radiation is given by Eq. (2.35).

$G_{in} = R_{sky} \cdot a^m(1 - 0.0065C^2)$ (2.35)

where;

G_{in} = incoming solar radiation (Wm^{-2})

R_{sky} = clear sky radiation and is a function of the solar constant and solar altitude (Wm^{-2})

a^m = factor for insulation by the atmosphere

C = cloud cover (in tenths)

No further detail is given on how the values of R_{sky} and a^m may be computed, Hence, adopting this approach for calculating the daily solar radiation could prove challenging.

c) Minhoto et al.'s (2005) Model

Equation (2.36) expresses Minhoto *et al*.'s (2005) approach to calculating the incident solar radiation.

$G_d = LS_cE_0\theta_z$ (2.36)

where;

G_d = total incident solar radiation (W/m^2)

L = loss factor accounting scattering and absorption of shortwave radiation by the atmosphere

S_c = solar constant =1,353 W/m^2

E_0 = eccentricity factor of the earth's orbit

θ_z = zenith angle

As there is no elaboration on how the loss factor (L) is obtained, implementing this model could be challenging.

2.10 Summary of Key Literature Review Findings

Based on the literature review, the following key findings are summarised:

i. Despite the different climatic zoning proposals, the climatic zoning by Bessah *et al*. (2022) that incorporates data from all 22 GMet synoptic stations over four decades appear to be realistic and simple to adopt for this study. Three climatic zones—the Savannah, Forest, and Coastal zones—were defined by Bessah *et al*. in 2022.

ii. The impacts of pavement temperature on material properties have been factored in the M-E pavement design concepts for a more robust pavement analysis and design.

iii. Asphalt pavement temperature prediction models can be categorised into empirical, numerical or analytical models.

iv. Empirical models are easy to develop and user-friendly but their accuracy is generally limited to the scope of the original data used in developing them.

v. Numerical and analytical models might have a wider application due to their consideration of physical processes, however, they are not user friendly.

vi. Asphalt pavement temperature prediction may employ climatic variables (e.g., air temperature, solar radiation, wind speed, etc.) and material factors (e.g., surface albedo, emissivity and absorptivity, specific heat capacity and conductivity). The material factors are usually selected from literature and may sometimes be characterised by approximation errors.

vii. Techniques employed in the evaluation of empirical models include error statistics, good-of-fit parameters and line of equality plots. Also, t-tests may be used to check the statistical significance of the model predictions.

v. The literature review identified the following empirical asphalt pavement temperature prediction modes, namely, ELLS 3, Diefenderfer *et al*. (2006), Taamneh (2016), Gedafa *et al*. (2014), Park *et al*. (2001) and Asefzadeh *et al*. (2017), having practical relevance and being straightforward to use.

viii. A well-fitted multiple linear regression model must satisfy the linearity, non-multicollinearity, normality and equal variance assumptions. A different dataset is used to validate the fitted and the t-test is used to check the statistical significance. The error statistics, the line of equality and R^2 are also verified as part of the validation.

ix. The incident global solar radiation on a horizontal surface is either measured with a pyranometer or estimated using models. Several factors, ranging from meteorological factors such as sunshine duration and air temperature to geographic factors, including latitude and day of the year, have been used to compute global solar radiation.

x. Interviews provide an in-depth understanding of a subject matter. They help explore emerging subjects that could escape the interviewer in designing the questions. Thematic analysis is a common approach for analysing interview data.

CHAPTER 3: METHODOLOGY

3.1 Study Areas

The study focussed on the Forest and Savannah zones of Ghana (Bessah *et al.,* 2022) for the following reasons. First, the Savannah and Forest zones constitute the largest area by land area and the share of the country's road network. Secondly, most of the climatic factors are severest in the Savannah and the Forest zones. For instance, while both the Forest and Coastal have bimodal rainfall patterns, the Savannah zone has only one rainfall pattern. Again, average sunshine duration is highest in the Savannah zone (9 hours) and lowest in the Forest zone (7 hours) (Tutu *et al*., 2022). Also, while the Savannah zone has the highest mean monthly maximum air temperature, the Forest zone records the lowest mean monthly minimum air temperature.

The study was conducted on selected roads in the cities of Kumasi (Ashanti Region) and Tamale (Northern Region) of Ghana. The choice of Kumasi and Tamale in the Forest and Savannah climatic zones, respectively, was influenced by their approximate central locations in their respective climatic zones. Two roads were selected in each city—one for collecting data for calibration of new model and evaluation of existing models, and the other for validation of new model. The selection process for the study roads are described below:

i. QGIS was used to geo-reference the two GMet synoptic weather stations located in Kumasi and Tamale.
ii. Open street maps served as raster data (image maps) to locate the coordinates of the weather stations with the help of a control point to align the raster data.
iii. A 3-km buffer was created around the GMet synoptic weather stations. The roads enclosed by the buffers were noted for further inquiries from the respective owners (KNUST Development Office and DUR).

iv. Pavement construction and maintenance information was obtained from the road owners.

v. Only asphalt roads that had been rehabilitated or reconstructed within the previous two years (2020 - 2022) were considered.

vi. Where several roads met the criteria above, only those with a flatter terrain were considered for safety reason.

vii. Two asphalt-surfaced roads in Kumasi—the Mango Road and the Antoa Road and two similar roads in Tamale—the RSM Road and Air Force Road, were selected for the study.

There are two GMet synoptic stations in Kumasi, located at 6°42´36´´N and 1°36´0´´W at the Kumasi Airport area and at 6°41´0´´N and 1°33´0´´W on the Kwame Nkrumah University of Science and Technology (KNUST) Campus. Kumasi has a Forest climate, with a bimodal rainfall pattern, moderate temperature, and humidity. Mean monthly rainfall in Kumasi peaks in June. The mean monthly maximum relative humidity of 70% occurs between June and September while the lowest value occurs around January. The highest mean monthly maximum air temperature of 34 °C is recorded in February while the lowest mean monthly minimum air temperature of 21 °C occurs in January (Bessah *et al.*, 2022).

The Mango Road, classified by the DUR as a collector road, was the data collection site for the calibration of new models and evaluation of existing selected models. The road was overlaid with asphalt (wearing course) in 2021, with layer thickness varying from 75 to 100 mm. The road has two lanes with a total width of 8.6 m, abutted by concrete U-drains on either side. The section of the Mango Road where the temperature data were collected has a flat terrain, with no vegetation cover and is about 0.8 m from the GMet station.

The Antoa Road is classified by DUR as a major arterial. The data collected on it were used for validation of new models. The Antoa Road links the Airport Roundabout to Kenyasi via Buokrom and is dualized at some sections. It was rehabilitated in 2020 up to the binder course. The binder course has a thickness of 70 mm. The dualized section, where the data were collected, has flat terrain and is approximately 1.0 km from the GMet station located at the Kumasi Airport. The road width for each carriageway is 7.5 m, with concrete U-drains on either side of the carriageway. Figure 3.1 shows the Mango and Antoa Roads.

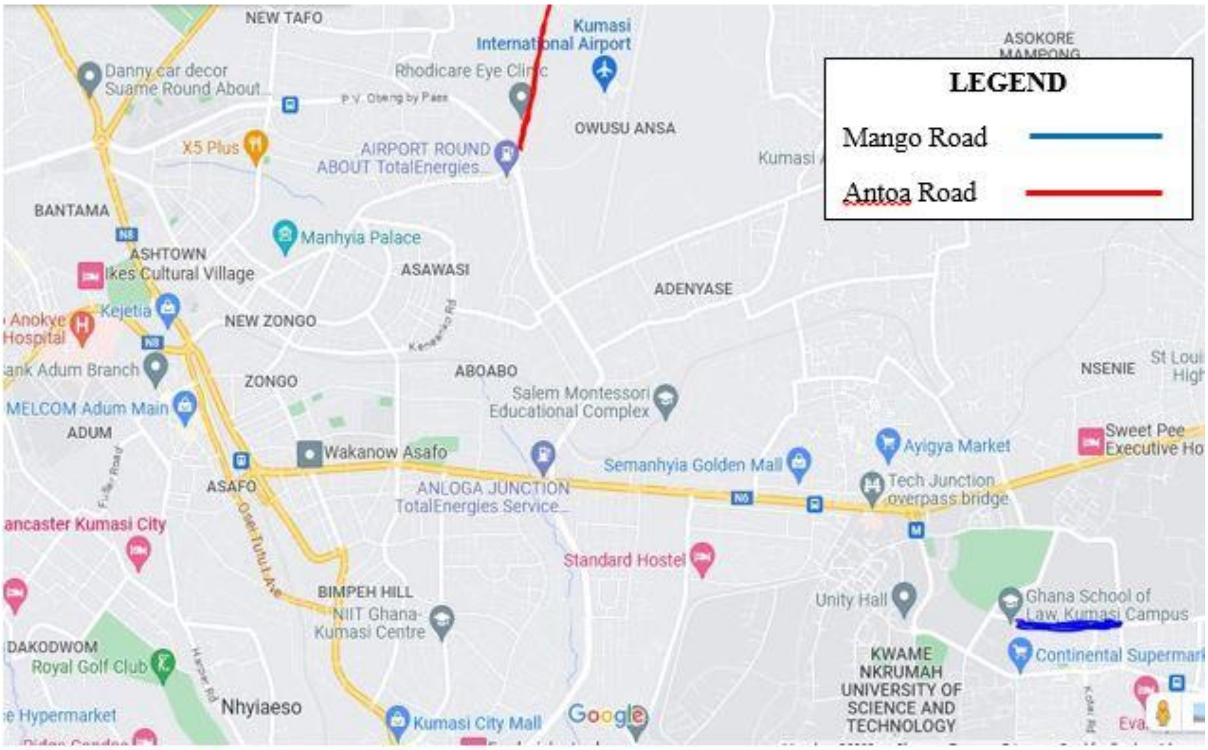

Figure 3.1. Google Map Showing the Mango Road and Antoa Road in Kumasi

Tamale's GMet synoptic station is located on latitude 9°34´48´´N and longitude 0°51´36´´W and it is 169 m above sea level (Bessah *et al*., 2022). Tamale has a Savannah climate with one rainfall season. The mean monthly rainfall peaks in September at 200 mm but reaches a lowest of nearly zero in January. During the rainy season in August, Tamale records its highest mean monthly humidity of 70% compared to at most 20% in January. The mean monthly maximum air temperature is highest between November and March whiles the mean monthly minimum air temperature reaches its lowest in December or January (Bessah *et al*., 2022).

The two study roads in Tamale (RSM Road and the Air Force Road) are both located within the Bawah Barracks, near the Tamale Airport. The RSM Road was used for the collection of data for the calibration of new models and evaluation of existing asphalt temperature prediction models, while data for the validation of the new models were collected on the Air Force Road. Both roads are classified as local roads by DUR. The widths of the RSM and Air Fore Roads are, respectively, 6.7 m and 5.8 m. The roads have flat terrain and are without any side drains. The RSM and Air Force Roads are approximately 1.99 km and 2.49 km, respectively, from the GMet synoptic station located at the Tamale Airport. Both roads received asphalt overlay in 2021 on the wearing course by the Department of Urban Roads. The roads have asphalt layer thickness of 70 mm. It is worth mentioning that the sections of the roads where the data were collected were not shaded by any vegetation. A map of Tamale showing the study roads is shown in Figure 3.2.

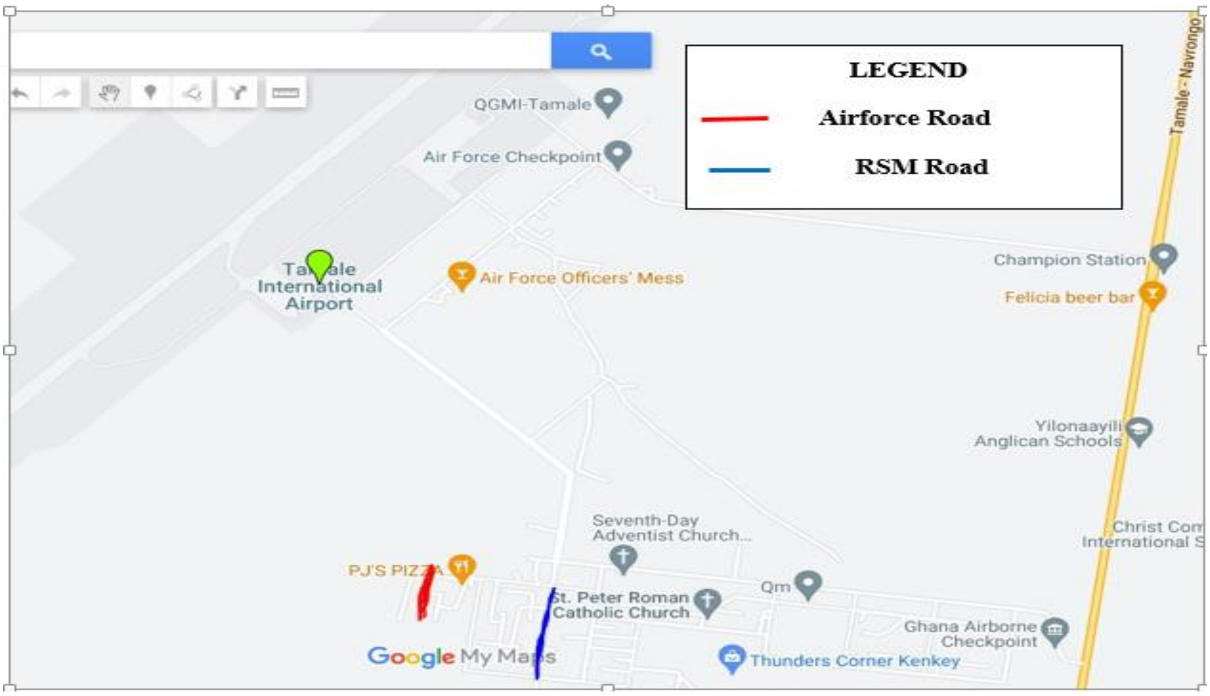

Figure 3.2. Google Map Showing the RSM Road and Air Force Road in Tamale

3.2 Research Design

The first objective of this study, was to establish the state of practice of asphalt pavement temperature determination in Ghana. This was achieved through the use of interview. The choice of a qualitative approach allowed the respondents to freely share their views without restriction. With a small sample size anticipated for the study, a qualitative approach provided in-depth information from the participants. The nature of the study design afforded the researcher opportunity to ask probing or follow-up questions, which other approaches would not have provided.

A longitudinal survey design, which involved the collection of data repeatedly over a certain period and allowed for hypothesis testing and correlation analysis, was employed for Objectives 2 & 3. Objective 2 sought to evaluate the prediction accuracy of some foreign asphalt pavement temperature prediction models for Ghana while Objective 3 developed new models for predicting asphalt pavement temperature in Ghana.

3.3 Interview Procedure

The population of interest was all public sector civil engineers, consulting engineers, and road construction contractor staff who have experience in pavement structural evaluation using FWD, asphalt mixture design and Superpave PG binder grade selection. Purposive sampling was initially used to identify engineers from organisations who fell in the above criterion for interview. Three organisations—CSIR-Building and Road Research Institute, Ablin Consult, and Memphis Metropolitan Limited—were initially sampled. A snowball sampling approach was then used to locate interviewees. The snowball sampling method is a non-probability sampling method that allows study participants to recommend the next qualified prospective participant. Two road agencies—the Ghana Highway Authority (GHA) and the Department of Urban Roads (DUR)—were identified during the sampling process as the main agencies that conduct FWD testing on their road network. However, only personnel from their Head Office in Accra and the Ashanti Regional Office (Kumasi) had experience in FWD testing.

The field instrument for the interview data collection was designed as semi-structured, open-ended questions. A sample of the interview guide is provided in Appendix A. The necessary ethical clearance was obtained from the Committee on Human Research Publication and Ethics (CHRPE) at KNUST. A copy of the Ethical Clearance Letter is provided in Appendix B.

Seven interviews were conducted, involving four respondents from the road agencies (GHA and DUR), one pavement engineering consultant, and two road contractor staff. The distribution of the respondents is shown in Table 3.1.

Table 3.1. Interview Respondents

Organisation	**City**		**Total**
	Accra	**Kumasi**	
Road Agencies (GHA and DUR)	3	1	4
Pavement Engineering Consultants	-	1	1
Road Contractors	2	-	2
Total Respondents	**5**	**2**	**7**

3.4 Climate Data Collection

Climate data were sourced from the GMet offices in Kumasi and Tamale. The data comprised daily minimum air temperature, daily maximum air temperature, daily relative humidity, daily wind speed, and daily sunshine duration over the period from 1st May, 2022 to 30th April, 2023. For each location and day, the minimum air temperatures were checked to ensure they were not higher than the maximum air temperatures. Daily solar radiation was computed by using the solar radiation formula by Diefenderfer *et al*. (2006), presented in Eq. (2.30). The latitudes of the GMet stations at KNUST (on Mango Road) and Tamale Airports, are respectively 6.68 and 9.58 decimal degrees.

$$G_d = \left(\frac{24}{\pi}\right) \times I_{sc} \times E_0 \times \sin(\varphi)\sin(\delta) \times \left\{\frac{\omega_s \times \pi}{180} - \tan(\omega_s)\right\} \qquad (2.30)$$

G_d = solar radiation received everyday on a horizontal surface (kJ/m^{2}day)

I_{sc} = solar constant =4,871 kJ/m^2 h

φ = location latitude (degrees)

δ = solar declination angle (degrees)

ω_s = sunrise hour angle (degrees)

E_0 = eccentricity factor and is calculated using Eq. (2.31)

$$E_0 = 1.000110 + 0.034221 \cos T + 0.001280 \sin T + 0.000719 \cos 2T + 0.000077 \sin 2T \quad (2.31)$$

where;

T = day angle (radians). T is computed with Eq. (2.32)

$$T = 2\pi(d_n - 1)/365 \quad (2.32)$$

d_n = day number (e.g., d_n = 25 for January 25, 40 for February 9 and so on).

Equation (2.33) and (2.34) are used to respectively calculate the δ and ω_s

$$\delta = (0.006918 - 0.399912 \cos T + 0.070257 \sin T - 0.006758 \cos 2T + 0.000907 \sin 2T - 0.002697 \cos 3T + 0.00148 \sin 3T) \times \frac{180}{\pi} \quad (2.33)$$

$$\omega_s = cos^{-1}(- \tan \varphi \tan \delta) \quad (2.34)$$

3.5 Asphalt Pavement Temperature Data Measurement

3.5.1 Thermometer Calibration Verification

An infrared thermometer (Figure 3.3) was used for the measurement of pavement surface temperatures, while a digital asphalt thermometer (Figure 3.4 a, b), connected by a temperature sensor probe (Figure 3.4 c), was used for AC layer mid-depth temperature data measurement. The infrared thermometers and the temperature probes were manufactured by Electronic Temperature Instruments Limited (ETI) under the brand name RayTemp 38, while the digital thermometers have the brand name “Impact Test Equipment Limited”, with a model number LH44T.

Figure 3.3. RayTemp 38 Infrared Thermometer Used for Pavement Surface Temperature Measurement

The digital thermometer (LH44T) measures temperatures ranging from -50°C to +1370°C, with a resolution of 1°C, while the RayTemp 38 infrared thermometers has resolution of 0.1°C and measurement range of -59.99°C to +999.99°C.

(a) Back View

(b) Front View

(c)

Figure 3.4. Digital Thermometer (a and b) and Probe (c) Used for In-depth Pavement Temperature Measurement

Both digital and infrared thermometers came with certificates of calibration from the UK manufacturers. However, the digital thermometers were calibrated against a reference digital thermometer before their use. The process involved simultaneously immersing the new and reference digital thermometers in boiling water, and recording temperatures at specified time intervals. The average readings on the new and reference thermometers were computed, as shown in Table 3.2. The average temperature difference between the new and reference thermometers was very small (1 ºC), showing the thermometers presented similar temperature reading.

Table 3.2. Calibration Reading of Digital Thermometers

Time interval (mins)	**New Thermometer Reading (ºC)**				**Reference Thermometer Reading (ºC)**
	EDT001	**EDT002**	**EDT003**	**EDT004**	
0	100	100	100	100	99
2	100	100	100	100	99
4	100	100	100	100	99
6	100	100	100	100	99
8	100	100	100	100	99
Average	100	100	100	100	**99**

Similarly, all four new and reference digital thermometers were installed at one of the study sites, Mango Road, on 29th April, 2022, to measure the pavement temperature trend at a depth of 38 mm from the pavement surface at 30-minute intervals for 6 hours (6:00 GMT to 12:00 GMT). The results shown in Figure 3.5 indicate that the new and reference digital thermometers recorded similar temperature data.

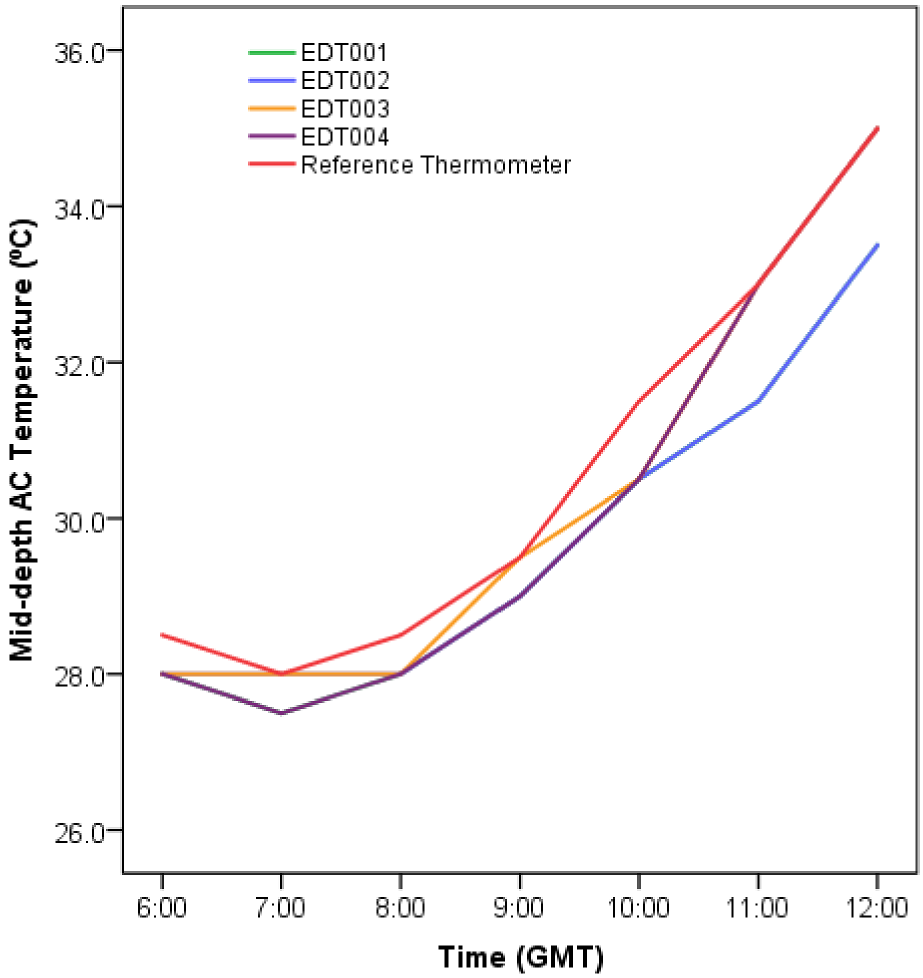

Figure 3.5. Thermometer readings on Mango Road (Kumasi)

An ANOVA test was performed on the digital thermometer readings and the results are shown in Table 3.3. The results indicated that all the means of measured asphalt pavement temperatures were statistically equal (P = 0.97) at a 5% significance level. It was concluded that the new digital thermometers measured asphalt pavement temperatures similar to the reference thermometer.

Table 3.3. ANOVA Results for Digital Thermometers Calibration

Source	**DF**	**SS**	**MS**	**F**	**P-value**
Factor	4	3.54	0.89	0.14	0.97
Residual	30	194.86	6.50		
Total	34	198.40			

A reference infrared thermometer was used for road surface temperature measurement on Mango Road on 1st May, 2022, simultaneously with the new infrared thermometer. The temperature data were recorded at 30-minute intervals for four hours from 10:00 GMT to 14:00 GMT. The results, shown in Figure 3.6**,** indicated the pavement surface temperatures recorded by the new infrared thermometers (IR1 – IR4) and the reference infrared thermometer were similar.

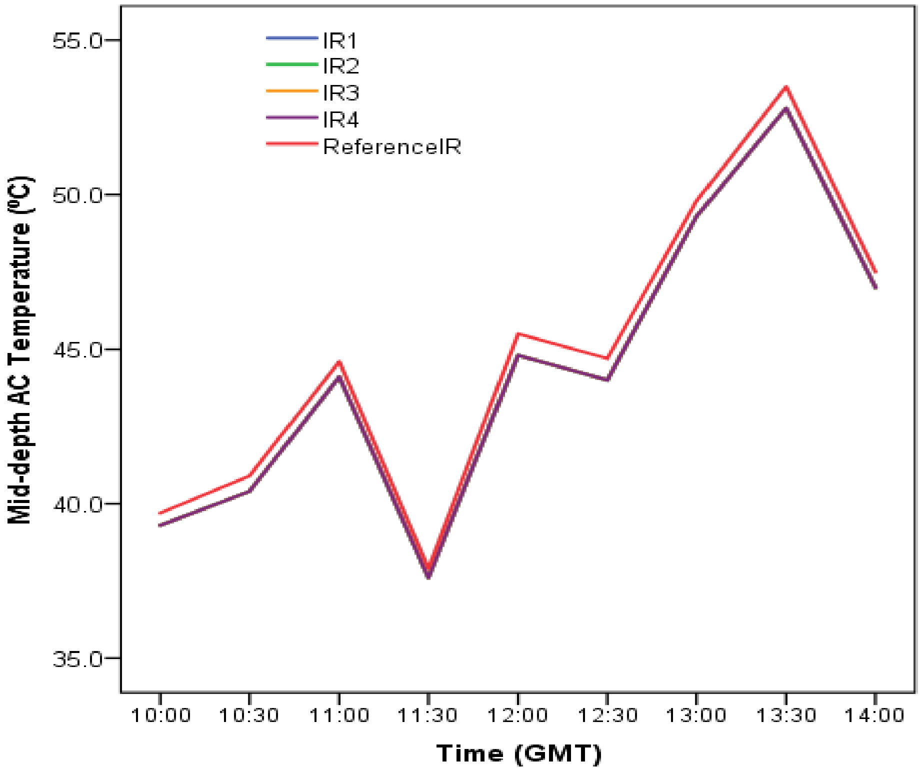

Figure 3.6. Comparison of Infrared Thermometers Readings on Mango Road (Kumasi)

There was a need to predict the daily duration of actual pavement temperature measurement by knowing when the maximum and minimum hourly pavement temperatures occurred. This informed temperature data measurement at 38 mm from the pavement surface for 24 hours (6:00 GMT to 6:00 GMT) on Mango Road, with one of the verified digital thermometers. This was plotted to determine the hourly trend in pavement temperature, as shown in Figure 3.7.

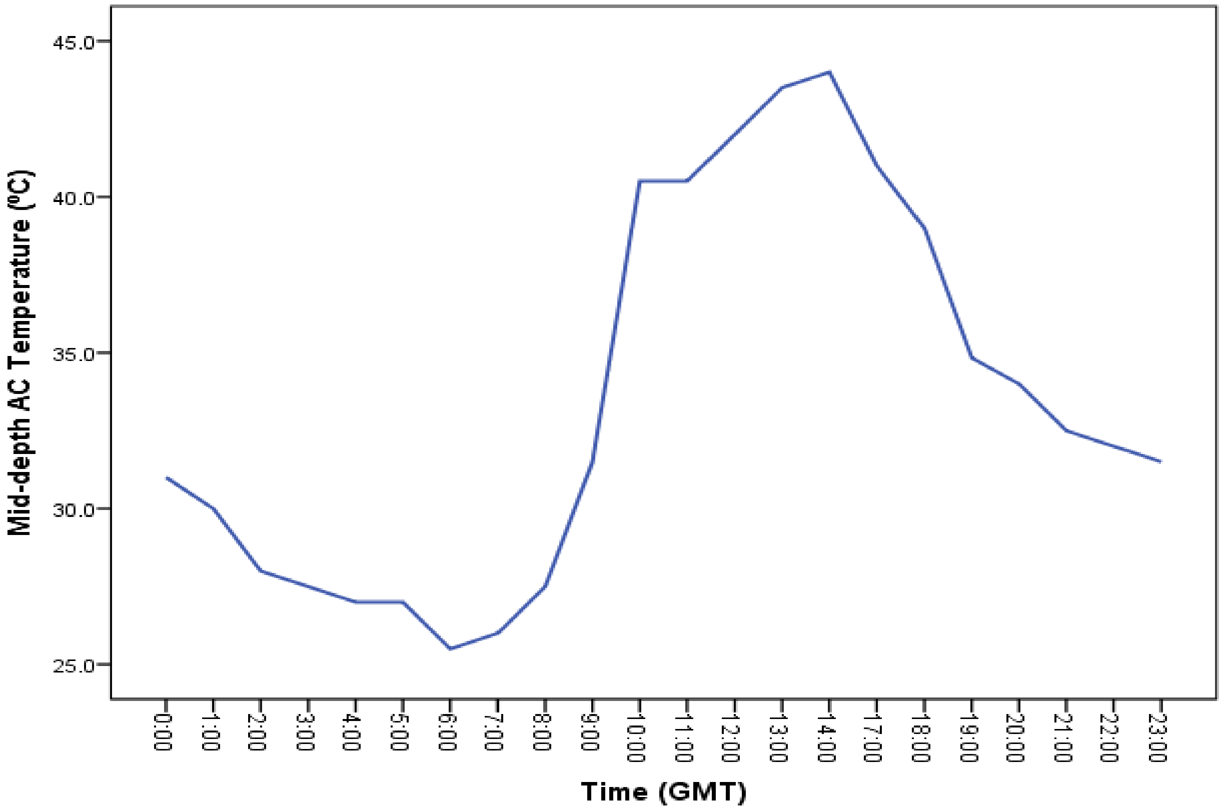

Figure 3.7. Hourly Pavement Temperature Variation on Mango Road (Kumasi)

From Figure 3.7**,** the minimum and maximum pavement temperature occurred at 6:00GMT and 14:00GMT, respectively. Based on this exercise, the in-situ pavement temperature data collection was designed to last for 12 hours from 6:00GMT to 18:00GMT at all data collection sites, as critical pavement temperatures (lowest and highest) occurred during the day.

3.5.2 Pavement Temperature Measurement

A. Pavement Temperature Data Collection Schedules

The calibration data collection was scheduled as follows:

i. A stratified random sampling was used

ii. A calendar year was divided into 12 strata (calendar months).

iii. Each stratum (calendar month) was further divided into sampling units of four (4) weeks.

iv. A simple random sampling was used to select the specific week number in a month for data collection. This was done by using a random number generator (www.random.org). The calibration data collection dates are shown in Table 3.4.

Table 3.4. Model Calibration Data Collection Dates

Month	**May 2022**	**June 2022**	**July 2022**	**Aug 2022**	**Sept 2022**	**Oct 2022**	**Nov 2022**	**Dec 2022**	**Jan 2023**	**Feb 2023**	**Mar 2023**	**Apr 2023**
Week No.	4	4	1	2	1	4	4	3	3	1	2	2
Date	23rd – 29th	22nd – 28th	4th – 10th	8th – 14th	1st – 7th	24th – 30th	22nd – 28th	15th – 21st	16th – 22nd	1st – 7th	8th – 14th	12th – 18th

Similarly, a stratified random sampling was used to design a data collection schedule for the model validation data. The process is described below:

i. The calendar year was divided into two strata – dry season and rainy seasons. The months of November, December, January, February, and March constituted the dry season, while the April, May, June, July, August, September, and October formed the rainy season.

ii. A simple random sampling was used to select two months in the dry season – November and February, as well as two months in the rainy season namely, July and April.

iii. The sampling unit of interest for each selected month was the week's number. Thus, each selected month was divided into four weeks.

iv. Purposive sampling was used to select the specific week numbers in each selected month without coinciding with the selected week numbers for the model calibration dates. The model validation data collection dates, shown in Table 3.5, were selected based on the selected week numbers.

Table 3.5. Model Validation Data Collection Dates

Month	**July 2022**	**Nov 2022**	**Feb 2023**	**Apr 2023**
Week No.	2	2	4	1
Date	11th – 17th	8th – 14th	22nd – 28th	5th – 11th

B. Pavement Temperature Data Measurement Procedure

The as-built asphalt layer thicknesses of the selected roads were confirmed on site by drilling. The data collection spots were free from tree shade and buildings to ensure accurate pavement temperature measurement. Pavement temperatures were measured at mid-depth of the AC layer using the digital thermometers. The temperatures were measured at asphalt layer depths of 38 mm in Kumasi and 35 mm in Tamale from the pavement surface using the Impact model LH445 digital thermometers. Pavement surface temperatures were measured using the ETI RayTemp38 infrared thermometers concurrently with the mid-depth measurements at half-hourly intervals for 12 hours (6:00GMT to 18:00GMT) for seven consecutive days per month.

The steps followed to obtain temperature measurements, at each study location, are outlined below:

- An 8-mm diameter hole was drilled near the pavement edge to half the depth of the AC layer and cleared of debris using a vacuum blower.
- The hole was filled with glycerine up to about 12 mm from the base of the hole to prevent heat transfer loss by radiation.
- The digital thermometer was inserted in the hole to measure the AC temperature half-hourly intervals for 12 hours on each testing day.
- The infrared thermometer was used to measure the pavement surface temperature concurrently with the mid-depth temperature measurements.

- The time for both temperature measurements was recorded in a 24-hour clock system.

The installed digital thermometer was left in place until the last reading was taken at 18:00GMT on each day. For the next data collection day, a new hole was drilled and the process described above repeated. The data collection setup on the Mango Road and Air Force Road are shown in Figures 3.8 and 3.9, respectively.

Figure 3.8. Pavement data collection set-up on Mango Road (Kumasi)

Figure 3.9. Pavement data collection setup on Air Force Road (Tamale)

The pavement temperature data was checked for any inconsistency and missing data. Any missing data in the daily mid-depth AC and surface temperatures for each location were interpolated based on the data available. The pattern of hourly mid-depth AC temperature for each location and day was compared with the established pattern from the pilot study for conformity.

3.6 Data Analysis Procedures

3.6.1 Interview Data Analysis

The interview data were analysed using thematic analysis (Braun and Clarke, 2013; SAGE, 2019). The interview responses (text and recordings) were transcribed and analysed manually. The data were coded and identified patterns were used to create themes to interpret the interviewee responses.

3.6.2 Evaluation of Existing Asphalt Pavement Temperature Prediction Models

Based on the Literature Review, the following asphalt pavement temperature prediction models—the BELLS 3, Park *et al*. (2001), Diefenderfer *et al*. (2006), Gedafa *et al*. (2014), Taamneh (2016) and Asefzadeh *et al*. (2017)—were selected for evaluation. The model calibration data from May 2022 to December 2022 for each zone were used for the evaluation of the selected asphalt pavement temperature prediction models. In the evaluation of the selected models, values of the predictor variables were entered into each model to predict asphalt pavement temperature and then compared with the field-measured temperature. Line of Equality (LOE) was used to assess whether the predicted pavement temperatures were balanced with the measured temperatures. The two-sample t-test was used to compare the means of the predicted temperatures with the means of the measured temperatures at 5% significance level. Though the normality test is a prerequisite for use of parametric tests such as the two- sample t-test, the large number of data points used in this study (56 to 1400) justified the assumption that the sampling distribution was normal (Ghasemi and Zahediasl, 2012). The coefficient of determination (R^2) was the goodness-of-fit parameter used for the model evaluation. Error analysis parameters—including the Root Mean Square Error (RMSE), Mean Percentage Error (MPE), and Mean Bias Error (MBE)—were computed for each model's predictions. The R-Studio statistical software was used for the statistical significance testing, while the SPSS Statistics (Version 23) was used for the scatter plot development.

3.6.3 Development New Asphalt Pavement Temperature Prediction Model

a) Model Calibration

Multiple regression was used to calibrate the models for predicting AC mid-depth pavement temperatures for Kumasi (Forest zone) and Tamale (Savannah zone). The mid-depth AC temperature has been found to be representative of the effective temperature of an AC layer

(Fernando *et al*., 2001) and, has been used to develop models by some researchers (e.g., Park *et al*., 2001; Gedafa *et al*., 2014).

The SPSS Statistics (Version 23) was used in fitting the models by checking that the proposed models fulfil the assumptions of multiple linear regression—linearity, non-multicollinearity, normality and equal variance of residuals. Mid-depth AC layer temperature was the response variable (dependent variable) with a number of potential predictor variables (independent variables), namely, pavement surface temperature, mean air temperature of preceding day and time of day. In checking the non-multi-collinearity assumption, a Pearson correlation matrix was performed for the response and predictor variables, in addition to, some interaction terms and non-linear transformation (e.g., sine of time). The threshold for identifying multi-collinearity between two potential predictor variables is a Pearson correlation coefficient of 0.7 minimum (Shrestha, 2020). The variance inflation factor was also used to investigate the non-multi-collinearity assumption. Secondly, a scatter plot of the mid-depth AC layer temperature versus each predictor variable was done to visualise the type of relationship between the variables. Only predictor variables linearly related with the response variable (mid-depth AC layer temperature) were considered in fitting the model. Both models eventually had the sine the time, mean ambient temperature of previous day and temperature of pavement surface as predictor variables.

Scatter plots of model residuals were drawn to check conformity with the equal variance assumption. Finally, histogram with a normal curve was used to check if the fitted model followed the normal distribution.

b) Model Validation

In validating the models, the fitted models were used to predict mid-depth AC layer temperature using the model validation data for each zone. The model-predicted temperatures were compared against measured temperatures, and the error statistics (RMSE and MPE) and R^2 determined. Scatter plots of the predicted and measured pavement temperatures for each zone were prepared and LOE drawn to determine the accuracy of the models. A well-fitted model has the AC temperature data points balanced around the LOE. Also, to check for the statistical significance of the model predictions, a two-sample t-test was used to compare the mean of the predicted and measured pavement temperatures at 5% significance level. The two-sample t-tests were performed with the R-Studio software.

CHAPTER 4: RESULTS AND DISCUSSION

4.1 Interview Responses

Based on the interview responses from industry practitioners to examine the state of practice of asphalt pavement temperature determination in Ghana and to justify the relevance of the study, two themes were generated and explained as follows.

4.1.1 Pavement Temperature Measurement Practices

Interviewees indicated that all FWD testing is conducted by the Ghana Highway Authority (GHA). Personnel of the GHA measure asphalt pavement temperature directly with digital thermometers in the course of the test. The process involves drilling holes into the pavement to about half-depth of the asphalt layer thickness, using a chisel and a hammer. A viscous liquid, such as glycerin, is used to partially fill the drilled hole to about 10mm from the base of the hole and allowed to cool. A digital thermometer is then inserted in this glycerin environment to measure the pavement temperature. FWD testing is typically conducted at one kilometer intervals and, at each FWD test location, pavement temperature is measured as described above. During FWD testing, ambient air temperature and the pavement surface temperature are recorded by using infrared (IR) sensors installed on the FWD equipment.

Interview respondents indicated that the current manual method of determining pavement temperature during FWD testing was laborious, non-productive, and time-consuming. Other respondents held the view that, the process was not economical and temperature data was restricted to a particular spots making it very slow.

4.1.2 Superpave Binder Grade Selection Practices

Superpave binder grade selection is gradually gaining acceptance in Ghana. Previous applications of the Superpave binder in Ghana included rehabilitation of the Bunso Junction to Apedwa Junction section of the National Road 6 (N6), sections of the N1, and the Osei Tutu II

Boulevard in Kumasi. In all these projects, the Superpave binder selection was undertaken by the road contractor executing the project.

It was noted that the non-existence of temperatures below 0ºC in Ghana gave room for guessing of the minimum pavement temperatures in the Superpave PG binder selection process. It was revealed that there was no clear procedure for the determination of the maximum pavement design temperatures. Interviewees also opined that Superpave PG binder selection in Ghana did not follow the full guidelines, and the final PG binder grades may not be justified. For instance, PG 70-10 was used for the N1, while PG 84-16 was used for the Bunso Junction – Apedwa Junction section of the N6, without adequate justification for use of such binders.

4.1.3 Discussion on Interview Responses

The direct measurement of asphalt pavement temperatures during FWD testing in Ghana conformed to research practices elsewhere (e.g., Chen *et al.*, 2000; Lukanen *et al*., 2000; Chang *et al.*, 2002) even though the emergence of asphalt pavement temperature prediction models have come to facilitate the process in some countries. It has been considered that the mid-depth AC temperatures measured during FWD testing is comparable to the average AC temperature measured at three depths (Fernando *et al*., 2001). Also, the AC modulus has a correlation with the mid-depth AC temperature (Park *et al*., 2001). For this reason, researchers, including Park *et al*. (2001), and Gedafa *et al*. (2014) focus on the mid-depth AC temperature during FWD testing, which gives credence to the practice of measuring mid-depth AC temperature during FWD testing in Ghana.

The interview responses indicated that manual asphalt pavement temperature measurement had some challenges, such as undue delays, uneconomical and labour-intensiveness, particularly on large projects. These challenges would be overcome if locally developed asphalt pavement temperature prediction models are employed.

The interview responses showed that Superpave PG binder selection does not follow any documented guideline. While Tutu *et al*.'s (2022) recommended PG 70-10 and PG 64-10 as base binder grades for the Northern Savannah zone and for the rest of the country was based on the LTPP models, it is important to develop local models for a more routine binder grade selection.

Finally, some road agency respondents indicated their resolve to have some of trunk roads instrumented with thermocouples so that pavement engineering applications requiring temperature would be enhanced. However, this appears to be a long-term vision and would have financial implications depending on the number of trunk roads in consideration. Even with such intervention, the problem of temperature data restriction to specific pavements cannot be eradicated as only the instrumented pavements would have temperature data readily available. Some interviewees expressed willingness to use locally-developed asphalt pavement temperature prediction models provided such models were practical and accurate. This interview response reinforced the need to develop asphalt pavement temperature prediction models for the climatic conditions of Ghana to facilitate pavement engineering in the country.

4.2 Evaluation of Existing Asphalt Pavement Temperature Prediction Models

The interview responses necessitated evaluation of the prediction accuracy of some popular asphalt pavement temperature prediction models to examine their potential adoption in Ghana. The following sections of the report explain the criteria used for the evaluation of the selected asphalt pavement temperature prediction models and the results.

4.2.1 Assessment by Statistical Significance

The statistical significance testing was performed using the two-sample t-test to compare whether the means of the predicted and measured asphalt pavement temperatures were equal at a 5% significance level. If the means were equal, it implied that the model predictions were satisfactory. While the two-sample t-test, and all other parametric tests thrive on normally distributed samples, Ghasemi and Zahediasl (2012) and Bluman (2012) noted that sample sizes larger than 30 can be assumed to be normally distributed and the test ignored. The sample size used ranged from 112 to 2800, hence a normal distribution was assumed to prevail. The data collection period of 8 months (8 weeks or 56 days) measured 1400 pavement temperatures. The BELLS 3, Gedafa *et al*. (2014) and Park *et al*. (2001) models utilised 2800 pavement temperature data each (1400 measured and 1400 predicted) during the t-test. In contrast, the Diefenderfer *et al*. (2006), Taamneh (2016) and Asefzadeh *et al*. (2017) models which predict daily maximum pavement temperature utilised 112 pavement temperature data (56 each for measured and predicted) for the t-test.   The hypothesis tests were set as follows:

Null hypothesis (H_0): The means of the measured and predicted pavement temperature are equal

Alternate hypothesis (H_A): The means of the measured and predicted pavement temperature are different

Results of the two-sample t-test are shown in Table 4.1.

Table 4.1. Two-sample t-test results: predicted vs measured pavement temperatures

Location	**Model**	**df**	**t**	**P-value**
Kumasi	BELLS3 (Lukanen *et al*., 2000)	2780.9	-8.704	<0.0001
	Park *et al*. (2001)	2676.1	1.602	0.1092
	Gedafa *et al*. (2014)	2761	8.965	<0.0001
	Diefenderfer *et al*. (2006)	59.6	-1.635	0.1074
	Taamneh (2016)	67.1	8.596	<0.0001
	Asefzadeh *et al*. (2017)	62.6	17.326	<0.0001
Tamale	BELLS3 (Lukanen *et al*., 2000)	2766.9	-9.762	<0.0001
	Park *et al*. (2001)	2660.9	0.014	0.989
	Gedafa *et al*. (2014)	2655.9	7.4895	<0.0001
	Diefenderfer *et al*. (2006)	63.9	-3.799	0.0003
	Taamneh (2016)	83.3	9.359	<0.0001
	Asefzadeh *et al*. (2017)	67.668	19.775	<0.0001

Based on Table 4.1, the following inferences are made:

a) In Kumasi, the means of asphalt pavement temperatures predicted by the BELLS3 (Lukanen *et al*., 2000), Gedafa *et al*. (2014), Taamneh (2016) and Asefzadeh *et al*. (2017) models are significantly different from the means of the measured asphalt pavement temperatures at a 5% significance level ($p < 0.0001$). This suggests that the asphalt pavement temperatures predicted by the models for Kumasi are not satisfactory.
b) Again, in Kumasi, the means of asphalt pavement temperatures predicted by the Park *et al*. (2001) and the Diefenderfer *et al*. (2006) models were statistically equal to the means of the measured asphalt pavement temperatures at a 5% significance level ($p > 0.05$). This indicates that asphalt pavement temperatures predicted by the Park *et al*. (2001) and Diefenderfer *et al*. (2006) models were comparable with the measured asphalt pavement temperatures.
c) In Tamale, the means of asphalt pavement temperatures predicted by the BELLS3 (Lukanen *et al*., 2000), Gedafa *et al*. (2014), Diefenderfer *et al*. (2006), Taamneh (2016) and Asefzadeh *et al*. (2017) models were significantly different from the means of the measured asphalt pavement temperatures at a 5% significance level ($p < 0.001$). This finding implies that asphalt pavement temperature predicted by these models were not comparable with the measured asphalt pavement temperatures; hence, these models were unsuitable for local application.
d) Also, in Tamale, the mean of asphalt pavement temperatures predicted by the Park *et al*. (2001) model was statistically equal to the mean of the measured asphalt pavement temperatures at a 5% significance level ($p = 0.989$). This suggests that the performance of Park *et al*.'s (2001) model in predicting asphalt pavement temperature in Tamale may be considered acceptable.

The best performing models, based on statistical significance testing, for the Forest zone (Kumasi) are the Park *et al*. (2001) and the Diefenderfer *et al*. (2006) models, while the Park *et al*. (2001) model exhibited best performance in the Savannah zone (Tamale).

The use of t-test to check for model satisfaction have been used by researchers such as Walia *et al*. (2022) and Gedafa *et al*. (2014). Also, Khan *et al*. (2019) and Ibili *et al*. (2022) both used the ANOVA to check for model satisfactory performance.

4.2.2 Assessment by Error Statistics and Coefficient of Determination

In Table 4.2, a comparison of the error statistics and the coefficient of determination (R^2) of the models is presented. Generally, all the models recorded higher R^2 values in the Savannah zone than in the Forest zone, except for Taamneh's (2016) model. Table 4.2 also indicates that prediction of asphalt pavement temperature using the model of Park *et al*. (2001) for the Savannah zone produced the lowest error statistics. Even in the Forest zone, the lowest error statistics (MPE and MBE) were produced by Park *et al*.'s (2001) model. However, the RMSE of the BELLS 3 model was lowest in the Forest zone. Thus, the model of Park *et al*. (2001) exhibited better performance based on error statistics, in both climatic zones than the other models while the BELLS 3 model performed better in considering R^2 values. The R^2 values, in this sense, indicate the proportion of the variability in the predicted asphalt pavement temperature that can be accounted for by the measured asphalt pavement temperature.

Also, both the MPE and MBE parameters portray under-prediction of asphalt pavement temperatures for both Kumasi and Tamale by the BELLS 3 (Lukanen *et al*. 2000) and Diefenderfer *et al*. (2006) models. The MPE and MBE also agree on the over-prediction of asphalt pavement temperature for both Kumasi and Tamale by the Gedafa *et al*. (2014), Taamneh (2016), and Asefzadeh *et al*. (2017) models. Meanwhile, the Park *et al*. (2001) model over-predicted for Kumasi, but its MPE for Tamale rather indicated under-prediction. The

Asefzadeh *et al*. (2017) and Taamneh (2016) models were the worst performing models in both climatic zones, in terms of error statistics. The Asefzadeh *et al*. (2017) and Taamneh (2016) models were associated with the lowest R^2 values for the study zones.

Table 4.2. Error Statistics and Coefficient of Determination of Model Predictions

Models	Kumasi				Tamale			
	RMSE (ºC)	**MPE (%)**	**MBE (ºC)**	**R^2**	**RMSE (ºC)**	**MPE (%)**	**MBE (ºC)**	**R^2**
BELLS 3	3.5	6.5	-2.3	0.866	3.6	7.9	-2.8	0.930
Park *et al*. (2001)	3.6	-0.9	0.5	0.825	3.2	0.8	0.0	0.905
Gedafa *et al*. (2014)	5.0	-7.2	2.2	0.558	4.8	-6.4	1.8	0.625
Diefenderfer *et al*. (2006)	4.8	1.2	-1.1	0.309	4.0	4.0	-2.2	0.599
Taamneh (2016)	7.5	-15.6	6.4	0.594	6.7	-13.2	5.9	0.443
Asefzadeh *et al*. (2017)	13.2	-29.6	12.4	0.305	12.1	-25.4	11.7	0.570

4.2.3 Assessment by Line of Equality.

Figures 4.1 through to 4.12 show the Line of Equality (LOE) drawn on graphs of predicted versus measured pavement temperatures. Figures 4.1 shows the BELLS 3 (Lukanen *et al*., 2000) model predictions versus measured asphalt pavement temperatures for Kumasi while Fig. 4.2 is a similar graph for Tamale. While there is under-prediction (more data points beneath the LOE compared to those above it) of asphalt pavement temperature for both locations, it is more pronounced for the Tamale data.

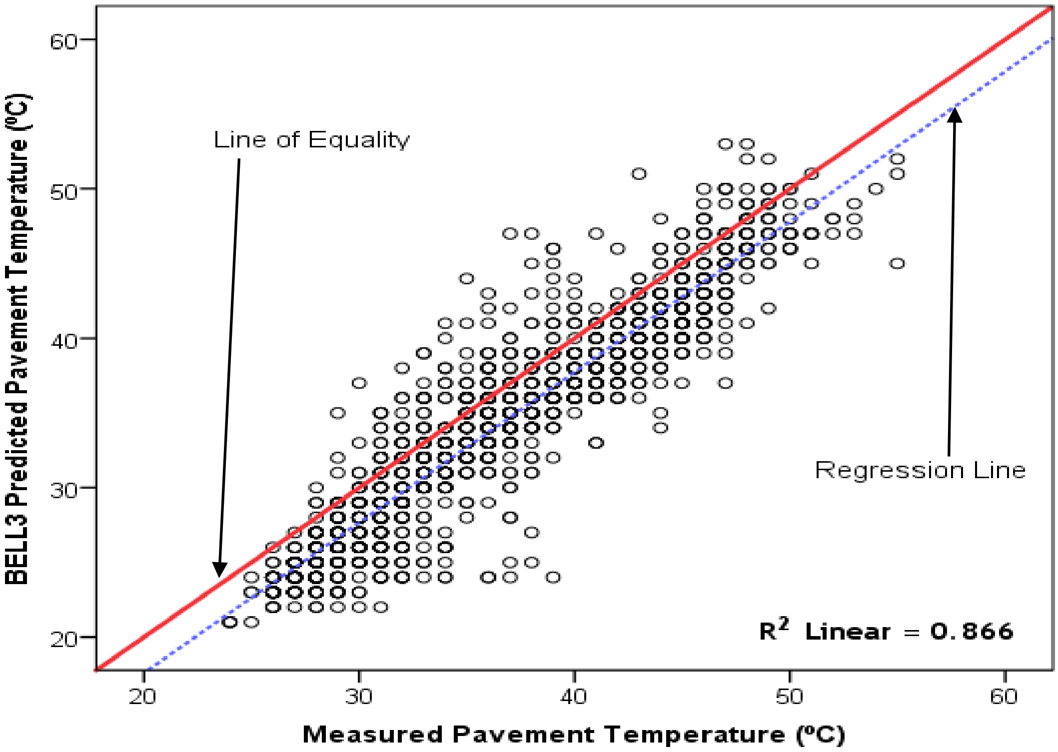

Figure 4.1. BELLS 3 model-predicted versus measured pavement temperature values on the Mango Road (Kumasi)

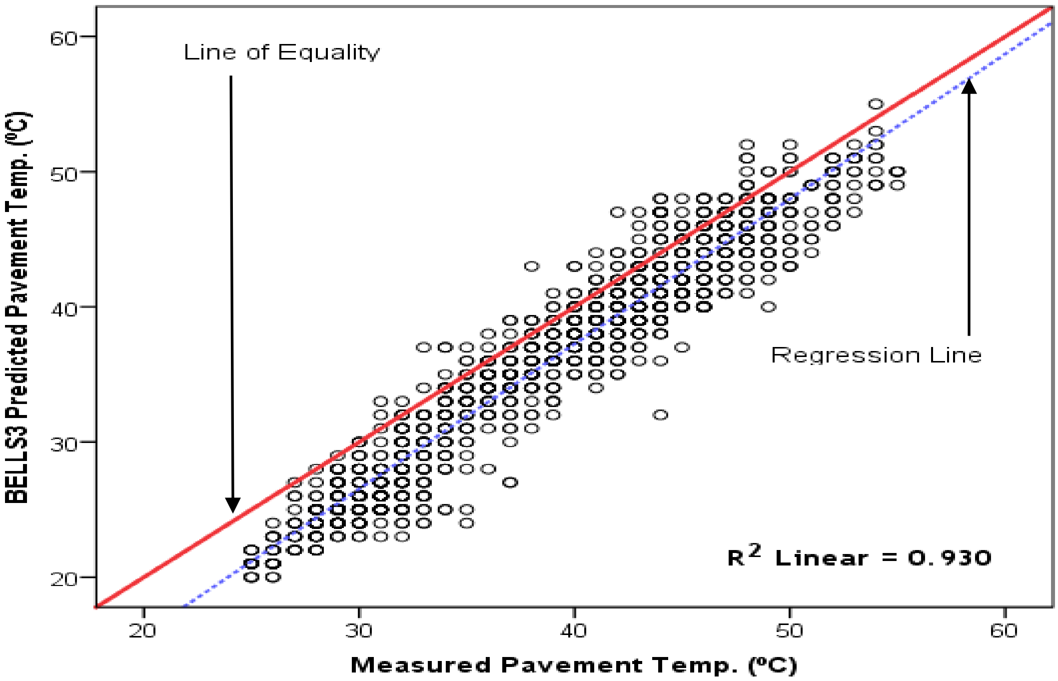

Figure 4.2. BELLS 3 model-predicted versus measured pavement temperature values on the RSM Road (Tamale)

Figures 4.3 and 4.4 show that the Gedafa *et al*. (2014) model over-predicted asphalt pavement temperature for both Kumasi and Tamale, as a relatively large number of data points plotted above the Line of Equality.

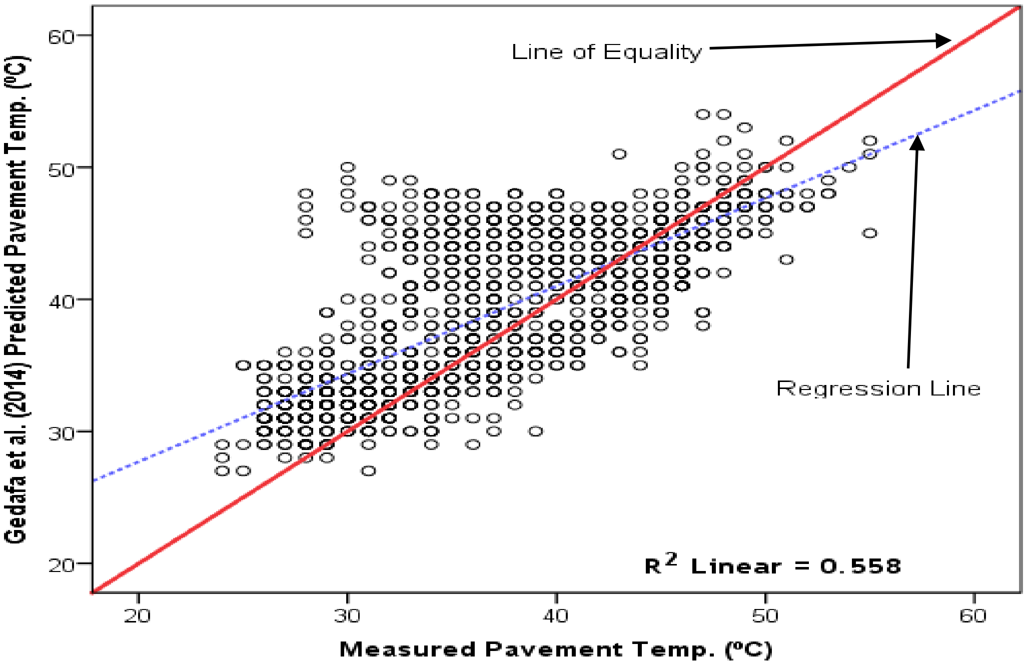

Figure 4.3. Gedafa *et al*. (2014) model-predicted versus measured pavement temperature values on the Mango Road (Kumasi)

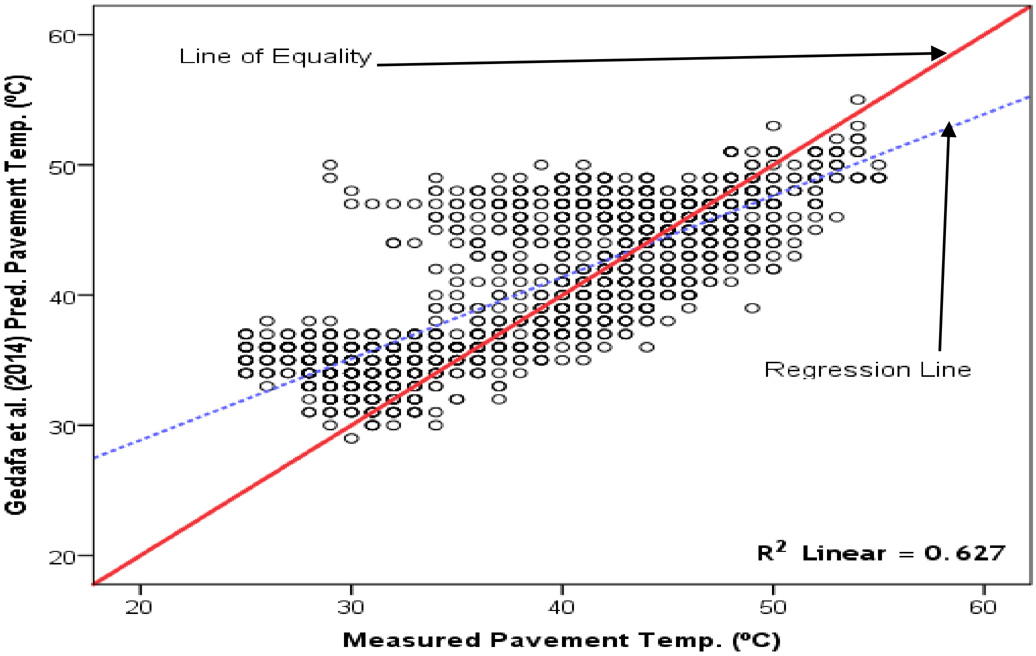

Figure 4.4. Gedafa *et al*. (2014) model-predicted versus measured pavement temperature values on the RSM Road (Tamale)

In Figures 4.5 and 4.6, it is seen that the measured and predicted asphalt pavement temperatures using Park *et al*.'s (2001) model for Kumasi and Tamale, respectively, are evenly distributed about the LOE, indicating a good prediction, although some amount of over-prediction could be seen for temperatures beyond 47ºC. This can be explained by the fact that the maximum temperature considered in the development of the Park *et al*. (2001) model was 43ºC (Park *et al*., 2001; Walia *et al*., 2022).

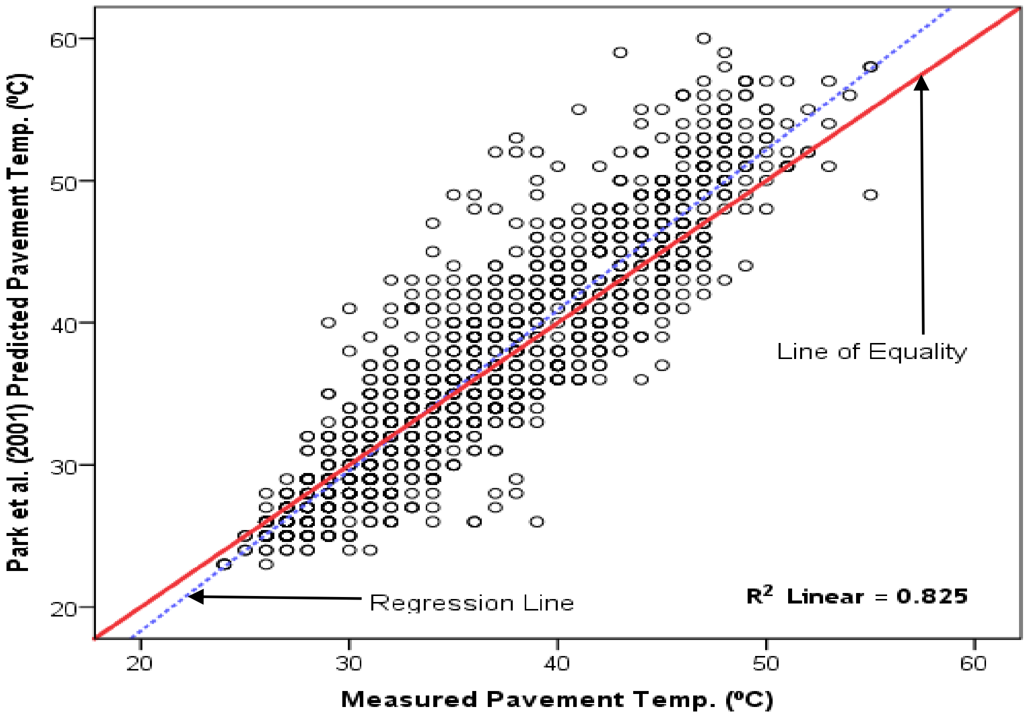

Figure 4.5. Park *et al*. (2001) model-predicted versus measured pavement temperature values on the Mango Road (Kumasi)

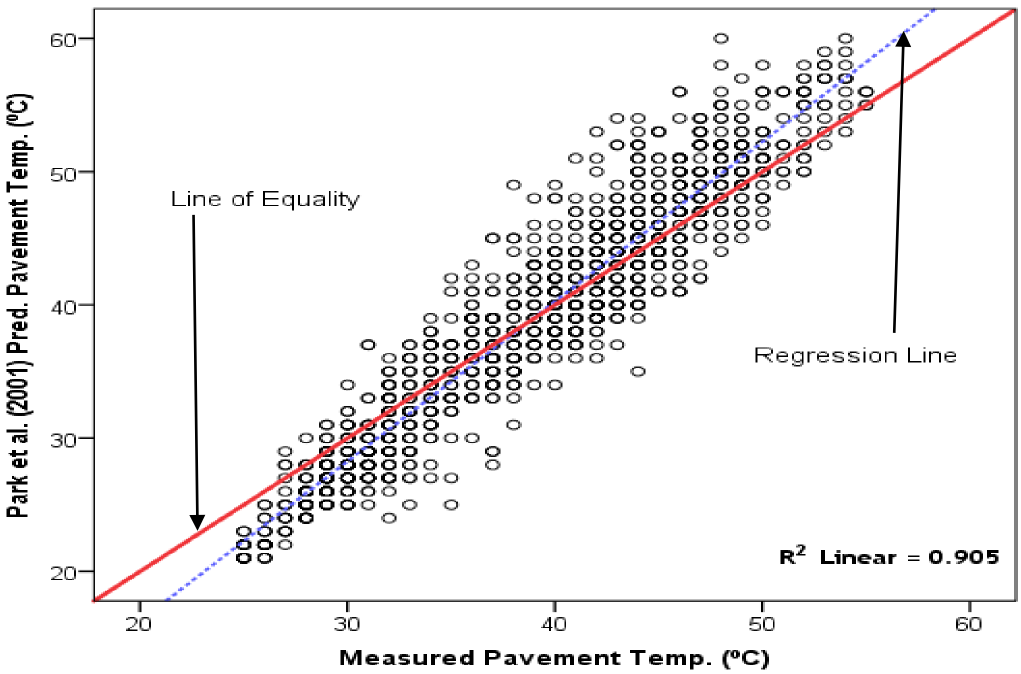

Figure 4.6. Park *et al*. (2001) model-predicted versus measured pavement temperature values on the RSM Road (Tamale)

Figures 4.1 through to 4.6 utilised a sample size of 1400 each.

It is evident in Figures 4.7 and 4.8 that there is disagreement between measured asphalt pavement temperatures and the predicted using the model of Diefenderfer *et al*. (2006). This suggests that there could be significant error to be incurred in using the Diefenderfer *et al*. (2006) model for asphalt pavement temperature prediction in both zones.

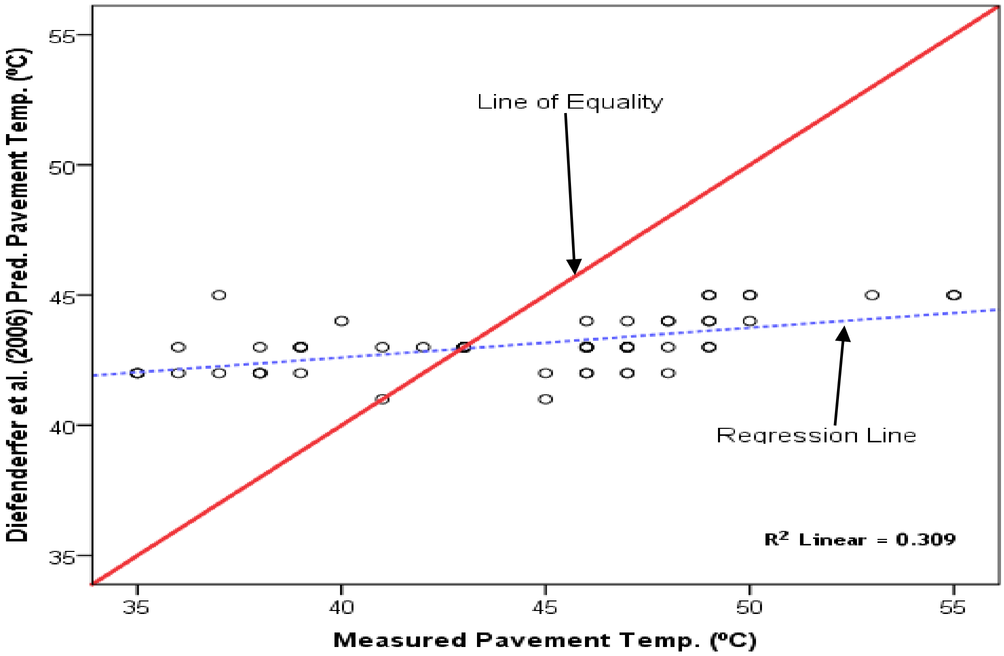

Figure 4.7. Diefenderfer *et al*. (2006) model-predicted daily maximum versus measured daily maximum pavement temperature values on the Mango Road (Kumasi)

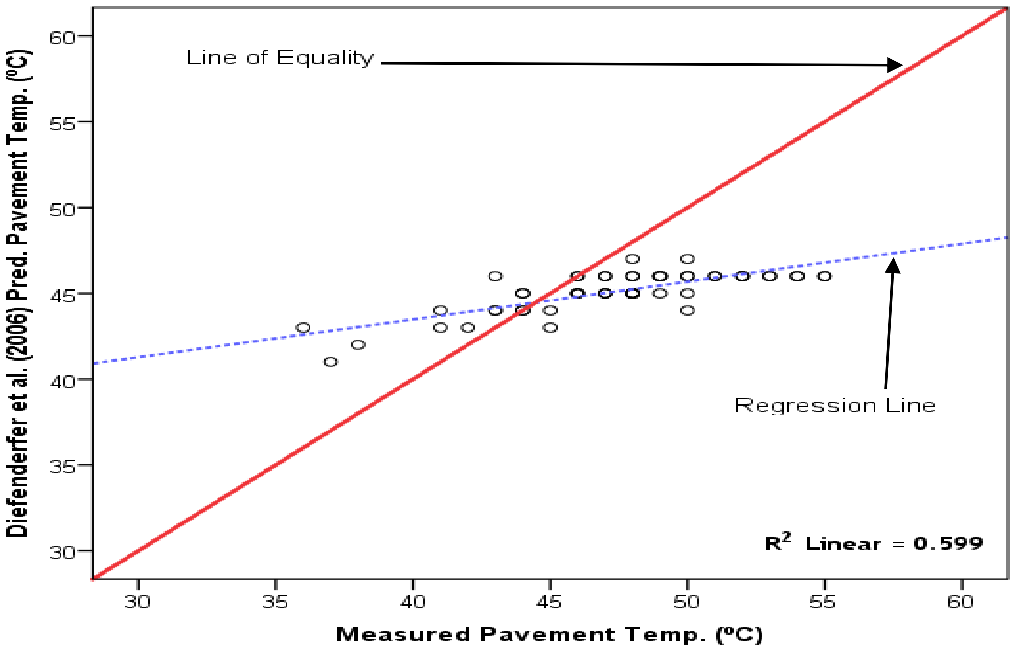

Figure 4.8. Diefenderfer *et al*. (2006) model-predicted daily maximum versus measured daily maximum pavement temperature values on the RSM Road (Tamale)

Figures 4.9 and 4.10 show that, using the Taamneh (2016) model for asphalt pavement temperature prediction for Kumasi and Tamale would not yield accurate results as almost all the data points plot above the Line of Equality.

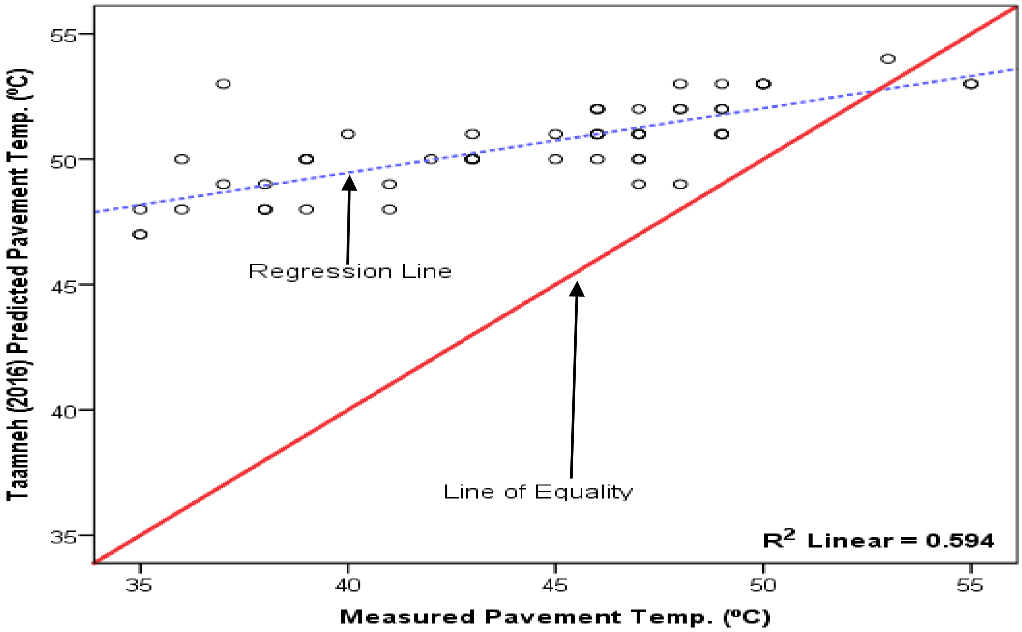

Figure 4.9. Taamneh (2016) model-predicted daily maximum versus measured daily maximum pavement temperature values on the Mango Road (Kumasi)

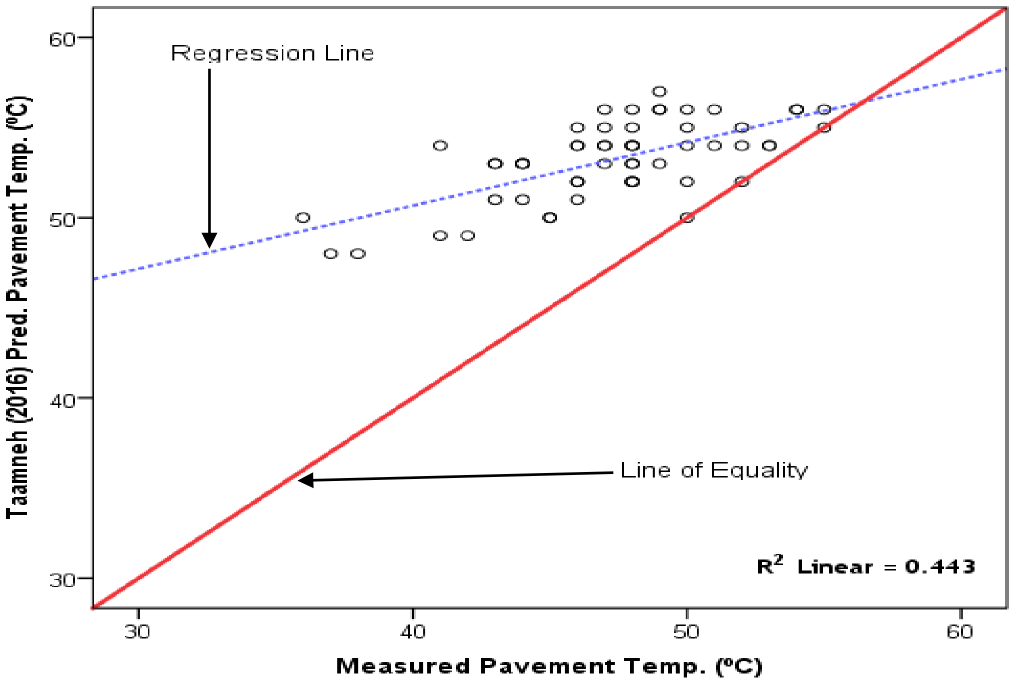

Figure 4.10. Taamneh (2016) model-predicted daily maximum versus measured daily maximum pavement temperature values on the RSM Road (Tamale)

In the case of the Asefzadeh *et al*. (2017) model, it over-predicts temperatures as all the data points in the plot of predicted versus measured temperatures at the two study sites are above the Line of Equality (see Fig. 4.11 for Kumasi and Fig. 4.12 for Tamale. This suggests that the model of Asefzadeh *et al*. (2017) is not suitable for predicting asphalt pavement temperatures for both the Forest and Savannah climatic zones in Ghana.

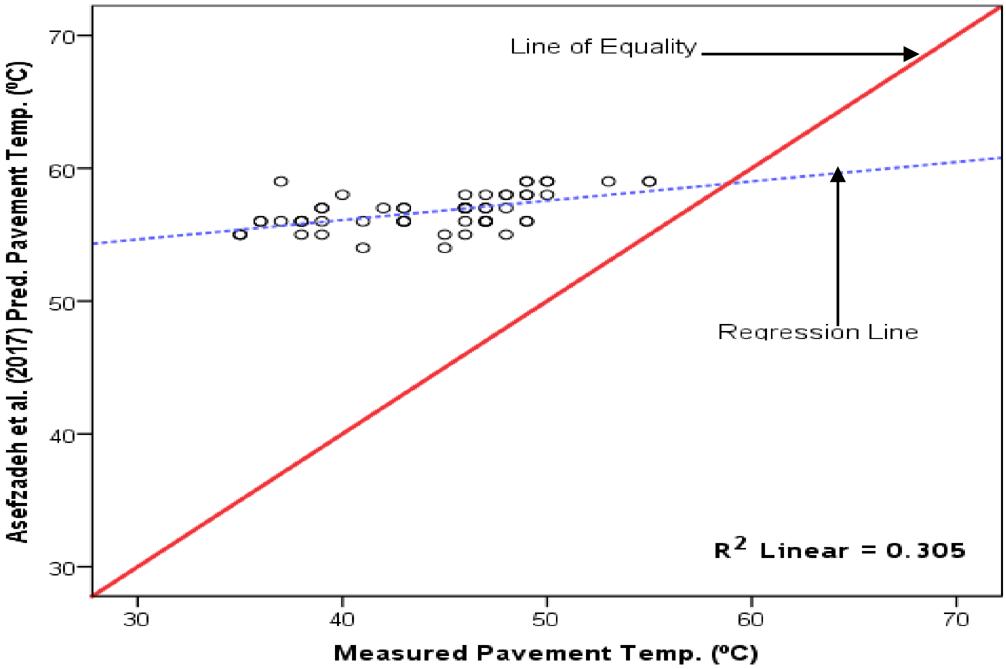

Figure 4.11. Asefzadeh *et al*. (2017) model-predicted daily maximum versus measured daily maximum pavement temperature values on the Mango Road (Kumasi)

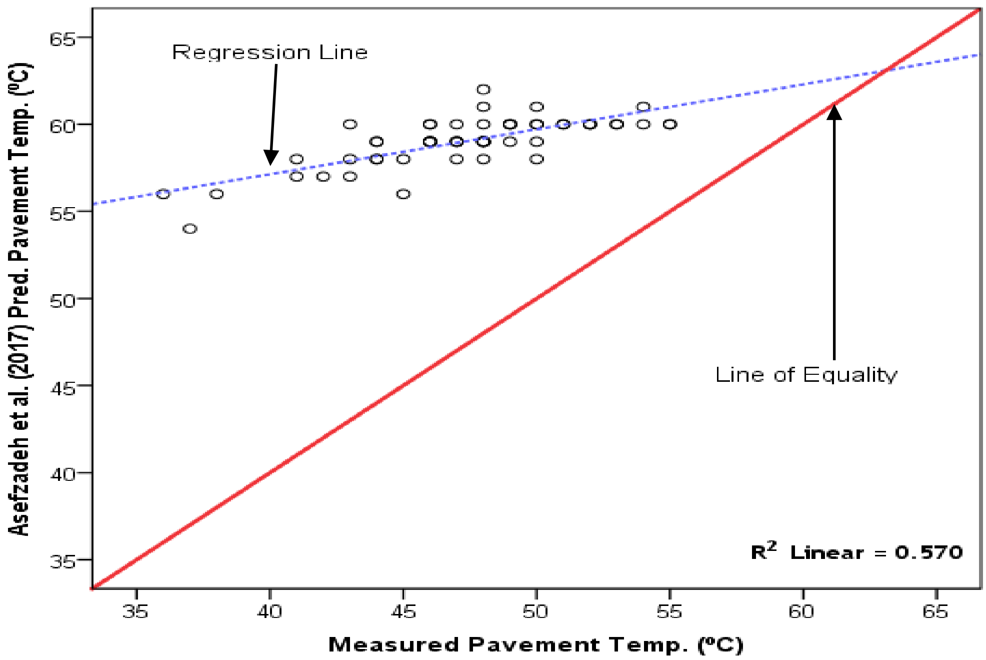

Figure 4.12. Asefzadeh *et al*. (2017) model-predicted daily maximum versus measured daily maximum pavement temperature values on the RSM Road (Tamale)

It is to be noted that there are few data points in Figures 4.7 through 4.12 (sample size of 56 each was used) because only daily maximum temperatures recorded within the data collection period were used for the model evaluation, as the Diefenderfer *et al*. (2006), Taamneh (2016) and Asefzadeh *et al*. (2017) models predict only daily maximum pavement temperatures.

4.2.4 Discussion on Asphalt Pavement Temperature Prediction Model Evaluation

The prediction accuracy of the BELLS 3 model in Ghana ($R^2 \geq 0.866$, RMSE ≤ 3.6) was better when compared to similar results obtained by Kassem *et al.* (2020) in the U.S. State of Idaho ($R^2 = 0.834$, RMSE =4.503) and by Walia *et al*. (2022) in India ($R^2 = 0.52$, RMSE =7.21). In spite of that, judging from the distribution of points about the LOE, the model under-performed in Ghana compared with its performance in Tennessee (US) as reported by Marshall *et al*. (2001). The poor prediction of the BELLS 3 model in Ghana may be due to the fact that the model was formulated for a maximum pavement temperature of 40ºC (Lukanen *et al*., 2000; Walia *et al*., 2022), which is below typical maximum pavement temperatures recorded in Ghana (60ºC). While the asphalt layer thicknesses of the study roads were in the range of 70 mm to 76 mm, the Gedafa *et al*. (2014) was originally developed for asphalt layer thicknesses in excess of 200 mm and this could have accounted for its poor prediction accuracy in Ghana.

From the statistical significance testing of the difference between the predicted and measured asphalt pavement temperatures, the best-performing models for the Forest zone were the Park *et al*. (2001) and Diefenderfer *et al*. (2006) models, whereas only the Park *et al*. (2001) model performed well in the Savannah zone. Based on Error Statistics, LOE and R^2, the Park *et al*. (2001) model outperformed the Diefenderfer *et al*. (2006) model for the Forest zone. Among the models evaluated, the Park *et al*. (2001) model was, therefore, ranked the best performing model for asphalt pavement temperature prediction for both Forest and Savannah zones. Overall, the performance of the Park *et al*. (2001) model for Tamale was better than that for Kumasi.

4.3 Development of New Asphalt Pavement Temperature Prediction Models

4.3.1 Asphalt Pavement Temperature Variation

A. Hourly Variation

Figure 4.13 shows the hourly pavement temperatures obtained for the Mango Road (Kumasi) and the RSM Road (Tamale) sites. Generally, the mid-depth AC and surface temperatures followed a similar pattern, except during the hours of 6:00 GMT to 7:00 GMT. There were low mid-depth AC and surface temperatures in the morning and late afternoon/evening (16:00 GMT to 18:00 GMT) compared with the mid-afternoon period. Both the mid-depth AC and surface temperatures attained their hourly maximum values at 14:00 GMT. However, the hourly minimum pavement temperature at mid-depth of the AC layer was recorded at 7:00 GMT and was preceded by that at the surface at 6:00 GMT. These findings corroborate those of Koranteng-Yorke (2012), who recorded the hourly maximum and minimum in-depth AC temperature in the Forest zone (Akumadan) at 14:00 GMT and 7:00GMT, respectively. Also, mid-depth AC and surface temperatures in Kumasi were consistently lower than in Tamale for most hours of the day. The consistently high surface and mid-depth AC temperatures recorded in Tamale confirm the higher mean daily insolation in Tamale (Savannah zone) than in Kumasi (Forest zone) (Asilevi *et al*., 2019).

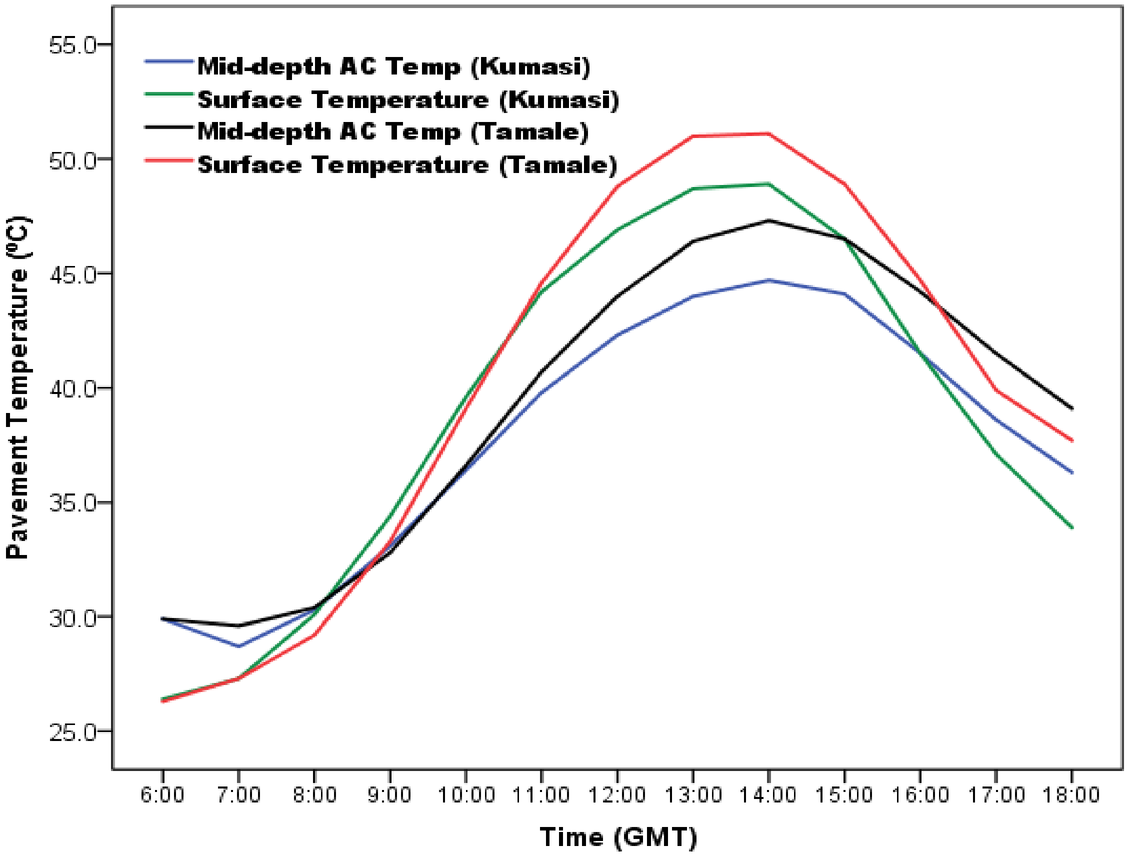

Figure 4.13. Hourly Pavement Temperatures on Mango Road (Kumasi) and RSM Road (Tamale)

B. Monthly Variation

The monthly pavement temperatures at the study sites are shown in Figure 4.14. The mid-depth AC and surface temperatures exhibited a similar pattern in a given city. In Tamale, mid-depth and surface temperatures were lowest in December and January but highest in March whereas in Kumasi, mid-depth temperatures were lowest in August and highest in April. Surface temperatures in Kumasi were lowest in September but highest in April and October. This is because both the Savannah and Forest zones experience maximum mean daily insolation from February to May, with the Forest zone experiencing another in October-November (Asilevi *et al.*, 2019). The high insolation leads to increased absorbed solar radiation in the asphalt pavements due to the low surface albedo of the new asphalt concrete (Chen *et al.*, 2019; Carnielo and Zinzi, 2013; Pomerantz *et al.*, 2000) of the Mango and RSM Roads, which were rehabilitated in 2021. These findings corroborate those of Koranteng-Yorke (2012) which established the maximum and minimum AC temperatures for the Forest zone (Akumadan) in April and August, respectively.

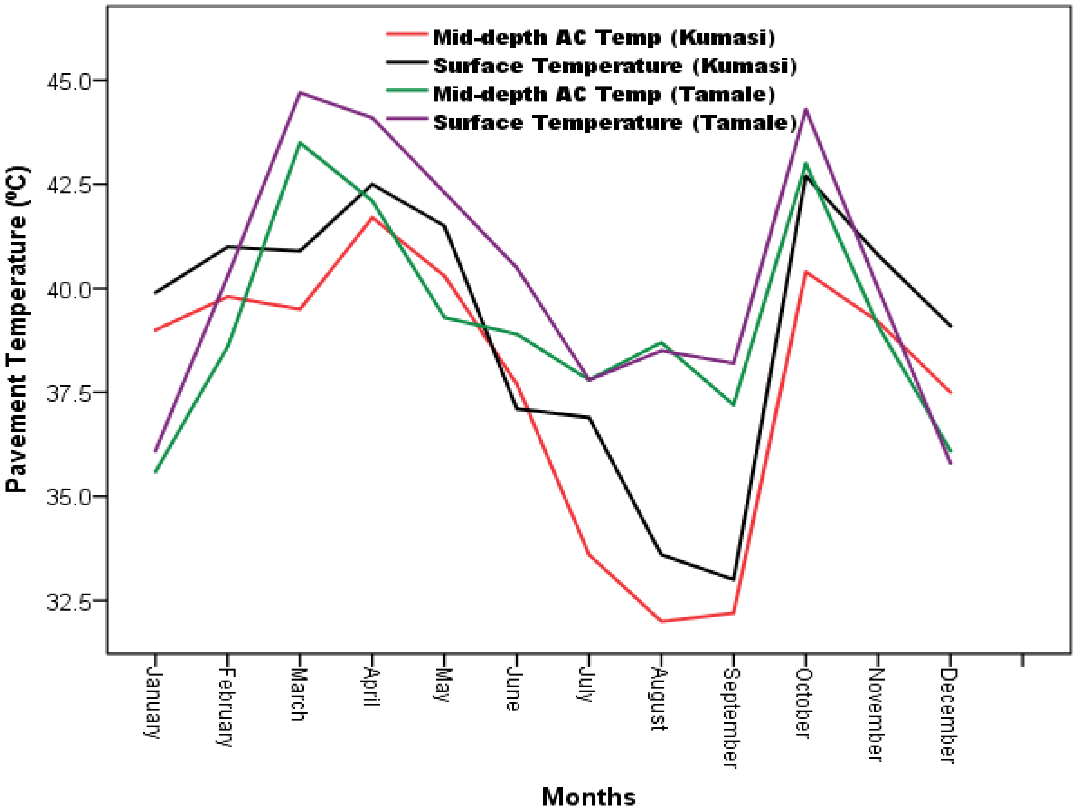

Figure 4.14. Monthly Pavement Temperatures on Mango Road (Kumasi) and RSM Road (Tamale)

4.3.2 Asphalt Pavement Temperature Prediction Models

Time- and depth-dependent asphalt pavement temperature prediction models are usually designed as non-linear regression (Chen *et al*., 2019). Such models may utilise the input parameters of pavement surface temperature, the average air temperature of previous day, asphalt layer depth and time of day (e.g., Lukanen *et al*., 2000; Park *et al*., 2001; Gedafa *et al*., 2014; Walia *et al*., 2022). Based on literature, temperature of pavement surface, air temperature and time of day are potential predictors of mid-depth pavement temperature and were used as such. Therefore, Eq. (4.1) is the generalized multiple non-linear regression equation proposed for predicting the AC mid-depth pavement temperature in each of the climatic zones considered.

$$T_{dmm} = \beta_0 + \beta_1 T_{sur} + \beta_2 T_{avg} + \beta_3 \sin(t) \quad (4.1)$$

where;

β_0, β_1, β_2, β_3 = model coefficients

T_{dmm} = AC pavement temperature (ºC) at mid-depth (d-mm) from the surface

T_{avg} = mean of air temperature (ºC) of the previous day

T_{sur} = pavement surface temperature (ºC)

t = time of pavement surface temperature measurement (recorded on a 24-hr time scale and divided by 24), days

A. Model Calibration for Kumasi

Data collected on the Mango Road, from May 2022 to April 2023, was used for the calibration of the proposed model above for Kumasi. The descriptive statistics associated with the model calibration for the Kumasi site for an asphalt concrete mid-depth of 38mm are shown in Table 4.3. It is seen in the table that the asphalt pavement temperature at a depth of 38mm (T_{38mm}) has a lower mean (37.7 ºC) compared to the mean (39.1 ºC) of pavement surface temperature (T_{sur}). This indicates that pavement surface temperatures are generally higher compared to mid-depth AC pavement temperatures in Kumasi but there is lower variability in the latter compared to the former.

Table 4.3. Descriptive Statistics associated with Model Calibration for Kumasi

Variable	**N**	**Mean**	**Std. Dev.**	**COV (%)**	**Minimum**	**Maximum**
T_{38mm}	2100	37.7	7.1	18.8	24.0	55.0
T_{sur}	2100	39.1	9.1	23.3	22.6	61.6
T_{avg}	2100	27.4	1.4	5.1	22.7	29.8
t	2100	0.50	0.2	40.0	0.25	0.75

*COV = coefficient of variation

T_{38mm} = AC pavement temperature (ºC) at 38mm mid-depth

T_{sur} = pavement surface temperature (ºC)

T_{avg} = mean air temperature (ºC) of previous day

t = time of pavement temperature measurement (days)

As discussed in the literature review section, one of the requirements of multiple linear regression is to check for multi-collinearity among the independent variables. This was accomplished using a Pearson correlation matrix. The Pearson correlation coefficient (R) are presented in Table 4.4. The results show a strong positive correlation (R=0.931) between T_{38mm} and T_{sur} but a weak positive correlation (R=0.295) of T_{38mm} and T_{avg}. T_{avg} values were computed from the daily minimum and maximum air temperature records. The sine function of time [$\sin(t)$] slightly improved the correlation with T_{38mm}.

Table 4.4. Pearson Correlation Matrix of the Kumasi Calibration Data

Variable	T_{38mm}	T_{sur}	T_{avg}	t	$\sin(t)$	$T_{avg}t$
T_{38mm}	1.000	0.931	0.295	0.601	0.618	0.644
T_{sur}	0.931	1.000	0.222	0.520	0.543	0.551
T_{avg}	0.295	0.222	1.000	0.000	0.000	0.166
t	0.601	0.520	0.000	1.000	0.999	0.985
$\sin(t)$	0.618	0.543	0.000	0.999	1.000	0.984
$T_{avg}t$	0.644	0.551	0.166	0.985	.984	1.000

To further strengthen the investigation of multi-collinearity among the potential predictor variables, the Variance Inflation Factor (VIF) presented in Table 4.5 was used. As shown in the Table 4.5, T_{avg}, $\sin(t)$ and $T_{avg}t$ recorded VIF above 10, indicating high correlation. Consequently, $T_{avg}t$ was not used as a predictor variable in fitting the model.

Table 4.5. Variance Inflation Factor for the Kumasi Model Calibration

Model		Variance Inflation Factor (VIF)
1	(Constant)	
	T_{sur}	1.849
	T_{avg}	10.610
	$\sin(t)$	322.464
	$T_{avg}t$	320.021

To check for the linearity assumption, mid-depth AC pavement temperature was plotted against pavement surface temperature, mean air temperature of the preceding day, and time of day, as shown in Figures 4.15 through 4.17. Figure 4.15 shows a linear relationship between the mid-depth AC pavement temperature and pavement surface temperature. Mid-depth AC pavement temperature versus mean air temperature of previous day is linear (Figure 4.16), while pavement temperature versus time of day is non-linear (Figure 4.17).

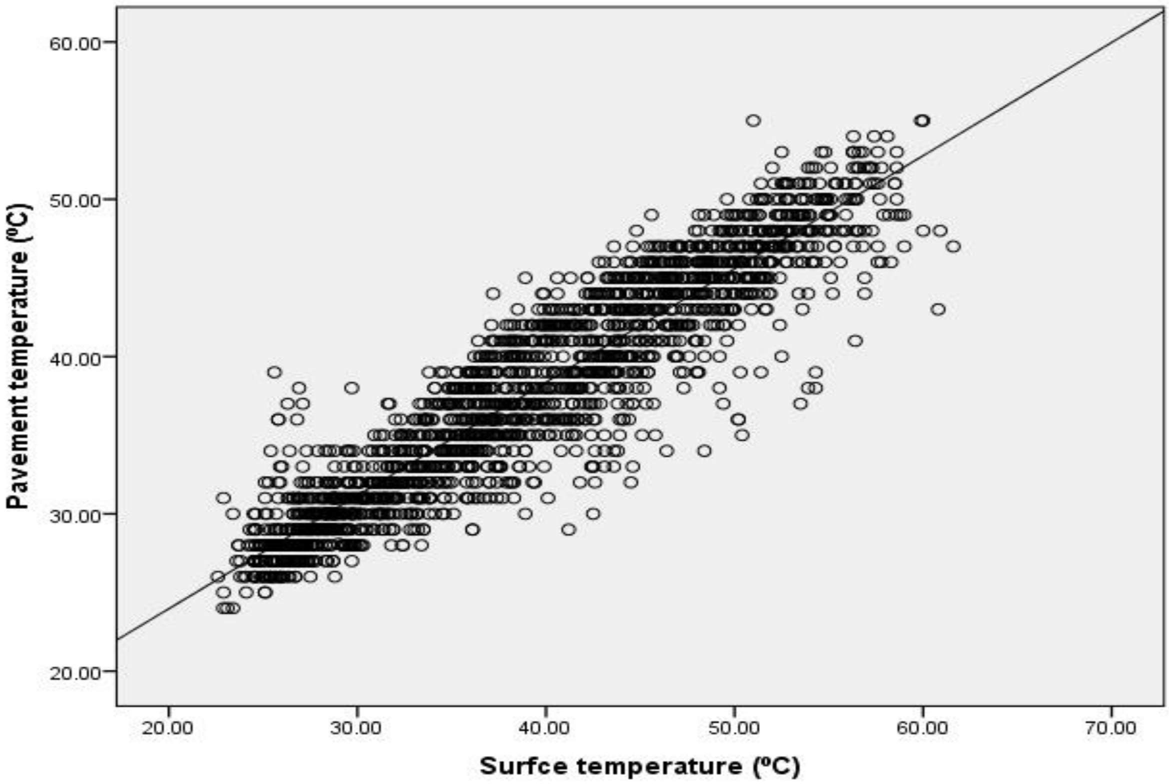

Figure 4.15. Mid-depth AC temperature versus pavement surface temperature on the Mango Road (Kumasi)

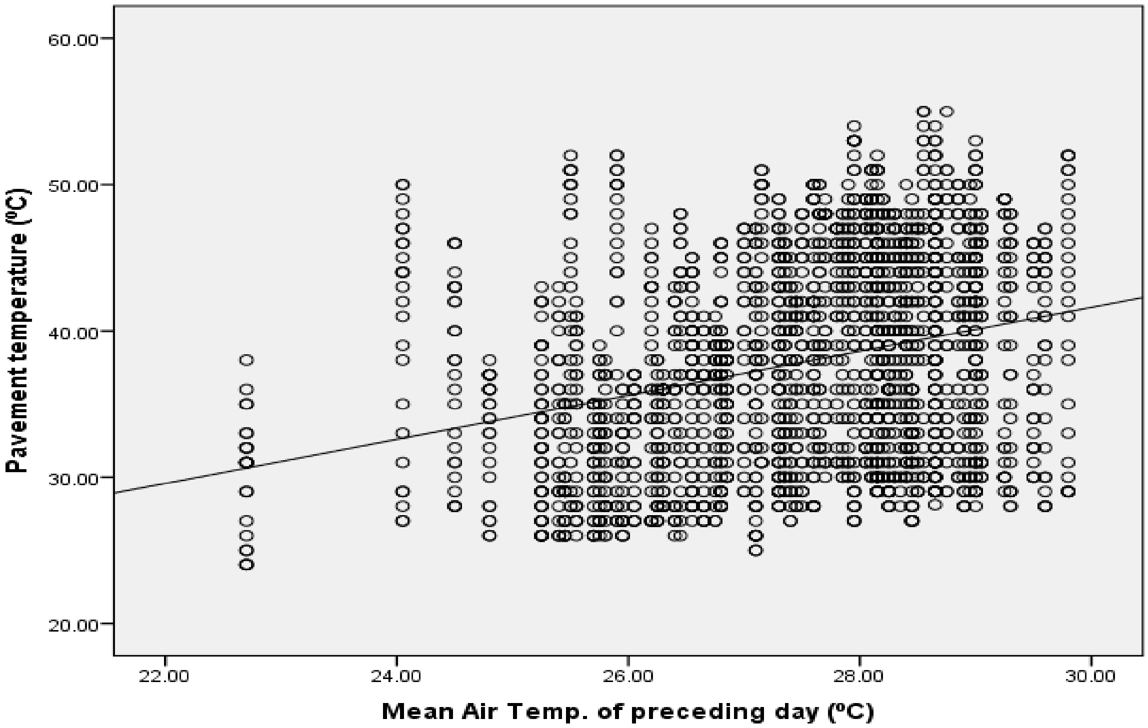

Figure 4.16. Mid-depth AC temperature versus Mean Air Temperature of the Preceding Day on the Mango Road (Kumasi)

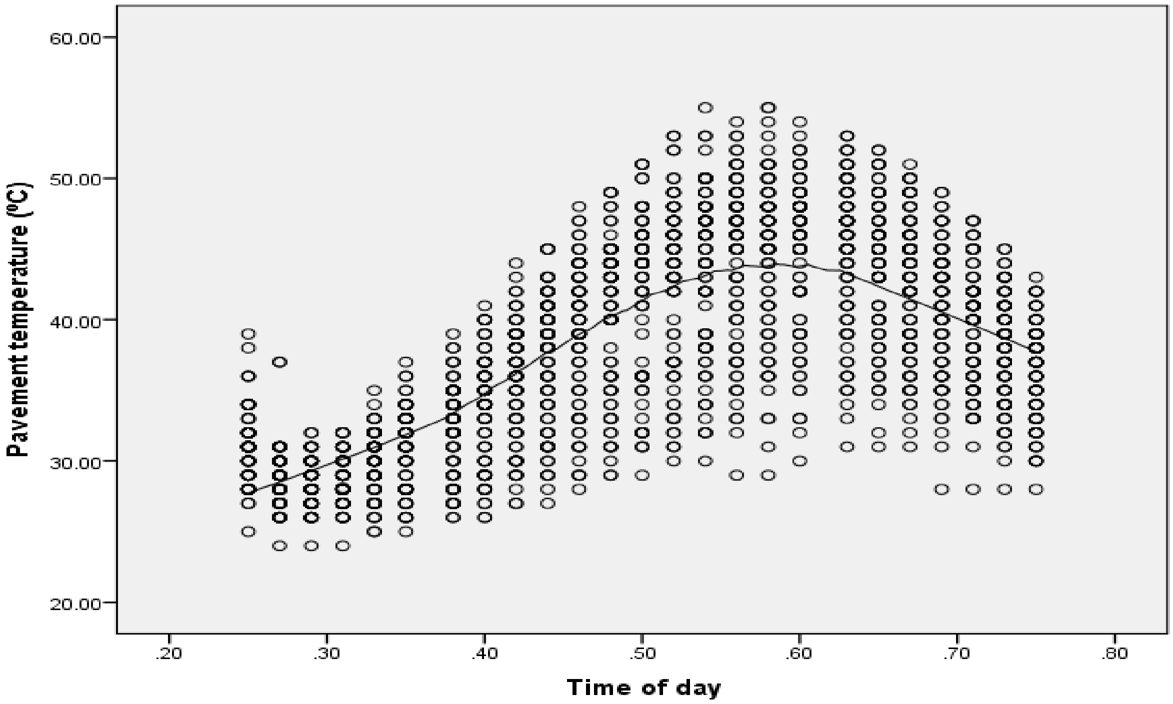

Figure 4.17. Mid-depth AC Temperature versus Time of Day on the Mango Road (Kumasi)

Due to the non-linear relationship of T_{38mm} with "t", the non-linear transformation, $\sin(t)$, was used instead of "t". The sine transformation of the time variable (t) is commonly used in modelling pavement temperature (e.g., Walia *et al*., 2022; Park *et al*., 2001; Lukanen *et al*., 2000). Therefore, the next phase of model calibration for Kumasi considered T_{avg}, T_{sur} and $\sin(t)$ as explanatory variables.

Multiple regression analysis was used to fit a model incorporating the predictor variables, T_{avg}, T_{sur} and $\sin(t)$ and the dependent variable T_{38mm}. The significance level was 5% ($\alpha = 0.05$), and the statistical summary for the Kumasi model is shown in Table 4.6.

Table 4.6. Summary Statistics of the Model Developed for Kumasi

Summary	**R**	**R^2**	**Adjusted R^2**	**SEE**	
	0.947	0.896	0.896	2.281	
ANOVA	**Degree of freedom**	**Sum of squares**	**Mean of squares**	**F statistic**	**P-value**
Regression	3	94220.7	31406.9	6034.3	0.000
Residual	2096	10909.1	5.2		
Total	2099	105129.8			
	Coefficients	**Standard error**	**t-statistic**	**VIF**	**P-value**
Intercept	-7.43	1.012	-7.345		0.000
T_{sur}	0.625	0.007	92.94	1.526	0.000
T_{avg}	0.589	0.037	15.789	1.075	0.000
$\sin(t)$	9.658	0.458	21.107	1.451	0.000

Note: SEE= Standard error estimate; VIF= Variance Inflation Factor

From Table 4.6, the combination of pavement surface temperature (T_{sur}), mean of air temperature of the previous day (T_{avg}), and sine of the time of pavement surface temperature measurement [$\sin(t)$] is significantly related to the AC mid-depth pavement temperature. The variance inflation factor (VIF) of each predictor variable is approximately 1, suggesting that the variables are not correlated. The adjusted R^2 value of 0.896 indicates that approximately 89.6% of the variability in the mid-depth AC pavement temperature (T_{38mm}) measured on the Mango Road (Kumasi) is accounted for by the prediction variables. Also, the p-values of the corresponding t-statistics of the T_{avg}, T_{sur} and $\sin(t)$ are all < 0.0001, indicating that the null hypothesis equating the coefficients of T_{avg}, T_{sur} and $\sin(t)$ to zero be rejected. The calibrated proposed regression equation for predicting the AC mid-depth pavement temperature in Kumasi (T_{38mm}) is given by Eq. (4.2);

$$\boldsymbol{T_{38mm} = -7.43 + 0.625\, T_{sur} + 0.589\, T_{avg} + 9.658 \sin(t)}\ ; \quad R^2 = 0.896 \qquad (4.2)$$

where;

T_{38mm} = AC pavement temperature (ºC) at 38mm mid-depth from the surface

T_{avg} = mean of air temperature (ºC) of the previous day

T_{sur} = pavement surface temperature (ºC)

t = time of pavement surface measurement (recorded on a 24-hr time scale and divided by 24), days

The assumption that the data used in the multiple regression model were normally distributed was checked using a histogram of the regression residuals, as shown in Figure 4.18. The residuals follow a normal distribution, indicating the model fulfils the normality assumption of multiple regression analysis. Again, the proposed model for Kumasi was checked for equality of variance of the residuals, using a scatter plot of the standardised residuals and predicted values, as shown in Figure 4.19. Since the data points are centred around the horizontal line through zero, it can be inferred that the variance of the residuals is equal. This also fulfils the equality of variance assumption of multiple linear regression.

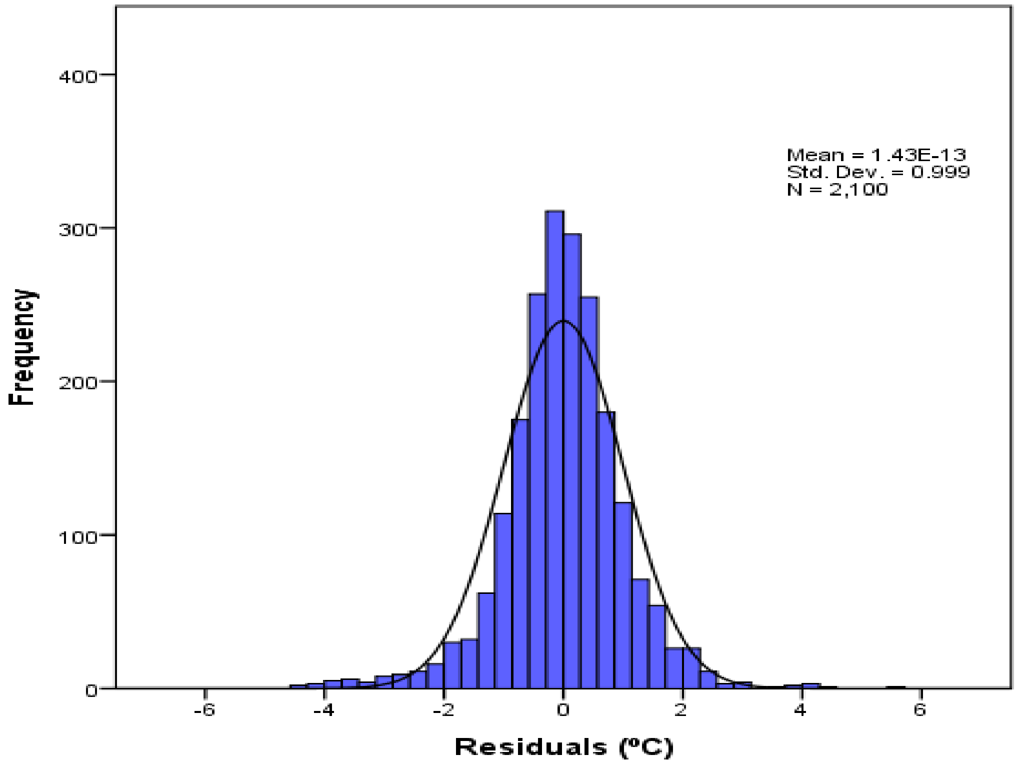

Figure 4.18. Distribution of Normalised Residuals for the Kumasi Model

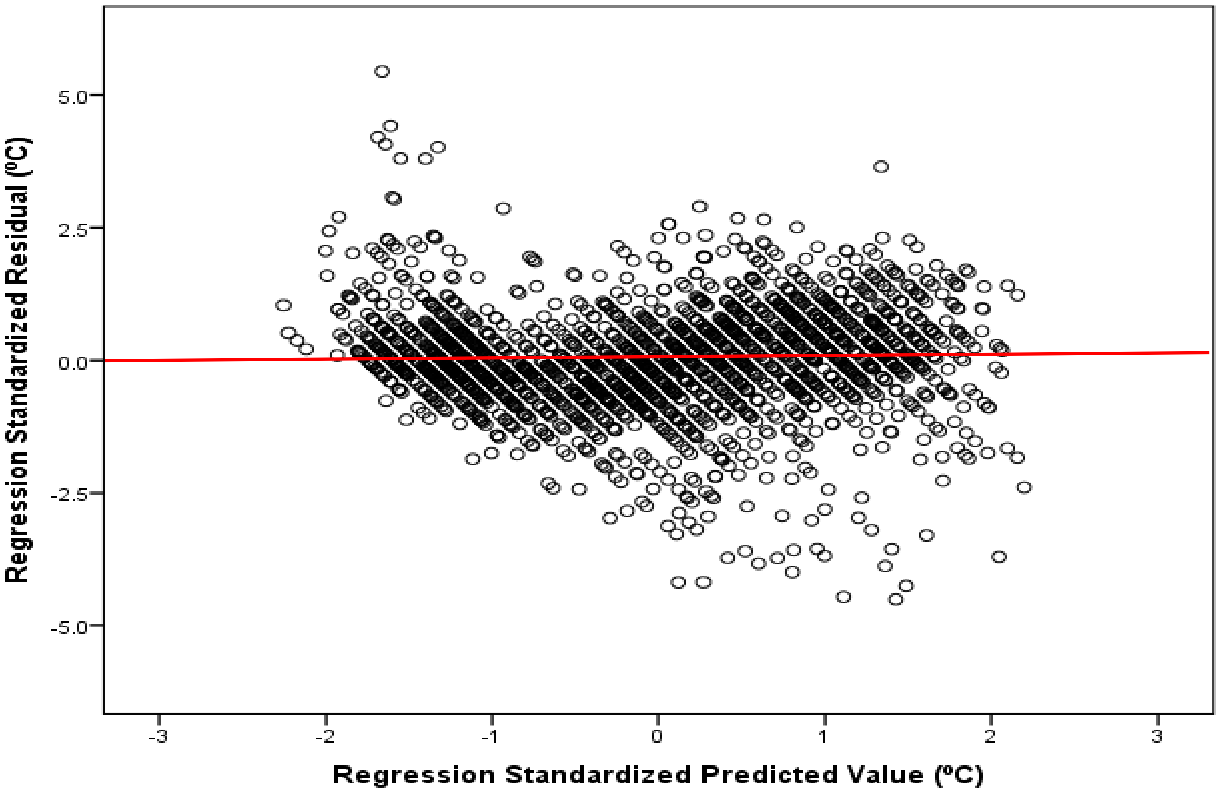

Figure 4.19. Standardised Residuals versus Predicted Values for the Kumasi Model

With the satisfaction of the fundamental assumptions of multiple linear regression and the high R^2, it was considered that the proposed model for predicting mid-depth asphalt pavement temperature for the Forest zone (represented by Kumasi) was well-fitted.

B. Validation of the Model for Kumasi

The next consideration in the model development was model validation. Model validation involves comparing model-predicted and measured asphalt pavement temperatures to identify if the difference between their average values is statistically significant, showing their distribution around a line of equality and computing the error statistics and the R^2. The model validation used a dataset independent of the data used for the model calibration. The data gathered from the Antoa Road in Kumasi (Table 3.5) was used for the validation. The descriptive statistics for the validation (Table 4.7) exhibit a similar characteristic to those of the calibration data. However, the mean of the T_{38mm} and T_{sur} were similar (36.5 ºC versus 36.7 ºC). Thus, the mean of mid-depth AC and surface temperatures on the Antoa Road (used for model validation) are lower than on the Mango Road (for model calibration). Meanwhile, the mean of T_{avg} for the validation dataset is equal to that of the model calibration data. The T_{38mm}, T_{sur} and "t" values had high variability compared to T_{avg}values.

Table 4.7. Descriptive Statistics of Validation Data for Kumasi Model

Variable	N	Mean	Std. Dev.	COV (%)	Minimum	Maximum
T_{38mm}	700	36.5	6.5	17.8	26.0	50.0
T_{sur}	700	36.7	7.7	21.0	23.3	53.4
T_{avg}	700	27.6	1.5	5.4	23.6	31.1
t	700	0.5	0.2	40.0	0.25	0.75

Note: Variables are as previously defined

The results of a two-sample t-test performed to compare the means of the measured and predicted AC pavement temperatures yielded a **p-value of 0.5979**. This suggested that the null hypothesis of equating the mean of the measured and predicted AC pavement temperatures is accepted. It is, therefore, inferred that the mean of observed pavement temperatures is statistically equal to the mean of predicted AC pavement temperatures. Due to the large data size (N=700), the normality check prior to conducting the t-test was ignored in line with the recommendation of Ghasemi and Zahediasl (2012).

The model was also validated by analysing a scatter plot of predicted versus measured pavement temperatures, as shown in Figure 4.20. As seen in the figure, there is a good prediction of pavement temperature, with majority of the data points distributed around the line of equality (LOE). The validated model had an R^2 of 0.919, RMSE of 1.924ºC, and MPE of 0.04%, indicating a high prediction accuracy.

The combination of the t-test and the residual analysis have been used to validate asphalt pavement temperature prediction models such as Walia *et al*. (2022) and Khan *et al*. (2019).

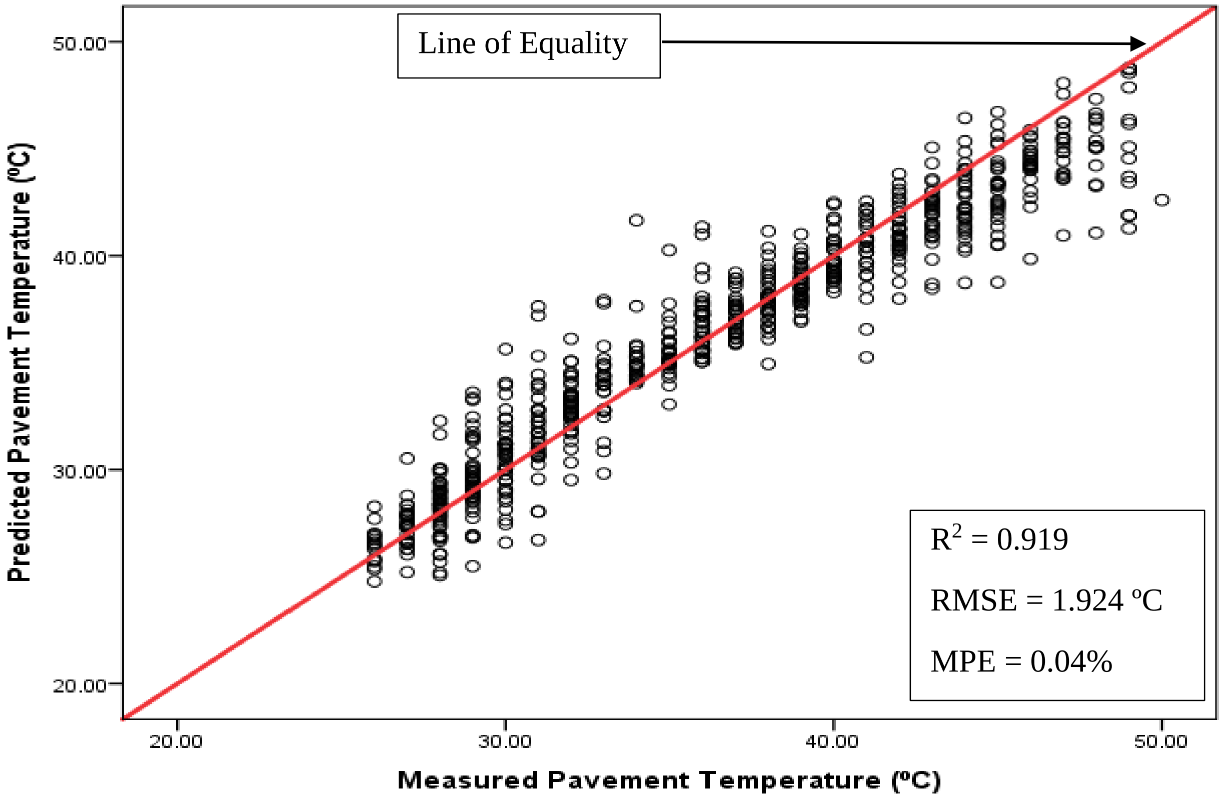

Figure 4.20. Kumasi Model Validation: Predicted versus Measured Pavement Temperature

C. Model Calibration for Tamale

The generalised model, Eq. (4.1), was calibrated for an AC pavement mid-depth of 35mm for the Tamale site. Data from the RSM Road from May 2022 to April 2023 were used for the model calibration. The descriptive statistics associated with the model calibration are presented in Table 4.8. The mean AC pavement temperature at a depth of 35mm (T_{35mm}) was close to the mean of the pavement surface temperature (T_{sur}) (39.1ºC versus 40.2ºC).

Table 4.8. Descriptive Statistics associated with Model Calibration for Tamale

Variable	N	Mean	Std. Dev.	COV (%)	Minimum	Maximum
T_{35mm}	2100	39.1	7.6	19.1	24.0	58.0
T_{sur}	2100	40.2	10.1	25.1	20.2	63.9
T_{avg}	2100	29.6	2.1	7.1	25.9	35.0
t	2100	0.50	0.2	40.0	0.25	0.75

In order to firm the potential predictor variables for the Tamale model, a correlation analysis was performed with the T_{35mm}, T_{sur}, T_{avg} and t variables as well as non-linear transformation of some of the variables and their interactions. This also helped to detect multi-collinearity between the predictor variables. The correlation analysis results are presented in Table 4.9. Similar to what was obtained for the Kumasi site, the table reveals that there is a strong relationship of T_{sur} with T_{35mm} (R = 0.947) but a weak correlation of $T_{avg}$with T_{35mm} (R = 0.228). While the time (t) has a moderate correlation with T_{35mm} (R =0.697), the sine transform of "t" slightly improved its correlation with T_{35mm} (R =0.713). Again, there was a strong correlation between two potential predictor variables, $\sin(t)$ and $T_{avg}t$ (R>0.7).

Table 4.9. Pearson correlation matrix for the Tamale model calibration data

Variable	T_{35mm}	T_{sur}	T_{avg}	t	$\sin(t)$	$T_{avg}t$
T_{35mm}	1.000	0.947	0.228	0.697	0.713	0.734
T_{sur}	0.947	1.000	0.207	0.619	0.640	0.651
T_{avg}	0.228	0.207	1.000	0.000	0.000	0.227
t	0.697	0.619	0.000	1.000	0.999	0.971
$\sin(t)$	0.713	0.640	0.000	0.999	1.000	0.971
$T_{avg}t$	0.734	0.651	0.227	0.971	0.971	1.000

Also, the variance inflation factor (VIF) presented in Table 4.10 was used to confirm possible multi-collinearity among the potential predictor variables. Higher VIF (>10) of T_{avg}, $\sin(t)$ and $T_{avg}t$ is an indication of higher correlations. Hence, $T_{avg}t$ was not used in the fitting of the model.

Table 4.10. Variance Inflation Factor for the Tamale Model Calibration

Model		Variance Inflation Factor (VIF)
1	(Constant)	
	T_{sur}	2.008
	T_{avg}	11.188
	$\sin(t)$	183.856
	$T_{avg}t$	185.475

A scatter plot of the T_{35mm} against T_{sur}, T_{avg}, and “t” is provided in Figures 4.21 through 4.23. Figure 4.21 shows a linear relationship between T_{35mm} and T_{sur}. There exists a linear relationship between T_{35mm} and T_{avg} (Figure 4.22), while a non-linear relationship exists between T_{35mm} and “t” (Figure 4.23). As a result, $\sin(t)$ was considered for the model instead of “t”.

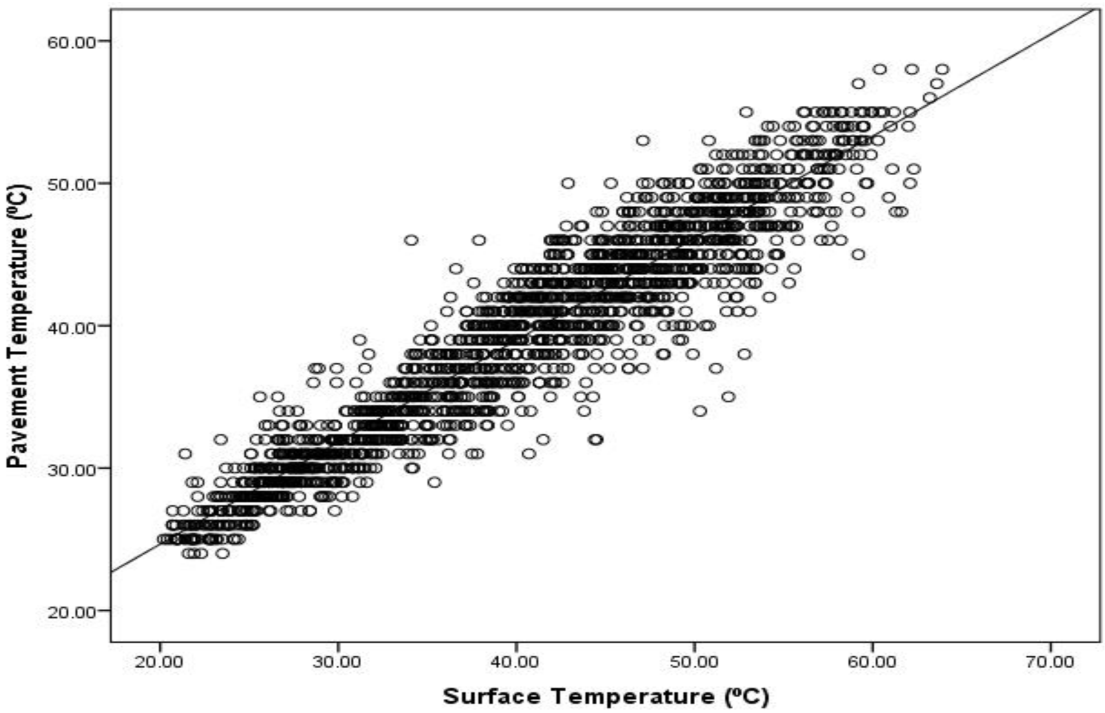

Figure 4.21. Mid-depth AC Temperature versus Surface Temperatures on the RSM Road (Tamale)

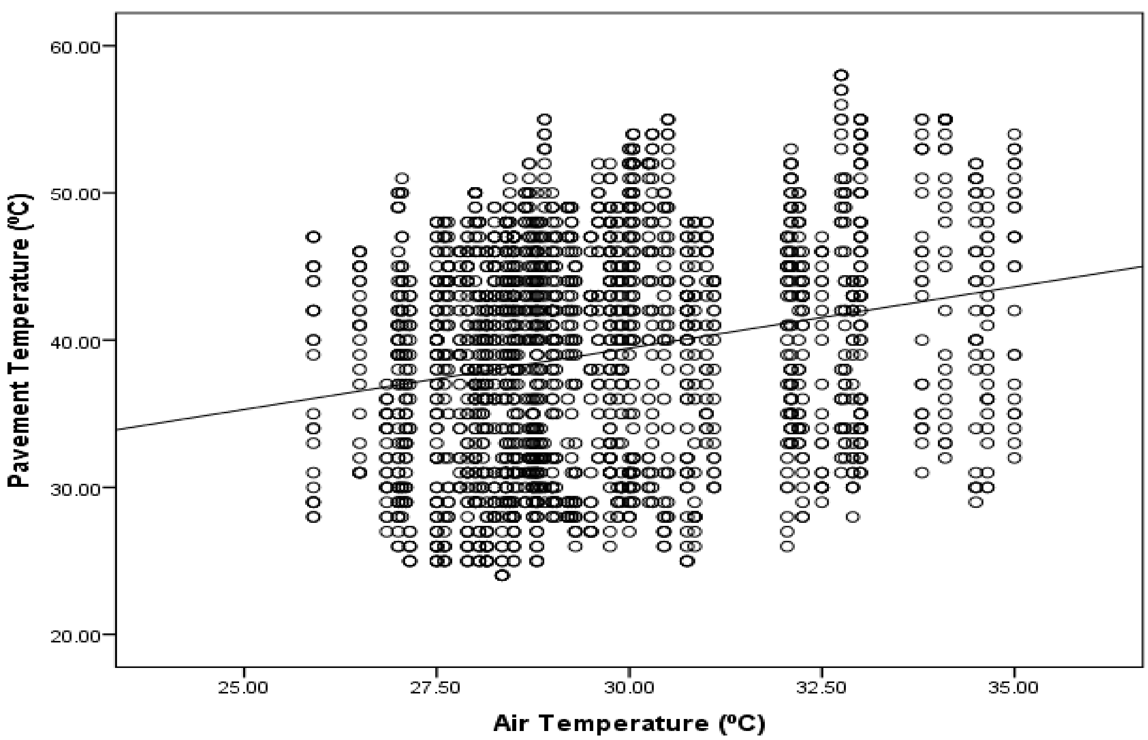

Figure 4.22. Mid-depth AC Temperature versus Air Temperature on the RSM Road (Tamale)

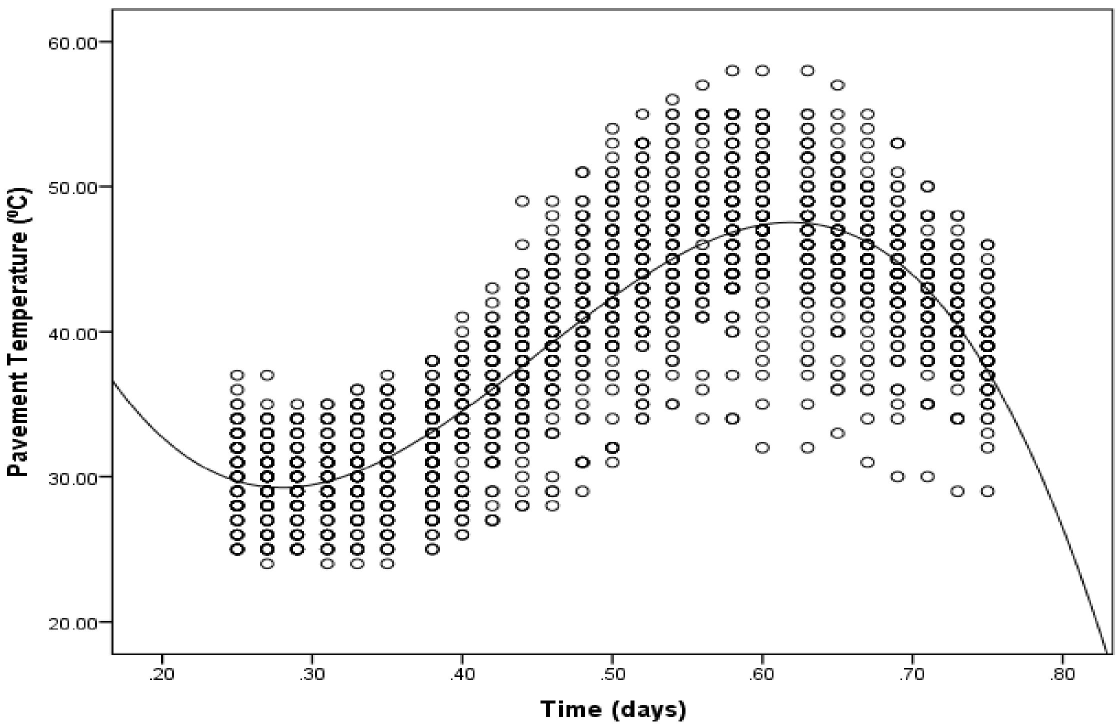

Figure 4.23. Mid-depth AC Temperature versus Time of Day on the RSM Road (Tamale)

The following independent variables were considered for predicting T_{35mm} in Tamale.

T_{sur} = pavement surface temperature (ºC)

T_{avg}= mean of the air temperature of the preceding day

$\sin(t)$ = sine of time (radians). Time (t) is a 24-hr time divided by 24 (days).

The model summary result for Tamale is shown in Table 4.11.

Table 4.11: Summary Statistics of Model Developed for Tamale

Regression Statistics	**Multiple R**	**R-square**	**Adj. R-sq.**	**SEE**	
	0.959	0.919	0.919	2.163	
ANOVA	**Degree of freedom**	**Sum of squares**	**Mean of squares**	**F statistic**	**P-value**
Regression	3	111625.2	37208.4	7952.0	0.000
Residual	2096	9807.5	4.7		
Total	2099	121432.7			
	Coefficients	**Standard error**	**t-statistic**	**VIF**	**P-value**
Intercept	2.644	0.700	3.777		0.000
T_{sur}	0.613	0.006	96.575	1.826	0.000
T_{avg}	0.22	0.024	9.324	1.078	0.000
$\sin(t)$	11.283	0.476	23.694	1.748	0.000

From Table 4.11**,** the adjusted R-square of 0.919 means that the independent variables (pavement surface temperature, mean air temperature of the preceding day, and time of pavement surface temperature measurement) explain about 92% of variation in the dependent variable (AC mid-depth pavement temperature). The variance inflation factor (VIF) of each predictor variable is approximately 1, suggesting that the variables are not correlated. The t-statistic of all the predictor variables yielded a p-value of < 0.0001, thus rejecting the null hypothesis that all the coefficients of the predictor variables are zero. It is then inferred that the linear combination of pavement surface temperature, mean air temperature of the preceding day and time of pavement surface temperature measurement significantly predict AC mid-depth pavement temperature in Tamale. The resulting regression equation for Tamale is given by Eq. (4.3).

$$\boldsymbol{T_{35mm} = 2.644 + 0.613\ (T_{sur}) + 0.22\ (T_{avg}) + 11.283\ \sin(t);}\quad R^2{=}0.919 \qquad (4.3)$$

where;

T_{35mm} = AC pavement temperature (ºC) at 35 mm from the surface

T_{sur} = pavement surface temperature (ºC)

t = time of pavement surface temperature measurement (24hrs divided by 24) (days).

T_{avg} = mean of air temperature (ºC) of the preceding day

The linear regression assumptions of normally distributed and equal variance of the residuals were investigated using a histogram (Figure 4.24) and a scatter plot (Figure 4.25). Figure 4.24 shows that the residuals follow the normal distribution, based on the bell shape curve. Also, the residuals have equal variance, as seen in Figure 4.25.

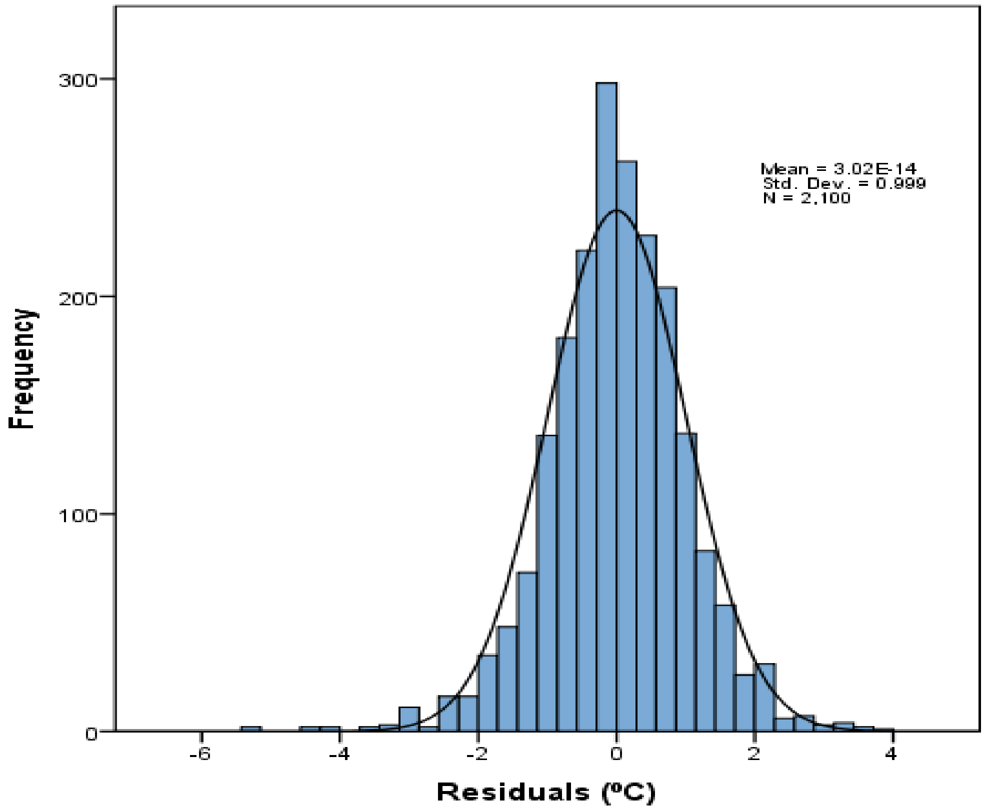

Figure 4.24. Distribution of Normalized Residual for the Tamale Model

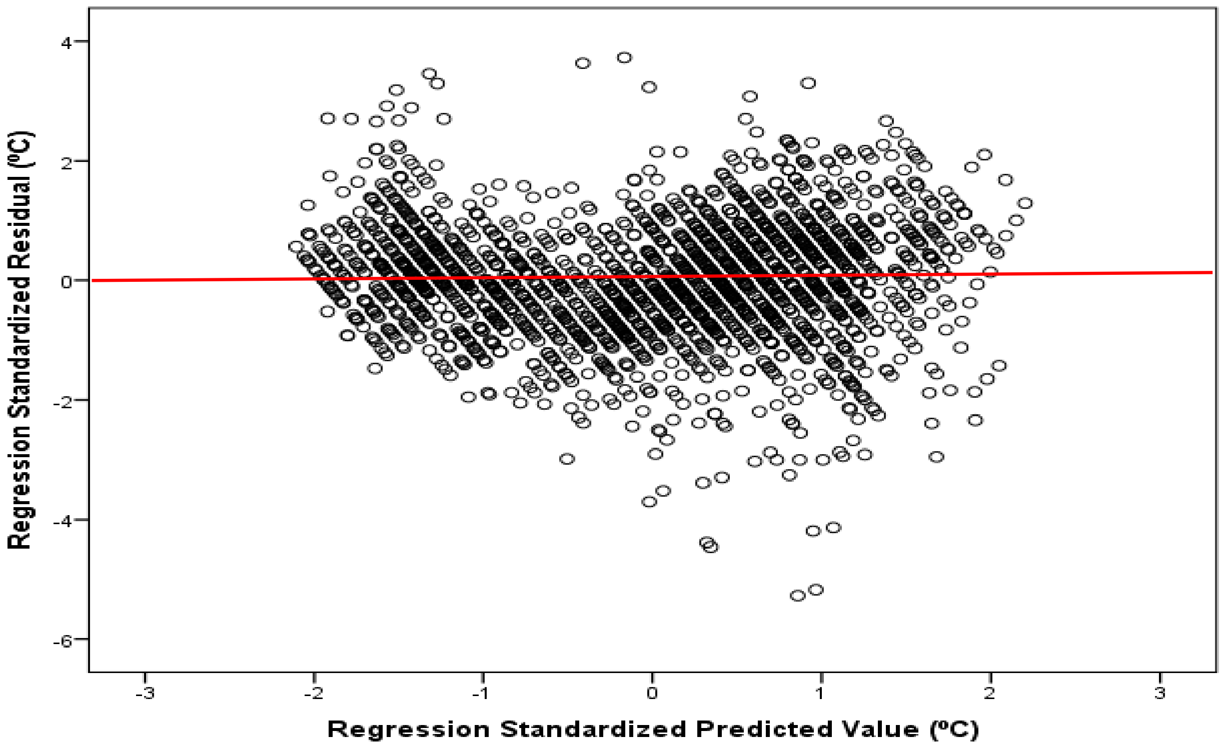

Figure 4.25. Standardised Residuals versus Predictor Values for the Tamale Model

Having satisfied the multiple linear regression assumptions and the high R^2, the proposed model for predicting mid-depth pavement temperature for the Savannah zone (Tamale) was deemed well-fitted.

D. Validation of the Tamale Model

A different dataset, collected from the Air Force Road in Tamale, was used to validate the newly-developed model. From Table 4.12, T_{sur} has a lower mean (40.8ºC) but with a large variability (Std. Dev. = 9.7 ºC) compared to T_{35mm} (mean = 41.1ºC, Std. dev. = 8.6ºC). T_{avg}, with a mean of 30.6ºC, was clustered around the mean (Std. Dev. = 2.1ºC).

Table 4.12. Descriptive Statistics of Validation Data for Tamale

Variable	N	Mean	Std. Dev.	COV (%)	Minimum	Maximum
T_{35mm}	700	41.1	8.6	20.9	25.0	58.0
T_{sur}	700	40.8	9.7	23.8	20.5	59.6
T_{avg}	700	30.6	2.1	6.9	26.9	34.5
t	700	0.5	0.2	40.0	0.25	0.75

In validating the model, a two-sample t-test was used to check if the means of the measured and predicted AC pavement temperatures were equal. A **p-value of 0.289** was obtained, which indicated that statistical parity existed between the means of the measured and anticipated AC pavement temperatures. The scatter plot in Figure 4.26 shows that the model predicts AC pavement temperatures at 35 mm with a high accuracy. The fitted model for Tamale had an R^2 of 0.920, RMSE of 2.679ºC, and MPE of 0.295%, which also indicates that the model has high accuracy.

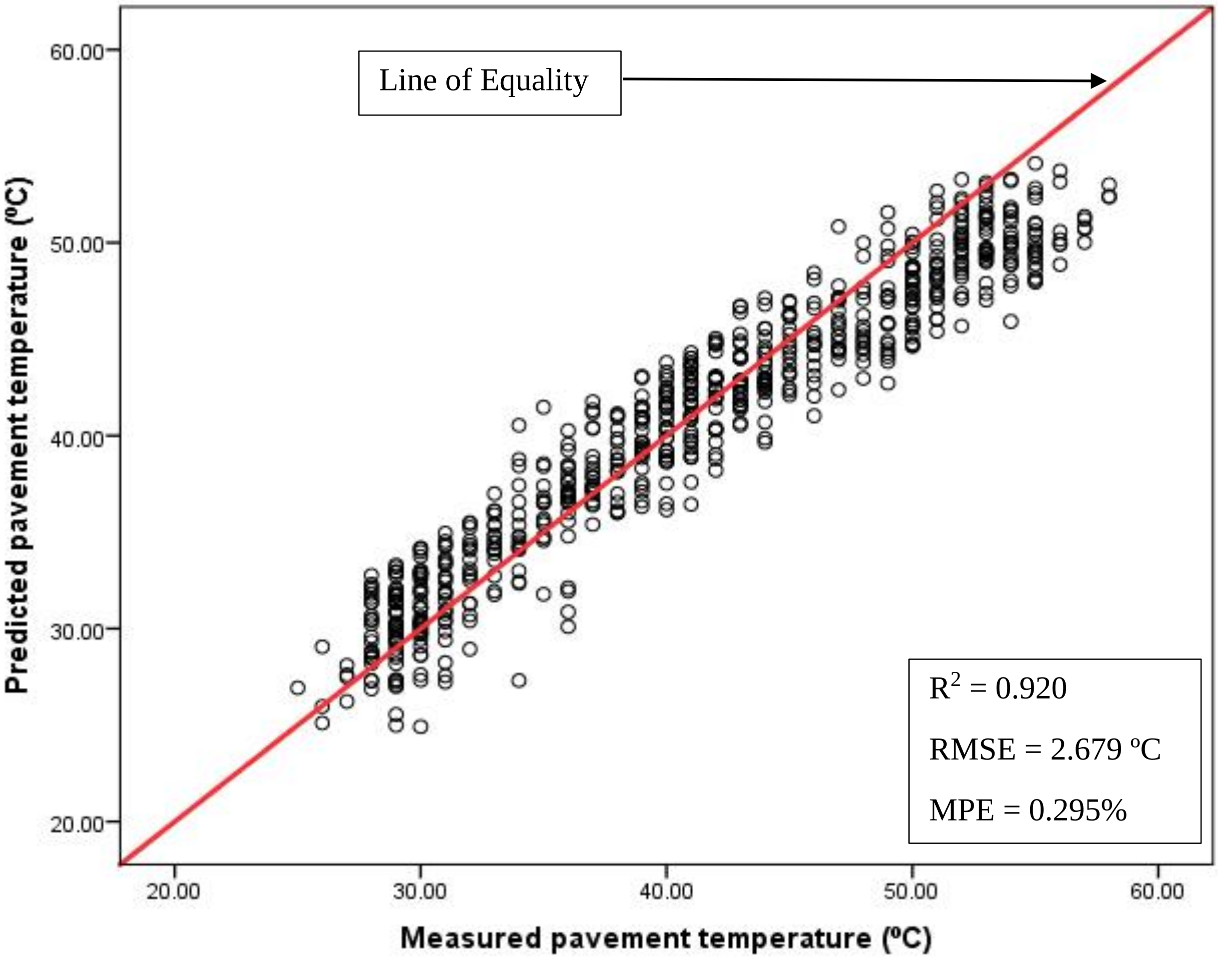

Figure 4.26. Tamale Model Validation: Measured versus Predicted Pavement Temperature

4.4 Performance Comparison of Proposed Models with Existing Ones

4.4.1 The Kumasi Model Versus Existing Models

To ensure a fair comparison of model prediction performance between the proposed Kumasi model and existing models, the validation data collected on the Antoa Road were used to validate the existing BELLS 3 and Park *et al*. (2001) models, and the results are presented in Table 4.13 and Figure 4.27. As shown in the table, the Kumasi model produced the lowest errors (RMSE, MPE and MBE), while the BELLS 3 (Lukanen *et al*., 2000) model recorded the highest R^2 value. Figure 4.27 reveals that the Kumasi model predictions were the closest to the measured temperature, compared with the BELLS 3 (Lukanen *et al*., 2000) and Park *et al*.

(2001) models. This observation confirmed that the Kumasi model has higher prediction accuracy than the BELLS 3 (Lukanen *et al*., 2000) and Park *et al*. (2001) models despite the highest R^2 value recorded by the BELLS 3 model.

Table 4.13. Comparison of the Kumasi Model with Some Existing Models

Model	**R^2**	**RMSE (ºC)**	**MPE (%)**	**MBE (ºC)**
Kumasi model	0.919	1.924	0.037	-0.173
BELLS 3 (Lukanen *et al*., 2000)	0.937	3.496	8.586	-3.105
Park *et al*. (2001)	0.899	2.388	2.481	-0.838

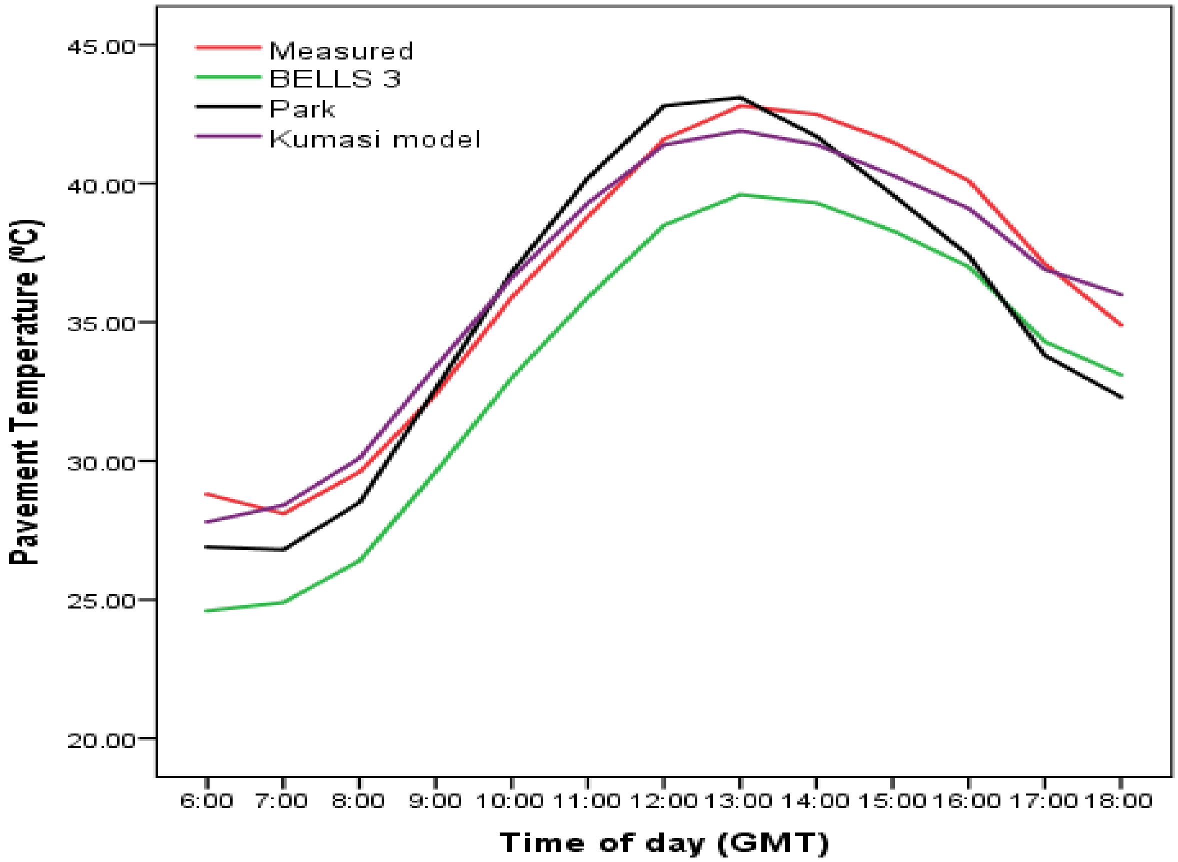

Figure 4.27. Measured and Predicted Mid-depth AC Temperatures: Some Existing Models and the Proposed Kumasi Model

4.4.2 The Tamale Model Versus Existing Models

The Tamale model was further validated by comparing its R^2 and errors (RMSE, MPE, and MBE) with those of the BELLS 3 (Lukanen *et al*., 2000) and Park *et al*. (2001) models, using the validation dataset collected on the Air Force Road. The results, shown in Table 4.14, indicated the Tamale model produced the lowest error levels, though the BELLS 3 (Lukanen *et al*., 2000) yielded the best R^2.

Table 4.14. Comparison of Some Existing Models Predictions with the Tamale Model

Model	**R^2**	**RMSE (ºC)**	**MPE (%)**	**MBE (ºC)**
Tamale model	0.920	2.679	0.295	-0.451
BELLS 3 (Lukanen *et al*., 2000)	0.940	4.557	9.807	-4.028
Park *et al*. (2001)	0.919	2.928	3.515	-1.332

However, Figure 4.28 shows that the pavement temperatures predicted by the fitted Tamale model were closest to measured temperatures, followed by the Park *et al*. (2001) model. This finding indicated the high prediction accuracy of the Tamale model compared with the BELLS 3 (Lukanen *et al*., 2000) and Park *et al*. (2001) models.

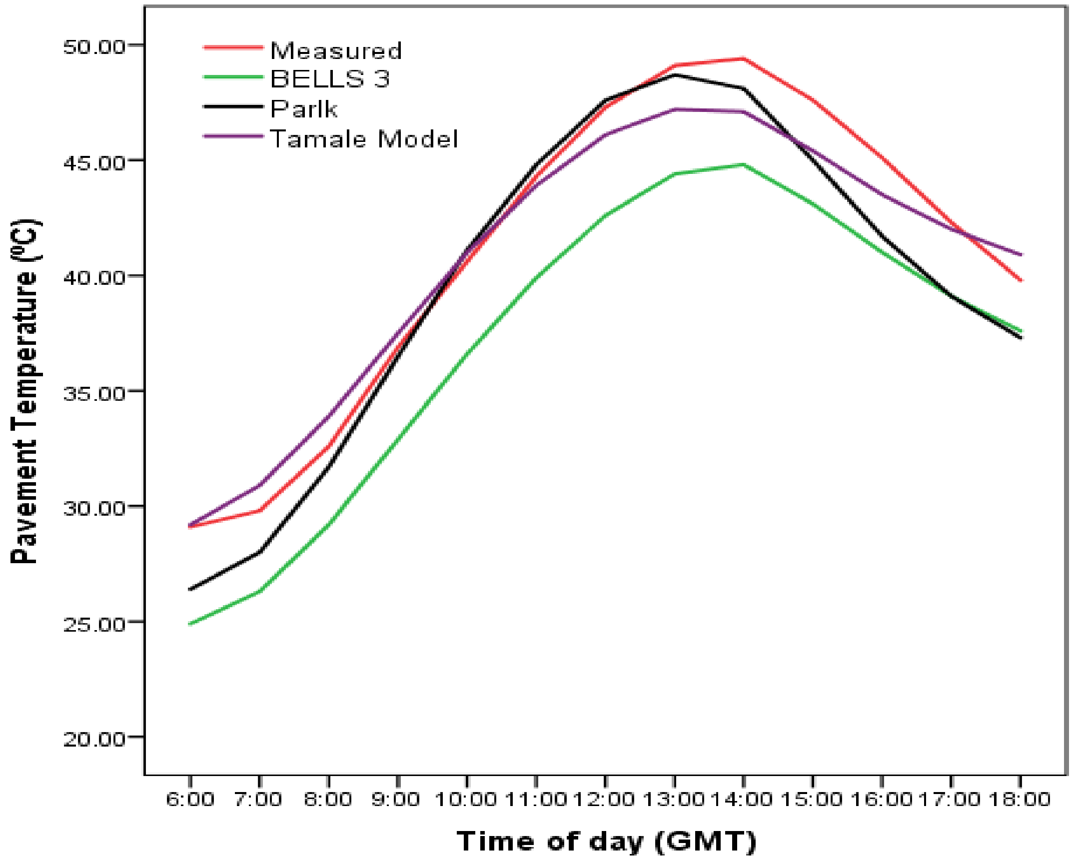

Figure 4.28. Measured versus Predicted Mid-depth AC Temperatures: Some Existing Models and the Proposed Tamale Model

4.4.3 Some Applications of Proposed Asphalt Pavement Temperature Prediction Models

This study is the first to develop and validate asphalt pavement temperature prediction models for different climatic zones in Ghana.

Potential applications of the proposed models include the following:

i. **Predicting mid-depth AC temperature for FWD data analysis**. Instead of manually measuring asphalt pavement temperatures from drilled holes during FWD testing, one can simply measure the pavement surface temperature with handheld infrared thermometer and record the time of the pavement surface temperature measurement. The mean air temperature of the previous day before the pavement surface temperature measurement is acquired and fed into the proposed models to predict the mid-depth AC temperature at given time of the day.

ii. **Superpave PG binder selection**. This will require the inputs of pavement surface temperature, mean preceding day's air temperature and time of surface temperature measurement for a minimum period of 20 years. This dataset will first be used to predict mid-depth AC temperature for different times of the day, and the daily maximum and minimum temperature determined for each year. Based on this, the 7-day moving average of the predicted daily maximum mid-depth AC temperature for each year is computed and the minimum for each year determined. The maximum pavement design temperature is the average of the yearly 7-day moving average for the entire duration of the data (minimum of 20 years).

iii. **Predicting asphalt pavement temperature to characterise long-term aging of asphalt concrete material**. This will require developing an aging model for Ghana (e.g., Zhang *et al*., 2019) before feeding the predicted pavement temperature, among other inputs, to characterize the asphalt mixture aging phenomenon.

iv. **Pavement Structural Design**. The proposed models could be used to determine monthly average asphalt pavement temperatures for various locations in the Forest and Savannah zones. The monthly pavement temperatures could then be used to predict monthly AC modulus for use in mechanistic-empirical pavement design systems.

v. **Asphalt Mixture Design**. The models could be used to investigate in-situ asphalt pavement temperatures to determine whether the current 60 ºC laboratory asphalt mixture conditioning temperature used for Marshall mix design needs revision for certain parts of the country.

CHAPTER 5: CONCLUSIONS AND RECOMMENDATIONS

5.1 Conclusions

This research sought to develop asphalt pavement temperature prediction models suitable for the Forest and Savannah climatic conditions of Ghana. The study established the state of practice of asphalt pavement temperature determination in Ghana, evaluated the prediction accuracy of selected foreign asphalt pavement temperature prediction models and developed new models. Based on the findings from this study, the following conclusions and recommendations are made.

a) Asphalt pavement temperature is determined manually in Ghana during FWD testing and is fraught with safety and delay challenges.

b) Of the six models evaluated using local data, the Park *et al*. (2001) model predicted mid-depth asphalt pavement temperatures for both the Forest and Savannah climatic zones of Ghana with relatively high accuracy up to about 47 ºC, beyond which there was either over-prediction or under-prediction.

c) The models developed in this study for the Forest zone (Kumasi) and the Savannah zone (Tamale) predicted mid-depth asphalt layer temperatures more accurately than any of the foreign-developed models evaluated using local data.

5.2 Recommendations

a) The proposed Kumasi models is recommended for predicting asphalt pavement temperature at a depth of about 38 mm in Forest climatic zone of Ghana based on its high prediction accuracy.

b) The proposed Tamale model is recommended for asphalt pavement temperature prediction at a depth of about 35 mm in the Savannah climatic zone of Ghana based on its high prediction accuracy.

5.3 Model Limitations and Future Research

a) The study was limited to a city each in the two climatic zones and also utilised in-situ pavement temperatures measured from asphalt layer mid-depths in the range of 35mm – 38 mm. Hence, the prediction accuracy of the models might not apply to asphalt layer depths significantly different from this range.
b) The models developed in the study may predict pavement temperatures accurately during daytime (6:00 GMT to 18:00 GMT) only.
c) Future attempts to improve the proposed models should include data from additional cities in all the climatic zones (Forest, Savannah and Coastal) and at different pavement depths and on aged asphalt pavements.
d) The pavement temperature data should be collected over a period longer than one year.
e) A study should be conducted to examine the prediction accuracy of the proposed models by using data from old pavements and shady areas.

REFERENCES

AASHTO (2015) *Mechanistic–Empirical Pavement Design Guide.* Second ed., *American Association of State Highway and Transportation Officials*. Second ed. United States of America: AASHTO.

Abbas, A.S. (2017) 'Temperature Zonging of Irag for asphalt mix design', *Journal of Engineering and Sustainable Development*, 21(5), pp. 54–63.

Alavi, M.Z., Pouranian, M.R. and Hajj, E.Y. (2014) 'Prediction of asphalt pavement temperature profile with finite control volume method', *Transportation Research Record*, 2456(2456), pp. 96–106. Available at: https://doi.org/10.3141/2456-10.

Alawi, M.H. and Helal, M.M. (2012) 'Mathematical modelling for solving nonlinear heat diffusion problems of pavement spherical roads in Makkah', *International Journal of Pavement Engineering*, 13(2), pp. 137–151. Available at: https://doi.org/10.1080/10298436.2011.633166.

Alshenqeeti, H. (2014) 'Interviewing as a Data Collection Method: A Critical Review', *English Linguistics Research*, 3(1), pp. 39–45. Available at: https://doi.org/10.5430/elr.v3n1p39.

Arulanandan, K., Turnbridge, H.D. and Saffo, A.O. (1963) 'A climatological approach to the estimation of moisture conditions under road paveemnts in Ghana.', *Journal of Science*, 3(1), pp. 66–75.

Aryee, J.N.A., Amekudzi, L.K., Quansah, E., Klutse, N.A.B., Atiah, W.A. and Yorke, C. (2018) 'Development of high spatial resolution rainfall data for Ghana', *International Journal of Climatology*, 38(3), pp. 1201–1215. Available at: https://doi.org/10.1002/joc.5238.

Asefzadeh, A., Hashemian, L. and Bayat, A. (2017) 'Development of statistical temperature prediction models for a test road in Edmonton, Alberta, Canada', *International Journal of Pavement Research and Technology*, 10(5), pp. 369–382. Available at: https://doi.org/10.1016/j.ijprt.2017.05.004.

Asi, I.M. (2007) 'Performance evaluation of SUPERPAVE and Marshall asphalt mix designs to suite Jordan climatic and traffic conditions', *Construction and Building Materials*, 21(8), pp. 1732–1740. Available at: https://doi.org/10.1016/j.conbuildmat.2006.05.036.

Asilevi, P.J., Quansah, E., Amekudzi, L.K., Annor, T. and Klutse, N.A.B. (2019) 'Modeling the spatial distribution of Global Solar Radiation (GSR) over Ghana using the Ångström-Prescott sunshine duration model', *Scientific African*, 4(May), p. e00094. Available at: https://doi.org/10.1016/j.sciaf.2019.e00094.

Ayasrah, U.B., Tashman, L., AlOmari, A. and Asi, I. (2023) 'Development of a temperature prediction model for flexible pavement structures', *Case Studies in Construction Materials*, 18(November 2022), p. e01697. Available at: https://doi.org/10.1016/j.cscm.2022.e01697.

Barber, E.S. (1957) 'Calculation of maximum pavement temperatures from weather reports', *Highway Research Board*, 168(3), pp. 1–8.

Beecroft, A. (2019) *Investigation of Asphalt Pavement Temperatures in WA Final Report*. Perth, Western Australia.

Bessah, E., Amponsah, W., Ansah, S.O., Afrifa, A., Yahaya, B., Wemegah, C.S., Tanu, M., Amekudzi, L.K. and Agyare, W.A. (2022) 'Climatic zoning of Ghana using selected meteorological variables for the period 1976–2018', *Meteorological Applications*, 29(1), pp. 0–15. Available at: https://doi.org/10.1002/met.2049.

Bluman, A. (2012) *Elementary Statistics: A Step by Step Approach*. 8th ed. New York: MCGraw-Hill. Available at: https://www.ptonline.com/articles/how-to-get-better-mfi-results.

Braun, V. and Clarke, V. (2013) *Successful qualitative research: A practical guide for beginners*. London, UK: SAGE.

Breakah, T.M., Williams, R.C., Herzmann, D.E. and Takle, E.S. (2011) 'Effects of Using Accurate Climatic Conditions for Mechanistic-Empirical Pavement Design', *Journal of Transportation Engineering*, 137(1), pp. 84–90. Available at: https://doi.org/10.1061/(ASCE)TE.1943-5436.0000195.

Bryce, J. and Ihnat, Z. (2020) 'Improved models of solar radiation and convective heat transfer for pavement temperature prediction', *International Journal of Pavement Engineering*, pp. 1–12. Available at: https://doi.org/10.1080/10298436.2020.1843037.

Carnielo, E. and Zinzi, M. (2013) 'Optical and thermal characterisation of cool asphalts to mitigate urban temperatures and building cooling demand', *Building and Environment*, 60, pp. 56–65. Available at: https://doi.org/10.1016/j.buildenv.2012.11.004.

Cengel, Y.A. (2003) *Heat Transference: A Practical Approach*. 2nd ed. New York: McGraw-Hill. Available at: http://dx.doi.org/10.1007/978-3-642-20279-7_5.

Chandrappa, A.K. and Biligiri, K.P. (2016) 'Development of Pavement-Surface Temperature Predictive Models: Parametric Approach', *Journal of Materials in Civil Engineering*, 28(3). Available at: https://doi.org/10.1061/(asce)mt.1943-5533.0001415.

Chang, J.-R., Lin, J.-D., Chung, W.-C. and Chen, D.-H. (2002) 'Evaluating the Structural Strength of Flexible Pavements in Taiwan Using the Falling Weight Deflectometer', *International Journal of Pavement Engineering*, 3(3), pp. 131–141. Available at: https://doi.org/10.1080/1029843021000067854.

Chen, D.H., Bilyeu, J., Lin, H.H. and Murphy, M. (2000) 'Temperature correction on falling weight deflectometer measurements', *Transportation Research Record*, (1716), pp. 30–39. Available at: https://doi.org/10.3141/1716-04.

Chen, J. qi, Li, L. and Wang, H. (2015) 'Analytical prediction and field validation of transient temperature field in asphalt pavements', *Journal of Central South University*, 22(12), pp. 4872–4881. Available at: https://doi.org/10.1007/s11771-015-3039-z.

Chen, J., Wang, H. and Xie, P. (2019) 'Pavement temperature prediction: Theoretical models and critical affecting factors', *Applied Thermal Engineering*, 158(December 2018). Available at: https://doi.org/10.1016/j.applthermaleng.2019.113755.

Chen, J., Wang, H. and Zhu, H. (2017) 'Analytical approach for evaluating temperature field of thermal modified asphalt pavement and urban heat island effect', *Applied Thermal Engineering*, 113, pp. 739–748. Available at: https://doi.org/10.1016/j.applthermaleng.2016.11.080.

Chowdhury, T. and Hossain, M. (1999) *Use of Falling Weight Deflectometer Data for Assessing Pavement Structural Values. Final Report*. Topeka, Kansas.

Cresswell, J.W. and Cresswell, J.D. (2018) *Research Design: Qualitative, Quantitative, and Mixed Methods Approaches*. 5th edn. Los Angeles: SAGE.

Denneman, E., Edmunds, A., Alex, P. and Wilson, G. (2022) 'Application of pavement temperature prediction algorithms in performance grade (PG) binder selection for Australia', *Australian Journal of Civil Engineering*, 00(00), pp. 1–9. Available at: https://doi.org/10.1080/14488353.2022.2082632.

Dickson, K.B. and Benneh, G. (1988) *A review of geography of Ghana*. Revised Ed. London: Longman Group UK Limited.

Diefenderfer, B.K., Al-Qadi, I.L. and Diefenderfer, S.D. (2006) 'Model to predict pavement temperature profile: Development and validation', *Journal of Transportation Engineering*, 132(2), pp. 162–167. Available at: https://doi.org/10.1061/(ASCE)0733-947X(2006)132:2(162).

FAO (2006) *Fertilizer Use by Crop - Fertiliser and Plant Nutrition Bulletin*. Rome.

Feng, D., Yi, J. and Wang, D. (2013) 'Performance and Thermal Evaluation of Incorporating Waste Ceramic Aggregates in Wearing Layer of Asphalt Pavement', *Journal of Materials in Civil Engineering*, 25(7), pp. 857–863. Available at: https://doi.org/10.1061/(asce)mt.1943-5533.0000788.

Fernando, E.G., Wenting Liu and Ryu, D. (2001) *Development of a Procedure for Temperature Correction of Backcalculated AC Modulus*. Austin, Texas.

Gedafa, D.S., Hossain, M. and Romanoschi, S.A. (2014) 'Perpetual pavement temperature prediction model', *Road Materials and Pavement Design*, 15(1), pp. 55–65. Available at: https://doi.org/10.1080/14680629.2013.852610.

Ghalandari, T., Shi, L., Sadeghi-khanegah, F. and Den, W. Van (2023) 'Case Studies in Construction Materials Utilizing artificial neural networks to predict the asphalt pavement profile temperature in western Europe', *Case Studies in Construction Materials*, 18(March), p. e02130. Available at: https://doi.org/10.1016/j.cscm.2023.e02130.

Ghasemi, A. and Zahediasl, S. (2012) 'Normality tests for statistical analysis: A guide for non-statisticians', *International Journal of Endocrinology and Metabolism*, 10(2), pp. 486–489. Available at: https://doi.org/10.5812/ijem.3505.

Gidigasu, M.D. (1972) 'Mode of formation and geotechnical characteristics of laterite materials of Ghana in relation to soil forming factors', *Engineering Geology*, 6(2), pp. 79–150. Available at: https://doi.org/10.1016/0013-7952(72)90034-8.

Gubrium, J.F. and Holstein, J.A. (2002) *Handbook of Interview Research: Context and Method*. Thousand Oaks CA: SAGE.

Gui, J.G., Phelan, P.E., Kaloush, K.E. and Golden, J.S. (2007) 'Impact of Pavement Thermophysical Properties on Surface Temperatures', *Journal of Materials in Civil Engineering*, 19(8), pp. 683–690.

Han, R., Jin, X. and Glover, C.J. (2011) 'Modeling Pavement Temperature for Use in Binder Oxidation Models and Pavement Performance Prediction', *Journal of Materials in Civil Engineering*, 23(4), pp. 351–359. Available at: https://doi.org/10.1061/(asce)mt.1943-5533.0000169.

Hasan, M.A. and Tarefder, R.A. (2017) 'Development of temperature zone map for mechanistic empirical (ME) pavement design', *International Journal of Pavement Research and Technology*, pp. 1–13. Available at: https://doi.org/10.1016/j.ijprt.2017.09.012.

Hermansson, Å. (2001) ‘Mathematical Model for Calculation of Pavement Temperatures’, *Transportation Research Record*, 1764(Paper No. 01-3543), pp. 180–188.

Ho, C. and Romero, P. (2009) ‘Low Design Temperatures of Asphalt Pavements in Dry – Freeze Regions Predicting by Means of Solar Radiation , Transient Heat Transfer, and Finite Element Method’, *Transportation Research Record*, (2127), pp. 60–71. Available at: https://doi.org/10.3141/2127-08.

Houston, W.N., Mirza, M.W. and Zapata, C.E. (2006) *Environmental Effects in Pavement Mix and Structural Design Systems. Calibration and Validation of the ICM Version 2.6. Preliminary Draft Final Report Part 2.* Tempe, AZ.

Huang, K., Zollinger, D.G., Shi, X. and Sun, P. (2017) ‘A developed method of analyzing temperature and moisture profiles in rigid pavement slabs’, *Construction and Building Materials*, 151, pp. 782–788. Available at: https://doi.org/10.1016/j.conbuildmat.2017.06.120.

Huber, G. a. (1994) *Weather Database for the SUPERPAVE Mix Design System. SHRP-A-648A*. Washington, D.C.

Ibili, F., Owolabi, A.O., Ackaah, W. and Ballack, A. (2022) ‘Statistical modelling for urban roads traffic noise levels’, *Scientific African*, 15, p. e01131. Available at: https://doi.org/10.1016/j.sciaf.2022.e01131.

Idham, M.K., Hainin, M.R., Yaacob, H., Warid, M.N.M. and Abdullah, M.E. (2013) ‘Effect of aging on resilient modulus of hot mix asphalt mixtures’, *Advanced Materials Research*, 723, pp. 291–297. Available at: https://doi.org/10.4028/www.scientific.net/AMR.723.291.

Islam, M.R., Ahsan, S. and Tarefder, R.A. (2015) ‘Modeling temperature profile of hot-mix asphalt in flexible pavement’, *International Journal of Pavement Research and Technology*, 8(1), pp. 47–52. Available at: https://doi.org/10.6135/ijprt.org.tw/2015.8(1).47.

Kassem, E., Bayomy, F.M.S., Williams, C., Saasita, E., Lamichane, S. and Permadi, D.D. (2020) *Development of Pavement Temperature Prediction Model, Report No. FHWA-ID-20-279*. Moscow, Idaho.

Kennedy, T.W., Huber, G.A., Harrigan, E.T., Cominsky, R.J., Hughes, C.S., Quintus, H. Von and Moulthrop, J.S. (1994) *Superior Performing Asphalt Pavements (Superpave): The Product of the SHRP Asphalt Research Program. Report SHRP-A-410*. Washington, D.C.

Khalil, S.A. and Shaffie, A.M. (2013) ‘Performance of Statistical Comparison Models of Solar Energy on Horizontal and Inclined Surface’, *International Journal of Energy and Power*, 2(1), pp. 8–25.

Khan, Z.H., Islam, M.R. and Tarefder, R.A. (2019) ‘Determining asphalt surface temperature using weather parameters’, *Journal of Traffic and Transportation Engineering (English Edition)*, 6(6), pp. 577–588. Available at: https://doi.org/10.1016/j.jtte.2018.04.005.

Klutse, N.A.B., Owusu, K., Adukpo, D.C., Nkrumah, F., Quagraine, K., Owusu, A. and Gutowski, W.J. (2013) ‘Farmer’s observation on climate change impacts on maize (Zea mays) production in a selected agro- ecological zone in Ghana’, *Research Journal of Agriculture and Environmental Management*, 2(12), pp. 394–402.

Koranteng-Yorke, J.B. (2012) *Proposed Framework for Asphaltic Concrete Pavement Design for Tropical Soils - Case Study of Ghana. A thesis submitted to the University of Birmingham for the degree of Doctor of Philosophy.* University of Birmingham.

Koranteng-Yorke, J.B. (2016) *Asphaltic Concrete Pavement Design Incorporating Life Cycle Analysis: Case Study of Benin*. Mombasa, Kenya.

Koranteng-Yorke, J.B., Ghataora, G. and Odoki, J. (2015) 'Rational approach for tropical pavement design using life-cycle principles: Case study of Ghana', *International Journal of Pavement Engineering*, 16(8), pp. 667–683. Available at: https://doi.org/10.1080/10298436.2014.943218.

Lee, J.S., Kim, J.H., Kwon, O.S. and Lee, B.D. (2018) 'Asphalt binder performance grading of North Korea for Superpave asphalt mix-design', *International Journal of Pavement Research and Technology*, 11(6), pp. 647–654. Available at: https://doi.org/10.1016/j.ijprt.2018.06.004.

Lekea, A. and Steyn, W.J. (2023) 'Performance of Pavement Temperature Prediction Models', *Applied Sciences*, 13(4164), pp. 1–12. Available at: https://doi.org/10.4324/9781315232140-14.

Li, H., Harvey, J. and Jones, D. (2014) 'Development and preliminary validation of integrated local microclimate model for numerical evaluation of cool pavement strategies', *Transportation Research Record*, 2444, pp. 151–164. Available at: https://doi.org/10.3141/2444-17.

Li, H., Harvey, J. and Kendall, A. (2013) 'Field measurement of albedo for different land cover materials and effects on thermal performance', *Building and Environment*, 59, pp. 536–546. Available at: https://doi.org/10.1016/j.buildenv.2012.10.014.

Li, Y., Liu, L. and Sun, L. (2018) 'Temperature predictions for asphalt pavement with thick asphalt layer', *Construction and Building Materials*, 160, pp. 802–809. Available at: https://doi.org/10.1016/j.conbuildmat.2017.12.145.

Lukanen, E.O., Stubstad, R. and Briggs, R. (2000) *Temperature Predictions and Adjustment Factors for Asphalt Pavement. Publication no. FHWA-RD-98-085*. McLean, VA.

Manikkunambi, M.C.R., Athukorallage, B., Senadheera, S. and James, D. (2023) 'Case Studies in Construction Materials Temporal and spatial temperature predictions for flexible pavement layers using numerical thermal analysis and verified with large datasets', *Case Studies in Construction Materials*, 18(March), p. e02008. Available at: https://doi.org/10.1016/j.cscm.2023.e02008.

Marchetti, M., Chapman, L., Khalifa, A. and Buès, M. (2014) 'New Role of Thermal Mapping in Winter Maintenance with Principal Components Analysis', *Advances in Meteorology*, 2014, pp. 1–11. Available at: https://doi.org/10.1155/2014/254795.

Marchetti, M., Khalifa, A. and Bues, M. (2015) 'Methodology to forecast road surface temperature with principal components analysis and partial least-square regression: Application to an urban configuration', *Advances in Meteorology*, 2015, pp. 1–10. Available at: https://doi.org/10.1155/2015/562621.

Marshall, C., Meier, R. and Welch, M. (2001) 'Seasonal temperature effects on flexible pavements in Tennessee', *Transportation Research Record*, (1764), pp. 89–96. Available at: https://doi.org/10.3141/1764-10.

Milad, A., Adwan, I., Majeed, S.A., Memon, Z.A., Bilema, M., Omar, H.A., Abdolrasol, M.G.M., Usman, A. and Yusoff, N.I.M. (2021) 'Development of a Hybrid Machine Learning Model for Asphalt Pavement Temperature Prediction', *IEEE Access*, 9, pp. 158041–158056.

Available at: https://doi.org/10.1109/ACCESS.2021.3129979.

Milad, A., Adwan, I., Majeed, S.A., Yusoff, N.I.M., Al-Ansari, N. and Yaseen, Z.M. (2021) ‘Emerging Technologies of Deep Learning Models Development for Pavement Temperature Prediction’, *IEEE Access*, 9, pp. 23840–23849. Available at: https://doi.org/10.1109/ACCESS.2021.3056568.

Minhoto, M.J.C., Pais, J.C., Pereira, P.A.A. and Picado-santos, L.G. (2005) ‘with a Three-Dimensional Finite Element Method’, *Transportation Research Record*, (1919), pp. 96–110. Available at: http://trb.metapress.com/content/060716883r685171/.

Mirza, M.W., Abbas, Z. and Rizvi, M.A. (2011) ‘Temperature Zoning of Pakistan for Asphalt Mix Design’, *Pakistan Journal of Engineering & Applied Science*, 8, pp. 49–60.

MOFA (2016) *Agriculture in Ghana. Facts and Figures (2015).* Accra, Ghana. Available at: http://www.agrofood-westafrica.com/fileadmin/user_upload/messen/agrofood-Westafrica/Brochure/AGRICULTURE-IN-GHANA-Facts-and-Figures-2015.pdf%0Ahttp://cairngorms.co.uk/discover-explore/facts-figures/.

Mohseni, A. (1998) *LTPP Seasonal Asphalt Concrete (AC) Pavement Temperature Models. FHWA-RD-97-103*. McLean, VA.

Nuijten, A.D.W. (2016) ‘Runway temperature prediction, a case study for Oslo Airport, Norway’, *Cold Regions Science and Technology*, 125, pp. 72–84. Available at: https://doi.org/10.1016/j.coldregions.2016.02.004.

Papagiannakis, A.T. (2013) ‘Mechanistic-empirical pavement design; A brief overview’, *Geotechnical Engineering*, 44(1), pp. 75–82.

Park, D., Buch, N. and Chatti, K. (2001) ‘Effective Layer Temperature Prediction Model and Temperature Correction via Falling Weight Deflectometer Deflections’, *Transportation Research Record*, 1764, pp. 97–111.

Pomerantz, M., Pon, B., Akbari, H. and Chang, S.-C. (2000) *The Effect of Pavements’ Temperatures on Air Temperatures in Large Cities*. Berkeley, CA.

Qin, Y. (2016) ‘Pavement surface maximum temperature increases linearly with solar absorption and reciprocal thermal inertial’, *International Journal of Heat and Mass Transfer*, 97, pp. 391–399. Available at: https://doi.org/10.1016/j.ijheatmasstransfer.2016.02.032.

Qin, Y. and Hiller, J.E. (2011) ‘Modeling temperature distribution in rigid pavement slabs: Impact of air temperature’, *Construction and Building Materials*, 25(9), pp. 3753–3761. Available at: https://doi.org/10.1016/j.conbuildmat.2011.04.015.

Qin, Y., Zhang, X., Tan, K. and Wang, J. (2022) ‘A review on the influencing factors of pavement surface temperature’, *Environmental Science and Pollution Research* [Preprint], (August). Available at: https://doi.org/10.1007/s11356-022-22295-3.

Qu, S.Q. and Dumay, J. (2011) ‘The qualitative research interview’, *Qualitative Research in Accounting and Management*, 8(3), pp. 238–264. Available at: https://doi.org/10.1108/11766091111162070.

Quansah, E., Amekudzi, L.K., Preko, K., Aryee, J., Boakye, O.R., Boli, D. and Salifu, M.R. (2014) ‘Empirical Models for Estimating Global Solar Radiation over the Ashanti Region of Ghana’, *Journal of Solar Energy*, 2014, pp. 1–6. Available at: https://doi.org/10.1155/2014/897970.

Rigabadi, A., Rezaei Zadeh Herozi, M. and Rezagholilou, A. (2021) ‘An attempt for development of pavements temperature prediction models based on remote sensing data and artificial neural network’, *International Journal of Pavement Engineering*, 23(9), pp. 2912–2921. Available at: https://doi.org/10.1080/10298436.2021.1873334.

Roulston, K. and Choi, M. (2018) ‘Qualitative Interview’, in U. Flick (ed.) *The SAGE Handbook of Qualitative Data Collection*. London: SAGE, pp. 233–249.

Roulston, K., DeMarrais, K. and Lewis, J.B. (2003) ‘Learning to Interview in the Social Sciences’, *Qualitative Inquiry*, 9(4), pp. 643–668. Available at: https://doi.org/10.1177/1077800403252736.

SAGE (2019) ‘Thematic Analysis of Interview Data in the Context of Management Controls Research’, *SAGE Research Methods Datasets*, 2. Available at: https://doi.org/10.4135/9781526474858.

Saliko, D., Ahmed, A. and Erlingsson, S. (2023) ‘Development and validation of a pavement temperature profile prediction model in a mechanistic-empirical design framework’, *Transportation Geotechnics*, 40(March), p. 100976. Available at: https://doi.org/10.1016/j.trgeo.2023.100976.

Shrestha, N. (2020) ‘Detecting Multicollinearity in Regression Analysis’, *American Journal of Applied Mathematics and Statistics*, 8(2), pp. 39–42. Available at: https://doi.org/10.12691/ajams-8-2-1.

Sirin, O., Paul, D.K. and Kassem, E. (2018) ‘State of the Art Study on Aging of Asphalt Mixtures and Use of Antioxidant Additives’, *Advances in Civil Engineering*, 2018, pp. 1–18. Available at: https://doi.org/10.1155/2018/3428961.

Solaimanian, M. and Kennedy, T.W. (1993) ‘Predicting Maximum Pavement Surface Temperature Using Maximum Air Temperature and Hourly Solar Radiation’, *Transportation Research Record*, (1417), pp. 1–11.

Solatifar, N., Abbasghorbani, M., Kavussi, A. and Sivilevičius, H. (2018) ‘Prediction of depth temperature of asphalt layers in hot climate areas’, *Journal of Civil Engineering and Management*, 24(7), pp. 516–525. Available at: https://doi.org/10.3846/jcem.2018.6162.

Swarna, S.T. and Hossain, K. (2022) ‘Asphalt binder selection for future Canadian climatic conditions using various pavement temperature prediction models’, *Road Materials and Pavement Design* [Preprint]. Available at: https://doi.org/10.1080/14680629.2021.2019093.

Taamneh, M. (2016) ‘Temperature profile prediction for flexible pavement structures’, *HKIE Transactions Hong Kong Institution of Engineers*, 23(3), pp. 150–156. Available at: https://doi.org/10.1080/1023697X.2016.1201439.

Tabrizi, S.E., Xiao, K., Van Griensven Thé, J., Saad, M., Farghaly, H., Yang, S.X. and Gharabaghi, B. (2021) ‘Hourly road pavement surface temperature forecasting using deep learning models’, *Journal of Hydrology*, 603(May), pp. 1–10. Available at: https://doi.org/10.1016/j.jhydrol.2021.126877.

Teltayev, B.B., Aitbayev, K. and Ablaliyev, S.A. (2016) ‘Modeling of transient temperature distribution in multilayer asphalt pavement’, *International Journal of Pure and Applied Mathematics*, 108(3), pp. 709–722. Available at: https://doi.org/10.12732/ijpam.v108i3.18.

Tsai, B.-W. and Wu, R. (2009) *Mn/Road Case Study Using CalBack and CalME*. Davis, California.

Tutu, K.A., Ntramah, S. and Tuffour, Y.A. (2022) ‘Superpave performance graded asphalt binder selection for asphalt mixture design in Ghana’, *Scientific African*, 17, p. e01348. Available at: https://doi.org/10.1016/j.sciaf.2022.e01348.

Ullidtz, P., Harvey, J., Basheer, I., Jones, D., Wu, R., Lea, J. and Lu, Q. (2010) ‘CalME, a mechanistic-empirical program to analyze and design flexible pavement rehabilitation’, *Transportation Research Record*, (2153), pp. 143–152. Available at: https://doi.org/10.3141/2153-16.

Viljoen, A. (2001) *Estimating Asphalt Temperatures from Air Temperatures and Basic Sky Parameters*. Pretoria, South Africa.

Walia, A., Rastogi, R., Kumar, P. and Jain, S.S. (2022) ‘Development of a temperature prediction model for asphalt pavements considering air temperature data of preceding hours’, *International Journal of Pavement Engineering*, pp. 1–17. Available at: https://doi.org/10.1080/10298436.2022.2132245.

Wang, D. (2012) ‘Analytical Approach to Predict Temperature Profile in a Multilayered Pavement System Based on Measured Surface Temperature Data’, *Journal of Transportation Engineering*, 138(5), pp. 674–679. Available at: https://doi.org/10.1061/(ASCE)TE.1943-5436.0000362.

Wang, D. (2013) ‘Prediction of asphalt pavement temperature profile during fwd testing: Simplified analytical solution with model validation based on LTPP data’, *Journal of Transportation Engineering*, 139(1), pp. 109–113. Available at: https://doi.org/10.1061/(ASCE)TE.1943-5436.0000449.

Wang, D. (2015) ‘Simplified Analytical Approach to Predicting Asphalt Pavement Temperature’, *Journal of Materials in Civil Engineering*, 27(12), pp. 1–7. Available at: https://doi.org/10.1061/(asce)mt.1943-5533.0000826.

Wang, D. (2016) ‘Prediction of time-dependent temperature distribution within the pavement surface layer during FWD testing’, *Journal of Transportation Engineering*, 142(7), pp. 1–5. Available at: https://doi.org/10.1061/(ASCE)TE.1943-5436.0000854.

Wang, D. and Roesler, J.R. (2014) ‘One-dimensional temperature profile prediction in multi-layered rigid pavement systems using a separation of variables method’, *International Journal of Pavement Engineering*, 15(5), pp. 373–382. Available at: https://doi.org/10.1080/10298436.2011.653358.

Wang, D., Roesler, J.R. and Guo, D.-Z. (2009) ‘Analytical Approach to Predicting Temperature Fields in Multilayered Pavement Systems’, *Journal of Engineering Mechanics*, 135(4), pp. 334–344. Available at: https://doi.org/10.1061/(asce)0733-9399(2009)135:4(334).

Wistuba, M.P. and Walther, A. (2013) ‘Consideration of climate change in the mechanistic pavement design’, *Road Materials and Pavement Design*, 14(SUPPL.1), pp. 227–241. Available at: https://doi.org/10.1080/14680629.2013.774759.

Xu, B., Dan, H.C. and Li, L. (2017) ‘Temperature prediction model of asphalt pavement in cold regions based on an improved BP neural network’, *Applied Thermal Engineering*, 120, pp. 568–580. Available at: https://doi.org/10.1016/j.applthermaleng.2017.04.024.

Yamba, E.I., Aryee, J.N.A., Quansah, E., Davies, P., Wemegah, C.S., Osei, M.A., Ahiataku, M.A. and Amekudzi, L.K. (2023) ‘Revisiting the agro-climatic zones of Ghana: A re-classification in conformity with climate change and variability’, *PLOS Climate*, 2(1), p.

e0000023. Available at: https://doi.org/10.1371/journal.pclm.0000023.

Yavuzturk, C., Ksaibati, K. and Chiasson, A.D. (2005) ‘Assessment of Temperature Fluctuations in Asphalt Pavements Due to Thermal Environmental Conditions Using a Two-Dimensional, Transient Finite-Difference Approach’, *Journal of Materials in Civil Engineering*, 17(4), pp. 465–475. Available at: https://doi.org/10.1061/(asce)0899-1561(2005)17:4(465).

Yinfei, D., Qin, S. and Shengyue, W. (2015) ‘Bidirectional heat induced structure of asphalt pavement for reducing pavement temperature’, *Applied Thermal Engineering*, 75, pp. 298–306. Available at: https://doi.org/10.1016/j.applthermaleng.2014.10.011.

Zhang, D., Birgisson, B., Luo, X. and Onifade, I. (2019) ‘A new long-term aging model for asphalt pavements using morphology-kinetics based approach’, *Construction and Building Materials*, 229, p. 117032. Available at: https://doi.org/10.1016/j.conbuildmat.2019.117032.

APPENDICES

Appendix A: Interview Guide

Topic: State of Practice Regarding the Determination of Asphalt Pavement Temperature in Ghana

Interviewee:

Organisation:

Designation:

Date: Interviewer:

Part one: Falling weight deflectometer (FWD) testing

Q1. Briefly describe how your organisation determines pavement temperature during FWD testing.

Q2. Describe the challenges (if any) associated with the current method of asphalt pavement temperature determination in FWD testing

Q3a. Do you anticipate a change in this practice for a more robust type in the future?

Q3b. What could be some of the challenges that such new methods may be associated with?

Q4. How is the determined pavement temperature used in the structural evaluation of the pavement?

Q5. Could you please share with me any improved asphalt pavement temperature determination technique that, if implemented, will help improve FWD analysis in your organization?

Part Two: Superpave Performance-Graded (PG) Binder Selection

Q6. Describe how Superpave PG binder grades were determined for past projects in your organisation?

Q7. Describe some of the challenges (if any) experienced in determining Superpave PG binder grades for past projects.

Q8. As you might know (or as you said), the Superpave binder grades are determined using minimum and maximum pavement temperatures. Would you consider using a mathematical model developed locally for predicting the minimum and maximum pavement temperatures for selecting Superpave PG binder grades?

Q9. What obstacles do you foresee in the use of such models?

Appendix B: Ethical Clearance Letter

Kwame Nkrumah
University of Science
and Technology, Kumasi

College of Health Sciences
SCHOOL OF MEDICINE AND DENTISTRY

COMMITTEE ON HUMAN RESEARCH, PUBLICATION AND ETHICS

Our Ref: CHRPE/AP/568/22

31st August, 2022

Mr. Simon Ntramah
Department of Civil Engineering
KNUST-KUMASI.

Dear Sir,

LETTER OF APPROVAL

Protocol Title: ***"State of Practice Regarding Determination of Asphalt Pavement Temperature in Ghana."***

Proposed Site: ***Kumasi and Accra (Memphis Metropolitan Ltd, Ablin Consult Engineers and Planners ltd and CSIR Building and Road Research Institute), Ghana.***

Sponsor: ***Self Sponsored.***

Your submission to the Committee on Human Research, Publications, and Ethics on the above-named protocol refer.

The Committee reviewed the following documents:

- Notification letters of 1st August 2022 from the Memphis Metropolitan Ltd, Ablin Consult Engineers and Planners ltd and CSIR Building and Road Research Institute (study site) indicating approval for the conduct of the study at the Municipality.
- A Completed CHRPE Application Form.
- Participant Information Leaflet and Consent Form.
- Research Protocol.
- Questionnaire.

The Committee has considered the ethical merit of your submission and approved the protocol. The approval is for a fixed period of one year, beginning **31st August, 2022** to **30th August, 2023** renewable thereafter. The Committee may, however, suspend or withdraw ethical approval at any time if your study is found to contravene the approved protocol.

Data gathered for the study should be used for the approved purposes only. Permission should be sought from the Committee if any amendment to the protocol or use, other than submitted, is made of your research data.

The Committee should be notified of the actual start date of the project and would expect a report on your study, annually or at the close of the project, whichever one comes first. It should also be informed of any publication arising from the study.

Thank you for your application.

Yours faithfully,

Rev. Prof. John Appiah-Poku.
Honorary Secretary
FOR: CHAIRMAN

Room 7, Block L, School of Medicine and Dentistry, KNUST, University Post Office, Kumasi, Ghana
Tel: +233 (0) 3220 63248 **Mobile:** +233 (0) 20 5453785 **Email:** chrpe.knust.kath@gmail.com/chrpe@knust.edu.gh